Title
Dissection of Medial Prefrontal Cortex Circuitry and its Dopaminergic Modulation

Author
Gee, Steven

Publication Date
2014

Peer reviewed|Thesis/dissertation

Dissection of Medial Prefrontal Cortex Circuitry and its Dopaminergic Modulation

by

Steven Gee

DISSERTATION

Submitted in partial satisfaction of the requirements for the degree of

DOCTOR OF PHILOSOPHY

in

Neuroscience

in the

GRADUATE DIVISION

of the

UNIVERSITY OF CALIFORNIA, SAN FRANCISCO

[redacted]

Acknowledgements

First and foremost, I need to thank my family –my brother, Ryan Gee, my mother, Lila Gee, and father, Gary Gee— for their guidance, encouragement, and continual support. Since childhood, my brother has been my best friend and we remain close to this day. Like any close sibling would feel, he was deeply saddened by my move to another city. I am grateful for his support and understanding, despite his reservations about me leaving, and am so proud of the smart, creative, and driven young man he has matured into today. I am especially thankful to have such a loving and caring mother. All the phone calls, care packages, and entire meals that she would prepare and send sustained me and were invaluable throughout my time in graduate school. I am also grateful to my father, whose example of constant persistence in the midst of setbacks served as an important motivator in my graduate career. Thank you Mom and Dad.

I want to thank Dr. Michael Levine, Dr. Carlos Cepeda, and Dr. Damian Cummings for giving me my first opportunity to participate in neuroscience research as an undergraduate. I definitely could not be at this point in my career without that experience.

I have had the great pleasure to meet and know such smart and talented classmates, colleagues, and friends throughout graduate school. I would like to thank Osama Ahmed, Moses Lee, Karuna Meda, Kartik Pattabiraman, Phil Parker, Stephanie Redmond, Dina Juarez-Salinas, and Bryan Seybold. Not only

were they instrumental in my development as a scientist, but they also made my time at UCSF incredibly fun and enjoyable outside the laboratory. I could not imagine myself making it through graduate school without them. Thank you all.

I would like to also thank people outside of the UCSF neuroscience program. My former roommates, Eugene Chen and Peter Westcott, created an amazing ‘home away from home’ during my initial years in graduate school and have been very dear friends ever since. Thank you both. I would also like to thank my family and friends in Southern California: Daryl, Tracey, and Kimberly Anacleto, Christian and Monica Bowman, Ahmad Adam, and Jasmine Le. Thanks for all the support, humorous conversations, and the fun times we’ve shared both here and back home.

I also thank the UCSF faculty members who have advised, taught, and mentored me through the years. I would like to thank, my graduate advisor, Dr. David Copenhagen for all the encouraging conversations when I first entered graduate school. Dr. Eric Huang was an extremely helpful and reassuring faculty member during the neuroscience core courses. I would also like to thank Dr. Susan Voglmaier for all her support and useful discussions regarding career paths. My thesis committee members, Anatol Kreitzer, Kevin Bender, and Andrea Hasenstaub, have been outstanding in training me to think critically about my own work and present this work coherently. I would also like to thank Dr. John Huguenard for kindly serving as the outside member of my thesis committee.

I must also thank Dr. Louis Reichardt and Roger Nicoll, the program directors for the Neuroscience Graduate Program, as well as Pat Veitch, the

Neuroscience Program coordinator, and Lucita Nacionales, the Neuroscience Program assistant. They have done an amazing job creating a cohesive and supportive environment for all their students.

I also owe many thanks to the members of the Sohal lab with whom I have worked and collaborated. I have also had the great pleasure to know these individuals as friends. Dr. Ian Ellwood is one of the most brilliant and insightful scientists I'm sure I will ever meet and has played a very significant role in my graduate career. I thank Anthony Lee, a great friend, and extremely intelligent and industrious graduate student. I also thank Tosha Patel, a close friend, and lab manager, who consistently does an amazing job making sure the Sohal lab runs smoothly. She has always been nothing short of kind and encouraging to me.

Finally, I owe a great debt of gratitude to Dr. Vikaas Sohal, my thesis mentor. Dr. Sohal accepted me into his lab in the summer of 2010 as his first graduate student. At the time, his laboratory was in its nascent stages, comprising of only Dr. Ellwood and Tosha Patel. I am extremely grateful to Dr. Sohal for seeing potential in me, and dedicating his time and effort towards my success. I am constantly inspired by Dr. Sohal's breadth of knowledge, incredible ability to identify and tackle important scientific questions, and his unassuming nature despite his numerous successes. It has been an absolute pleasure working in his lab and I feel very fortunate to have been trained in his lab. I could not thank him enough.

Author Contributions

The text of Chapter 2 of this thesis is largely a reprint of the material as it originally appeared in The Journal of Neuroscience (Gee*, Ellwood*, et. al., 2012). Steven Gee and Ian Ellwood contributed equally to the electrophysiology experiments in this chapter. Vikaas Sohal, the senior author on the publication, directed and supervised the research, and wrote the paper.

The text of Chapter 3 of this thesis is a reprint of the material as it originally apperared in Neuron (Lee*, Gee* et al., 2014). Steven Gee and Anthony Lee contributed equally to the electrophysiology experiments in this chapter. Dan Vogt and Tosha Patel, the third and fourth author on the publication, constructed the viruses for the experiments. Vikaas Sohal, the senior author on the publication directed and supervised the research. Vikaas Sohal, Anthony Lee, and Steven Gee co-wrote the paper.

The text of Chapter 4 of this thesis is a reprint of material submitted to The Journal of Neuroscience (Gee, Sohal, 2014). Steven Gee performed the electrophysiology experiments in this chapter. Vikaas Sohal, the senior author on the publication directed and supervised the research. Vikaas Sohal and Steven Gee co-wrote the paper.

Table of Contents

List of Tables and Figures

Abstract

The prefrontal cortex (PFC) is comprised of a network of excitatory and inhibitory neurons that are critical for a number of cognitive processes including the ability to make decisions. PFC dysfunction causes deficits in these domains and major aspects of psychiatric disorders. Notably, layer V of the PFC is thought to play an important role in regulating these higher order processes and contains heterogeneous subpopulations of pyramidal neurons with distinct morphologies and projections. Layer V of PFC is also the major site of dopaminergic modulation. However, unlike the striatum, where D1 or D2 receptors are known to differentially express in separate projection subtypes of medium spiny neurons, the distribution of D1 and D2Rs in layer V projection neurons within PFC is unclear. Notably, Dopamine D2 receptors (D2Rs) play major roles in both normal and pathological PFC function. Thus, knowing their expression and effects in layer V neurons can provide helpful insights into important mechanisms that underlie prefrontal activity, and ultimately cognitive function. Chapter 1 of this thesis examines the expression of D1Rs and D2Rs in layer V projection subtypes. We also describe a novel mechanism by which D2R activation can drastically enhance the excitability of a D2R-expressing layer V pyramidal subtype. In Chapter 2, we explore differences in how long range excitation and feedforward inhibition is processed in D2R-expressing and D2R-lacking layer V pyramidal neurons. We propose that these differences might confer these

subtypes with separate computational properties important for normal PFC function.

CHAPTER 1

General Introduction

Normal and pathological roles of the PFC

The ability to make decisions based on our representation of the environment and our past experiences is integral for our survival. This ability to is thought to be primarily mediated by the prefrontal cortex (PFC), which also facilitates other aspects of executive function including attention, reward prediction, working memory, efference copy, behavioral flexibility, and the capacity to suppress socially unacceptable behaviors. Patients with psychiatric diseases such as schizophrenia or autism or individuals with damage to the PFC suffer from deficits in these domains (Roberts and Bruton, 1995). These deficits are thought to be due, in part, to impaired PFC circuitry and/or aberrant dopamine modulation. This thesis focuses on understanding the components of PFC circuitry, the long-range and inhibitory connections within, and the role of dopamine. By understanding these mechanisms, we hope to better understand the neural basis for higher cognitive function and how these mechanisms are potentially altered in psychiatric disease

Long-range and recurrent connections in the PFC

The PFC is heavily interconnected with other regions of cortex, sending and receiveing inputs to and from sensory cortices, contralateral PFC, and subcortical regions like the thalamus and basal ganglia. Furthermore, aberrant functional connectivity (Wernicke et al., 1906; Marenco et al., 2012; Brennan et al., 2008), in addition to decreased synchrony (Sigurdsson et al., 2010), between the PFC and other brain regions has been implicated as a major

pathophysiological mechanism underlying schizophrenia, autism, and attention deficit hyperactivity disorder. It is important to note that, in addition to sending and receiving long-range projections to and from other cortical regions, pyramidal neurons within the form highly recurrent connections with other pyramidal neurons in the PFC (Morsishima, 2006) and these connections are thought to underlie reverberant excitation important for information processing, decision making, and mnemonic activity (Anderson et al., 2000; Wang et al., 2004; Curtis et al., 2010; Shepherd, 2013).

Finally, inhibition plays an important role in PFC function. At least three types of inhibitory interneurons exist in the PFC (Rudy, 2011). Substantial focus has been directed to the role of the parvalbumin-positive, fast-spiking (FS) interneurons owing to their role in generating gamma rhythms (Sohal, 2009) and their implications in schizophrenia.

The effects of dopamine on the PFC

In addition to long range, and recurrent, excitatory connections, the PFC also receives strong mesocortical dopaminergic inputs from the ventral tegmental area (VTA). Traditionally, the activity of dopamine neurons within the VTA correlates with differences in expected and actual rewards (reward error prediction error). However dopaminergic projections from the VTA can also signal aversion, saliency, novelty, and uncertainty. (Schultz, 2007; Broomberg-Martin et al., 2010). Our understanding of the differential functions of

dopaminergic signals from the VTA to its targets (nucleus accumbens, prefrontal cortex, striatum, etc) is still being elucidated. Indeed, increases in catecholamine activity in response to novelty and reward have been reported in both the PFC and nucleus accumbens (Rebec et al., 1997). However, in a recent study, Lammel et. al demonstrated that dopaminergic cells projecting to the nucleus accumbens responded to rewarding stimuli whereas dopaminergic cells projecting to the medial prefrontal cortex responded to aversive stimuli (Lammel et al., 2013). Prefrontal dopamine is thought to play a critical role in higher cognitive processes and neuropsychiatric pathology, and is an area of extensive research (Seamans et al., 2004). Depletion of prefrontal dopamine by 6-hydroxy-dopamine had deleterious effects on spatial working memory in primates (Brozoski et al., 1979) and rats (Simon et al., 1981). Furthermore, aberrant dopaminergic modulation of PFC might contribute to cognitive dysfunction in psychiatric disorders including schizophrenia (Winterer and Weinberger, 2004; Durstewitz and Seamans, 2008). Specifically, aberrant D2R modulation, which will be discussed later, is thought to play a major role in the pathophysiology of schizophrenia.

Different effects of dopamine by D1R and D2Rs receptors in the PFC

Dopamine is thought to act through two classes of receptors, “D1-like” or “D2-like,” to modulate neurons and their activity. The coding of reward value and uncertainty signals is thought to occur via differential stimulation of D1 and D2Rs. High-affinity D2 receptors respond to low dopamine concentrations produced by

tonic release whereas low-affinity D1Rs respond to higher dopamine concentrations produced by phasic dopamine release (Schultz, 2007).

In the PFC, D1 and D2Rs are thought to have opposing affects on activity associated with cognitive tasks (Sawaguchi and Goldman-Rakic, 1994; Seamans and Durstewitz 2001; Wang and Goldman-Rakic 2004; Tseng and O'Donnell 2005). During a delayed working memory task in primates, Wang and Goldman-Rakic, recorded from prefrontal neurons and found that some neurons increased in their activity during the delay period when the monkey was required to store directional information in working memory (2004). Modulating D1Rs reversed this increase in activity whereas D2R modulation had no effect (Wang and Goldman-Rakic, 2004). A separate group of neurons increased their activity during the period following the delay period, when the monkey made a saccade to indicate its decision (Wang and Goldman-Rakic, 2004). In these neurons, infusion D2R antagonists reversed the increase in activity, while D1R modulation had no effect (Wang and Goldman-Rakic, 2004). In another study performed in rodents, infusion of D1R and D2R agonists and antagonists into the PFC had opposing effects in a probabilistic discounting task (St Onge et a., 2011). Rats were provided a choice between a small, certain and large, but probabilistic reward (St Onge et a., 2011). Blocking D1Rs in PFC led to a decreased preference for the large but risky option whereas D2R blockade led to an increased preference. Together, these findings support a contemporary theory about how D1 and D2Rs can exert opposing effects on decision-making (Durstewitz et al., 2000; Seamans

and Yang, 2004). According to this 'dual-state' model, D1Rs in the PFC stabilize network activity, decreasing the influence of weaker inputs, and strengthening single representations (Durstewitz and Seamans, 2008). D2Rs, on the other hand, are thought destabilize these representations, shifting the network towards a more flexible state that promotes fluctuations in representations (Durstewitz and Seamans, 2008).

Within the basal ganglia, D1Rs and D2Rs also play opposing roles in behavior and they are also dichotomously expressed on neuronal populations with specific projection targets. Approximately half of the medium spiny neurons (MSNs) in the striatum are part of the "direct pathway", express D1Rs, and project to the internal segment globus pallidus/substantia nigra pars reticulata, while half belong to the "indirect pathway", express D2Rs, and project to the external segment of the globus pallidus. Activity in the direct pathway is thought to facilitate movement whereas activity in the indirect pathway is thought to inhibit movement. While this model is likely an overgeneralization, it has nevertheless provided a useful framework for testing specific hypotheses about the role of specific circuits and cell populations in normal and pathological basal ganglia function (DeLong and Wichmann, 2009; Packard and Kowlton, 2002; Kravitz et. al., 2009). Such a framework is lacking for the PFC network. The work of Wang and Goldman-Rakic suggest that there exist populations of neurons in PFC that are sensitive to D2Rs and not D1Rs, and vice versa. However, due to the nature of in-vivo recordings, this work provided little information about the identity of the

neurons recorded. In chapter 2, we address whether, as in the striatum, D1Rs and D2Rs in the PFC are expressed on neurons with distinct projection targets. Knowing the identity of PFC neurons that express D1 or D2Rs can provide a vital framework to test the normal and pathological function of specific circuits and cell types. Further these data lend support to models of how D1Rs and D2Rs can influence the network activity that promote the stabilization or destabilization of representations in the environment (Durstewitz et al., 2000; Seamans and Yang, 2004). Understanding how D1 and D2Rs are expressed at the level of different cell populations will allow us to better understand how dopamine can have specific actions in a heterogeneous population of neurons and, potentially, the roles of these neurons in executive function.

Cellular heterogeneity in the PFC

Different neuronal cell types in cerebral cortex have long been postulated to modify the response of the patterns of the fibers coming into it (Hubel and Wiesel, 1962). In the example mentioned earlier, the subtype of medium spiny neuron in the striatum can predict its patterns of connectivity and, ultimately, its role in cognitive or motor function. The cortex, which is interconnected with both the basal ganglia and thalamus in large-scale loops, also serves a critical role in mediating these functions (Delong and Strick, 1986). Corticostriatal projections neurons are located almost uniformly across cortex and consist of both intratelencephalic (IT) neurons and pyramidal tract (PT) neurons (Shepherd, 2013; Ferino et al., 1987; Wilson 1987, Levesque et al., 1996). IT neurons project

contralaterally via the corpus callosum and can send both ispi- and bilateral projections to cortex and striatum (Shepherd, 2013; Figure 1). PT neurons project to ipsillaterally subcortical regions such as RTN and thalamus and, in some cases, may project to contralateral brainstem and spinal cord (Figure 1).

PT and IT neurons have distinct morphologies and intrinsic properties. PT subcortically-projecting neurons and tend to have thicker apical tufts than IT neurons, which project across the corpus callosum (Morishima and Kawaguchi, 2006; Hattox and Nelson, 2007; Otsuka and Kawaguchi, 2008). In PFC, neurons projecting to brainstem were found to have differences in the amount of h-current in response to hyperpolarizing current steps (Dembrow et al., 2010). These differences in h-currents may impart specific differences in signal propagation and network synchrony between cell types (Vaidya and Johnston 2013).

While the roles of PT and IT neurons in motor cortex have been explored in the context of movement control and locomotion (Beloozerova et al., 2003; Pasquereau and Turner, 2011; Bauswein, 1989), their roles in PFC and cognition are less well understood. If D1R and D2Rs play dissociated roles in behavior, do they act on distinct cell populations within layer V of PFC? And if so, are they differentially expressed on PT and IT pyramidal neurons? These questions will be explored here.

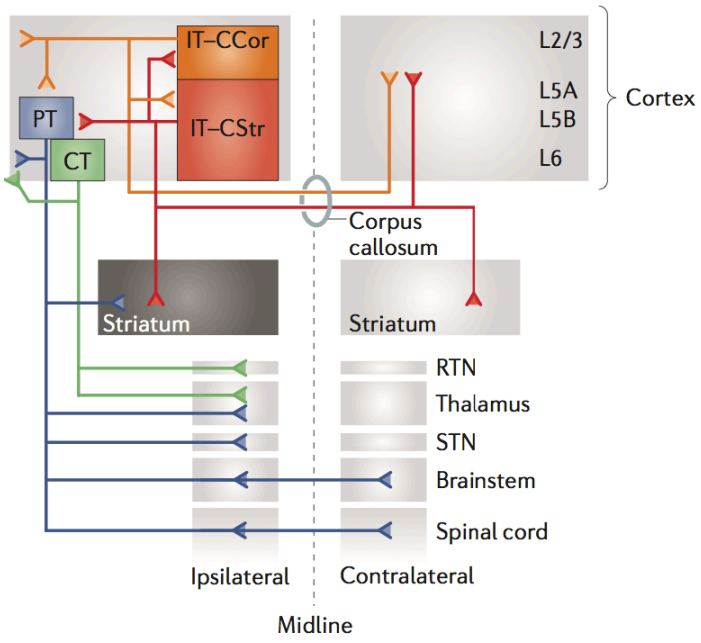

Figure 1. Long range connectivity defines two classes of corticostriatally projecting neurons. Cortical pyramidal tract (PT) neurons project to ipsilateral striatum, thalamus, subthalamic nucleus, and ispi- and contralateral brainstem and spinal cord regions. Intratelencenphalic (IT) neurons project to contralateral cortex and striatum via the corpus callosum. IT neurons also project to ipsilateral striatum. (adapted from Shepherd, 2013).

References

Anderson KL, Rajagovindan R, Ghacibeh GA, Meador KJ, Ding M
Theta oscillations mediate interaction between prefrontal cortex and medial temporal lobe in human memory. Cereb Cortex 2010; 20:1604–1612.

Bauswein E, Fromm C, Preuss A (1989) Corticostriatal cells in comparison with pyramidal tract neurons: contrasting properties in the behaving monkey. Brain Res 493:198 –203.

Beloozerova IN, Sirota MG, Swadlow HA. Activity of different classes of neurons of the motor cortex during locomotion. *J Neurosci* 23: 1087–1097, 2003a.

Brennan AR, Arnsten AF. Neuronal mechanisms underlying attention deficit hyperactivity disorder: the influence of arousal on prefrontal cortical function. Ann NY Acad Sci. 2008;1129:236–245.

Broomberg-Martin ES, Matsumoto M, Hikosaka O. Dopamine in motivational control: rewarding, aversive, and alerting. Neuron 2010; 68:815-34

Curtis, C.E., and Lee, D. (2010). Beyond working memory: the role of persistent activity in decision making. Trends Cogn Sci *14*, 216-222.

Delong M, Wichmann T. Update on models of basal ganglia function and dysfunction.Parkinsonism Relat. Disord..2009; 15: S237–S240

Dembrow NC, Chitwood RA, Johnston D (2010) Projection-specific neuromodulation of medial prefrontal cortex neurons. J Neurosci 30:16922-16937.

Durstewitz D, Vittoz NM, Floresco SB, Seamans JK (2010) Abrupt transitions between prefrontal neural ensemble states accompany behavioral transitions during rule learning. Neuron 66:438-448.

Ferino, F., Thierry, A. M., Saffroy, M. & Glowinski, J. Interhemispheric and subcortical collaterals of medial prefrontal cortical neurons in the rat. Brain Res. 417, 257–266 (1987).

Hattox AM, Nelson SB (2007) Layer V neurons in mouse cortex projecting to different targets have distinct physiological properties. J Neurophysiol 98:3330-3340.

Hubel D, Wiesel T Receptive fields, binocular interaction and functional architecture in the cat's visual cortex. 1962; 160:106-154

Kravitz AV, Freeze BS, Parker PR, Kay K, Thwin MT, Deisseroth K, Kreitzer AC (2010) Regulation of parkinsonian motor behaviours by optogenetic control of basal ganglia circuitry. Nature 466:622-626.

Lammel, S., Lim, B. K., Ran, C., Huang, K. W., Betley, M. J., Tye, K. M., et al. (2013). Input-specific control of reward and aversion in the ventral tegmental area. *Nature*, *491*(7423), 212–217. doi:10.1038/nature11527

Levesque, M., Charara, A., Gagnon, S., Parent, A. & Deschenes, M. Corticostriatal projections from layer V cells in rat are collaterals of long-range corticofugal axons. Brain Res. **709**, 311–315 (1996).

Marenco S, Stein JL, Savostyanova AA, Sambataro F, Tan, HY, Goldman AL, Verchinski BA, Barnett AS, Dickinson D, Apud JA*, et al.* (2012). Investigation of anatomical thalamo-cortical connectivity and FMRI activation in schizophrenia. Neuropsychopharmacology *37*, 499-507.

Morishima M, Kawaguchi Y (2006) Recurrent connection patterns of corticostriatal pyramidal cells in frontal cortex. J Neurosci 26:4394-4405.

Otsuka T, Kawaguchi Y (2008) Firing-pattern-dependent specificity of cortical excitatory feed-forward subnetworks. J Neurosci 28:11186-11195.

Packard MG, Kmowlton BJ. Learning and memory functions of the basal ganglia. Annu Rev Neurosci 2002; 25:563-93

Pasquereau B, Robert T. Primary motor cortex of the parkinsonian monkey: differential effects on the spontaneous activity of pyramidal tract-type neurons. Cereb Cortex 2011l; 21: 1362-1378

Rebec GV, Christensen JR, Guerra C, Bardo MT. Regional and temporal differences in real-time dopamine effluz in the nucleus accumbens during free-choice novelty Brain Res 1997 776:61-7

Roberts GW, Bruton CJ (1990): Notes from the graveyard: Neuropathology and schizophrenia. Neuropathol App Neurobiol 16:3–16

Rudy B, Fishell G, Lee S, Hjerling-Leffler J. Three groups of interneuons account for nearly 100% of neocortical GABAergic interneurons. Dev Neurobiol. 2011 71:45-61

Seamans JK, Durstewitz D, Christie BR, Stevens CF, Sejnowski TJ. (2001) Dopamine D1/D5 receptor modulation of excitatory synaptic inputs to layer V prefrontal cortex neurons. Proc Natl Acad Sci USA 98:301-6

Seamans JK, Yang CR (2004) The principal features and mechanisms of dopamine modulation in the prefrontal cortex. Prog Neurobiol 74:1-58.

Simon H (1981) Dopaminergic A10 neurons and the frontal system. J Physiol (Paris) 77:81–95.

Sohal VS, Zhang F, Yizhar O, Deisseroth K (2009) Parvalbumin neurons and gamma rhythms enhance cortical circuit performance. Nature 459:698-702.

Shepherd GM (2013) Corticostriatal connectivity and its role in disease. Nat Rev Neurosci 14:278-291.

Schultz W (2007) Multiple dopamine functions at different time courses. Annu Rev Neurosci 30:259-288.

Sigurdsson T, Stark KL, Karayiorgou M, Gogos JA, Impaired hippocampal-prefrontal synchrony in a genetic mouse model of schizohprenia. Nature 2010; 464, 763-7

St Onge JR, Abhari H, Floresco SB (2011) Dissociable contributions by prefrontal D1 and D2 receptors to risk-based decision making. J Neurosci 31:8625-8633.

Vaidya, S. P., & Johnston, D. (2013). Temporal synchrony and gamma-to-theta power conversion in the dendrites of CA1 pyramidal neurons. *Nature Publishing Group*, *16*(12), 1812–1820. doi:10.1038/nn.3562

Wang M, Vijayraghavan S, Goldman-Rakic PS (2004) Selective D2 receptor actions on the functional circuitry of working memory. Science 303:853-856.

Wernicke C (1906):Grundrisse der Psychiatrie. Leipzig, Germany: Thieme.

Wilson, C. J. Morphology and synaptic connections of crossed corticostriatal neurons in the rat. J. Comp. Neurol. **263**, 567–580 (1987).

Winterer G, Weinberger DR (2004) Genes, dopamine and cortical signal-to-noise ratio in schizophrenia. Trends Neurosci 27:683-690.

CHAPTER 2

Synaptic Activity Unmasks Dopamine D2 Receptor Modulation of a Specific Class of Layer V Pyramidal Neurons in Prefrontal Cortex

ABSTRACT

Dopamine D2 receptors (D2Rs) play a major role in the function of the prefrontal cortex (PFC), and may contribute to prefrontal dysfunction in conditions such as schizophrenia. Here we report that in mouse PFC, D2Rs are selectively expressed by a subtype of layer V pyramidal neurons that have thick apical tufts, prominent h-current, and subcortical projections. Within this subpopulation, the D2R agonist quinpirole elicits a novel afterdepolarization that generates voltage fluctuations and spiking for hundreds of milliseconds. Surprisingly, this afterdepolarization is masked in quiescent brain slices, but is readily unmasked by physiologic levels of synaptic input which activate NMDA receptors, possibly explaining why this phenomenon has not been reported previously. Notably, we could still elicit this afterdepolarization for some time after the cessation of synaptic stimulation. Besides NMDA receptors, the quinpirole-induced afterdepolarization also depended on L-type Ca^{2+} channels and was blocked by selective L-type antagonist nimodipine. To confirm that D2Rs can elicit this afterdepolarization by enhancing Ca^{2+} (and Ca^{2+}-dependent) currents, we measured whole-cell Ca^{2+} potentials that occur after blocking Na^{+} and K^{+} channels, and found quinpirole enhanced these potentials, while the selective D2R antagonist (-)sulpiride had the opposite effect. Thus, D2Rs can elicit a Ca^{2+}-channel dependent afterdepolarization that powerfully modulates activity in specific prefrontal neurons. Through this mechanism, D2Rs might enhance outputs to subcortical structures, contribute to reward related persistent firing, or increase the level of noise in prefrontal circuits.

INTRODUCTION

Dopamine plays a critical role in prefrontal cortex (PFC). First, depleting prefrontal dopamine impairs working memory in monkeys (Brozoski et al., 1979), and genetic variations in prefrontal dopamine catabolism affect both PFC-dependent executive function and prefrontal physiology in humans (Egan et al., 2001). Second, imbalanced prefrontal dopaminergic signaling may contribute to disorders including schizophrenia (Arnsten and Goldman-Rakic, 1998; Winterer and Weinberger, 2004; Kellendonk et al., 2006). Third, reward signals are typically mediated by dopamine (Schultz, 2007), and the past history of reward modulates prefrontal neuron excitability (Bernacchia et al., 2011) and can trigger persistent firing (Histed et al., 2009).

Prefrontal dopamine D2 receptors (D2Rs) play critical roles in cognition. Infusion of D2 agonists and antagonists into PFC modulates working memory and set-shifting in rodents (Druzin et al., 2000; Floresco et al., 2006; St Onge et al., 2011). Systemic administration of D2 agonists in non-human primates affects working memory and elicits “hallucinatory-like” behaviors (Arnsten et al., 1995). In non-human primates, prefrontal D2Rs are specifically necessary for neural activity associated with memory-guided saccades (Wang et al., 2004). Consistent with these animal studies, genetic variation in D2Rs modulates prefrontal activity and working memory in humans (Zhang et al., 2007).

Given that all antipsychotics block D2Rs, and that prefrontal D2Rs play a major role in tasks that are disrupted in schizophrenia, a major hypothesis is that excessive D2R activation contributes to prefrontal dysfunction in schizophrenia (Winterer and Weinberger, 2004; Durstewitz and Seamans, 2008). Prefrontal D2Rs may also contribute to Tourette syndrome and bipolar disorder (Simonic et al., 1998; Minzer et al., 2004; Yoon et al., 2007; Minton et al., 2009; Steeves et al., 2010). Thus, D2Rs play a major role in both normal and pathological prefrontal function. Specifically D2Rs may increase the variability of PFC activity (Winterer and Weinberger, 2004; Durstewitz and Seamans, 2008). Under normal conditions, such variability could facilitate adaptation to a changing environment (Durstewitz et al., 2010; St Onge et al., 2011). However, excessive or imbalanced D2R activation might produce pathological variability that contributes to “prefrontal noise” and cognitive dysfunction in schizophrenia (Winterer and Weinberger, 2004).

We focused on layer V pyramidal neurons in PFC because these neurons contain most prefrontal D2Rs (Lidow et al., 1998; Santana et al., 2009). A few studies have described ways that D2Rs enhance (Wang and Goldman-Rakic, 2004) or suppress (Gulledge and Jaffe, 1998; Tseng and O'Donnell, 2004) excitability in these neurons. A possibly related observation is that dopamine profoundly depolarizes frontal cortex pyramidal neurons *in vivo* (Bernardi et al., 1982). Nevertheless, specific mechanisms for D2R-modulation of layer V pyramidal neurons in PFC remain elusive.

Here we report two major results about D2Rs in layer V of PFC. First, D2Rs are not uniformly distributed across layer V cell populations, but rather restricted to a specific subpopulation of layer V pyramidal neurons with thick apical tufts, prominent h-current, and subcortical projections. Second, in these neurons, D2Rs elicit a novel afterdepolarization that depends on NMDA receptors and L-type calcium channels, and can drive spiking for hundreds of milliseconds.

METHODS

All experiments were conducted in accordance with procedures established by the Administrative Panels on Laboratory Animal Care at the University of California, San Francisco.

Slice preparation. Slice preparation and intracellular recording followed our published protocol (Sohal and Huguenard, 2005). We cut 250 micron coronal slices from 6-10 week old mice of either sex. Specifically, all electrophysiological experiments showing the quinpirole-induced afterdepolarization were from 9-10 week old mice, except for 4/7 perforated patch experiments, which were from 6-7 week old mice. We used the following mouse lines: wild-type C57Bl/6 mice (Charles River), Drd1::EGFP (line S118; www.gensat.org), Drd1::Cre (line EY262; www.gensat.org), Drd2::EGFP (www.gensat.org), and Drd2::Cre (line ER44; www.gensat.org). We secured the slice by placing a harp along the midline between the two hemispheres.

Intracellular Recording. We obtained somatic whole cell patch recordings from visually identified pyramidal cells in layer V of infralimbic (IL) or prelimbic (PL) cortex using differential contrast videomicroscopy on an upright microscope (BX51WI, Olympus). Recordings were made using a Multiclamp 700A (Axon Instruments). Except when otherwise noted, patch electrodes (tip resistance = 2–6 MOhms) were filled with (in mM): 130 K-gluconate, 10 KCl, 10 Hepes, 10 EGTA, 2 MgCl, 2 MgATP, and 0.3 NaGTP (pH adjusted to 7.3 with KOH). For

perforated patch recordings, the pipette solution included 0.02 mg/mL gramicidin D. ACSF contained (in mM): 126 NaCl, 26 $NaHCO_3$, 2.5 KCl, 1.25 NaH_2PO_4, 1 $MgCl_2$, 2 CaCl, and 10 glucose. In experiments that used TEA, the amount of NaCl was decreased by a corresponding amount (30 mM) to maintain the osmolarity of the extracellular solution. All recordings were at 32.5 ± 1 °C. Series resistance was usually 10–20 MΩ, and experiments were discontinued above 30 MΩ.

Injection of virus for ChR2 or EYFP expression. For Cre-dependent expression of ChR2 or EFYP, we used a previously described adeno-associated virus vector that drives Cre-dependent expression of a ChR2-EFYP fusion protein (Sohal et al., 2009). In other cases, we expressed ChR2-EFYP in pyramidal neurons using a previously described adeno-associated virus vector that contains a gene encoding ChR2-EYFP under control of the promoter for CaMKII (Yizhar et al., 2011). In each case, we injected 0.5 – 0.75 L of virus following previously described procedures (Sohal et al., 2009). For experiments in which we recorded from ChR2-negative neurons while stimulating ChR2-positive axons, we injected virus into the contralateral mPFC, and verified that we observed fluorescent soma on the injected side, but not on the contralateral side (which was the location for recording). In 3/5 of these experiments, we drove expression using the Cre-dependent virus in Drd1::Cre mice, while in the other 2/5 experiments we injected the virus carrying the CaMKIIα promoter into wild-type mice. We waited at least 3-4 weeks after virus injection before preparing

brain slices. Coordinates for injection into mPFC were (in mm relative to bregma): 1.7 AP, 0.3 ML, and -2.75 DV.

Injection of retrogradely transported microspheres for projection targeting experiments. Procedures for injection of these microspheres were similar to those for virus injection. We waited at least 48h after each injection before preparing brain slices. Coordinates for mPFC injections were the same as for virus injections. For injections into MD thalamus, coordinates were (in mm relative to bregma): -1.7 AP, 0.3 ML, and -3.5DV. For each experiment, we verified that microspheres were present in the correct target (MD thalamus or mPFC). For injections into MD thalamus we specifically verified that microspheres were not present in nearby structures (e.g. striatum).

Drug application. For electrophysiology, all drugs were dissolved in water (quinpirole, NMDA, DL-AP5, TEA) or DMSO (haloperidol, (-)sulpiride, nimodipine) before being diluted in ACSF, except for and TTX which was dissolved in a pH 4.8 citrate buffer. Throughout the text, “TEA” refers to tetraethylammonium chloride, “AP5” refers to DL-AP5, and “sulpiride” refers to (-)sulpiride.

ChR2 stimulation. We stimulated ChR2 in pyramidal neurons using flashes of light generated by a Lambda DG-4 high speed optical switch with a 300W Xenon lamp, and an excitation filter set centered around 470nm, delivered to the slice

through a 40x objective (Olympus). Illumination was delivered across a full high-power (40x) field.

Biocytin fills, morphological analysis, and confocal imaging. For experiments in which we studied cell morphology, the intracellular solution contained 0.3% biocytin. Cells filled with biocytin were fixed overnight in a buffered solution containing 4% paraformaldehyde. To visualize filled cells, we washed fixed slices in 0.1 M PBS, then incubated for 40 min in PBS with 1-2% Triton X-100, before incubating for 1 h in PBS with 0.5% Triton and Texas red Avidin D or Fluorescein Avidin D (1:500). Before mounting the slice, we washed it with PBS again. We measured the width of the apical dendritic shaft 5 mm above the soma. To visualize fluorescent cells, we followed a similar protocol omitting incubation with Avidin D. All imaging was carried out on a Zeiss LSM510.

Statistical analysis. We used Student's t-tests to compare of pairs of groups, unless there were repeated measurements or unpaired observations, in which case we used ANOVA. To compare time constants for 90% decay of the quinpirole-induced afterdepolarization, we first log-transformed these time constants, because their distributions in quinpirole were highly skewed and non-gaussian. Error bars indicate ± 1 S.E.M. unless otherwise specified.

RESULTS

H-current identifies a subpopulation of layer V pyramidal neurons in the PFC that express D2Rs

Initially, we studied whether D2Rs are selectively expressed in previously identified subpopulations of layer V pyramidal neurons. Previous studies have classified layer V pyramidal neurons from somatosensory or frontal cortex based on projection targeting or apical tuft morphology, and found that these characteristics are strongly correlated (Morishima and Kawaguchi, 2006; Hattox and Nelson, 2007). Specifically, layer V pyramidal neurons that project to the thalamus or brainstem have apical dendrites with wider arborizations, thicker shafts, and a greater number of primary branches, than do apical dendrites originating from layer V pyramidal neurons that project to contralateral cortex and/or striatum. This suggests that layer V pyramidal neurons in neocortex can be divided into at least two subpopulations, “thick-tufted” neurons that project to thalamus or brainstem, and “thin-tufted” neurons that project to striatum or contralateral cortex. Notably, excitatory and inhibitory connectivity differs between these subpopulations (Wang et al., 2006; Otsuka and Kawaguchi, 2008; Brown and Hestrin, 2009). A recent study found that in prefrontal layer V pyramidal neurons that project to contralateral cortex (CC) or brainstem, levels of the hyperpolarization-activated cyclic nucleotide gated cation h-current (I_h) are low or high, respectively (Dembrow et al., 2010). An analogous relationship holds in motor cortex (Sheets et al., 2011).

Given these previous findings, we first sought to confirm that we could use h-current to classify neurons that have different projection targeting. If prefrontal corticothalamic (CT) and corticopontine neurons have similar properties, since they are both thick-tufted, then the level of h-current in CT neurons should be greater than that in CC neurons. Indeed, we found that h-current could be used to reliably distinguish CT and CC neurons in layer V of medial PFC (Fig. 1A-D). To identify CT or CC neurons, we injected retrogradely transported fluorescently labeled latex microspheres (Retrobeads; Lumafluor) into the ipsilateral medial dorsal thalamus or the contralateral PFC. As illustrated in Fig. 1A, CT and CC neurons were distinct populations. We made whole cell patch-clamp recordings from identified CT or CC neurons in layer V of the medial PFC (mPFC). Although CT and CC neurons had similar resting membrane potentials and input resistances (Fig. 1D), they had significantly different levels of h-current (measured as the sum of the voltage sag and rebound depolarization in response to a hyperpolarizing current pulse) (Fig. 1B,C; $p < 0.01$; $n = 18$ and 8 CT and CC neurons, respectively). In fact, the distributions of h-current from CT and CC neurons were completely nonoverlapping (Fig. 1C).

Thus, we could define a threshold level of h-current that would unambiguously separate CT and CC neurons. We refer to layer V pyramidal neurons above this threshold as “type A”neurons, and those below this threshold as “type B neurons.” Based on the studies outlined above, we would predict that type A neurons (more h-current) would be thick-tufted whereas type B neurons

(minimal h-current) should be thin-tufted. Indeed, after filling layer V pyramidal neurons in mPFC with biocytin and visualizing them via confocal microscopy (Fig. 2A), we found that type A neurons (n = 4) had a greater number of primary branches ($p < 0.05$) and wider apical shafts ($p < 0.05$) than type B neurons (n = 4) (Fig. 2B). Thus, consistent with previous studies, the level of h-current differentiates two subpopulations of layer V pyramidal neurons that project to different targets and have different apical tuft morphologies.

Next, we asked whether D2Rs are selectively expressed within these two subpopulations of layer V pyramidal neurons in the PFC. To answer this question, we recorded from visually identified neurons expressing fluorescent proteins under control of promoters for D1Rs or D2Rs (Fig. 3A). Specifically, we recorded from fluorescent neurons in Drd1::EGFP transgenic mice (n = 4) (line S118), Drd1::Cre transgenic mice (line EY262) injected with virus containing a Cre-dependent construct for ChR2-EYFP (Sohal et al., 2009) (n = 6), Drd2::EGFP transgenic mice (n = 7), or Drd2::Cre transgenic mice (line ER44) injected with adeno-associated virus (AAV) containing a Cre-dependent construct for ChR2-YFP (n = 7). These transgenic mice have been widely used to study D1R and D2R-expressing neurons in the striatum (Gong et al., 2003; Lobo et al., 2006; Kravitz et al., 2010), and this AAV drives EYFP expression that is highly specific for Cre-expressing neurons (Sohal et al., 2009). We found that all of the presumed D2R-expressing neurons (fluorescent neurons from Drd2::EGFP or Drd2::Cre mice) were “type A”, i.e. had a level of h-current current above the

threshold that separates CT and CC neurons, whereas presumed D1R-expressing neurons included both type A and type B neurons (Fig. 3B).
Of course, other subpopulations of layer V pyramidal neurons might also express D2Rs, but not be labeled by either transgenic line we used. We identified D2R-expressing neurons using two distinct transgenic lines in order to minimize this possibility. The following experiments provide additional confirmation for our finding that D2R expression is restricted to a specific subpopulation of layer V neurons, by showing that activating D2Rs elicits a novel cellular effect that is also restricted to this same subpopulation.

Synaptic activity unmasks a quinpirole-induced afterdepolarization in Type A neurons

We measured effects of D2R activation in type A and B neurons, and surprisingly, at baseline, the D2R agonist quinpirole had minimal effects on the responses of type A neurons to depolarizing current pulses (300-400 pA, 250-500 msec; left panels of Fig. 4B-D). However, when these current pulses were preceded by optogenetic stimulation of excitatory synapses in layer V, quinpirole dramatically altered the responses of these neurons to depolarizing current. Specifically, under these conditions, quinpirole (5-20 μM) elicited a prominent afterdepolarization in 12/12 type A neurons (middle and right panels of Fig. 4C; Fig. 4E,F). This afterdepolarization could generate spikes and extend for up to several seconds after the end of the current pulse (Fig. 4F). In addition to this afterdepolarization, quinpirole caused a progressive decrease in spike height

during the current pulse (Fig. 4C-F). Despite eliciting this dramatic afterdepolarization, both 5 μM (-)quinpirole and 20 μM (±)quinpirole had minimal effects on the resting membrane potential (5 μM: control V_{rest} = -61.7 ± 1.4 mV, quinpirole V_{rest} = -60.8 ± 1.5 mV; p = 0.32, n = 8; 20 μM: control V_{rest} = -62.3 ± 1.8 mV, quinpirole V_{rest} = -60.9 ± 1.5 mV; p = 0.42, n = 5). For these experiments, we expressed ChR2 in pyramidal neurons in the contralateral mPFC using viral injection (Fig. 4A; Methods). We then recorded from type A neurons that did not express ChR2 while stimulating ChR2-positive corticocortical fibers with trains of randomly occurring light flashes (470 nm; 2.5 msec duration; intensity: ~2 mW; rate: 5-50 Hz; train duration: 2.5 sec; 5 trains were delivered with an intertrain interval of 13 sec). As illustrated in Fig. 4, this led to relatively weak synaptic input that usually evoked zero or only a few spikes in the postsynaptic neuron.

We quantified the quinpirole-induced afterdepolarization by measuring the time for the membrane potential to decay back to within 90% of the baseline membrane potential following a depolarizing current pulse (Fig. 4G). To confirm that D2Rs mediate the quinpirole-induced afterdepolarization, we used the selective D2R antagonist (-)sulpiride. Many studies have used sulpiride at doses up to 10 μM to confirm that various phenomena are mediated by D2Rs (Kreitzer and Malenka, 2005; Ramanathan et al., 2008; Ding et al., 2010). Indeed, we found that 5 μM (-)sulpiride eliminated the quinpirole-induced afterdepolarization in 4/4 cells (Fig. 4G). This dose is ~10-fold less than the K_i for (-)sulpiride binding to D1Rs in expression systems (Seeman and Van Tol, 1994), and should

thus be highly selective for D2Rs in brain slices. The quinpirole-induced depolarization could be reversed in other ways as well: by addition of the NMDA-R antagonist AP5 (50 μM; n = 3/3 cells; Fig. 4C,G); by addition of the selective L-type Ca^{2+} channel antagonist nimodipine (1 μM; n= 3/3 cells; Fig. 4C,G). Furthermore, as shown in Fig. 4G, the duration of the quinpirole-induced afterdepolarization was larger for 20 μM (±)quinpirole (n=6) than for 5 μM (-) quinpirole (n=7), although this difference did not reach statistical significance.

Many studies have activated D2Rs using 10 μM quinpirole (Wang and Goldman-Rakic, 2004; Kreitzer and Malenka, 2005; Ramanathan et al., 2008; Sidiropoulou et al., 2009), similar to the doses we have used (5 or 20 μM). Nevertheless, these doses are higher than those used in other studies of PFC, e.g. 1-2 μM (Tseng and O'Donnell, 2007; Tseng et al., 2008). We will address possible reasons for these discrepancies in the Discussion, although we remain confident that D2Rs are required for the quinpirole-induced afterdepolarization because this phenomenon (1) can be elicited by moderate doses of quinpirole (5 μM), (2) occurs selectively in D2R-expressing neurons, and (3) is blocked by the specific D2R antagonist sulpiride (5 μM). Of course, we cannot rule out the possibility that in addition to D2Rs, other receptors also play a role. Since we obtained the most prominent afterdepolarization using 20 μM (±)quinpirole, we used this dose for subsequent experiments. As described below, all of the effects we observed using 20 μM (±)quinpirole were reversed by (-)sulpiride (5 μM), confirming that they require D2Rs.

Activating NMDA receptors also unmasks the quinpirole-induced afterdepolarization

Given that AP5 blocks the ability of synaptic stimulation to unmask the quinpirole-induced afterdepolarization, we tested whether modest levels of NMDA receptor activation might suffice to unmask this effect. Indeed, we observed the quinpirole-induced afterdepolarization when we included a low concentration of NMDA (4 μM) in the bath (Fig. 5A,B; n=4). Notably, the afterdepolarization was not induced by this concentration of NMDA alone, and was reversed by (-)sulpiride (5 μM; Fig. 5A,B; n=4). Fig. 5B quantifies and summarizes these effects. The concentration of NMDA we used is within the range used by previous studies to elicit network activity in prefrontal brain slices (3-8 μM) (Tseng and O'Donnell, 2005; Stewart and Plenz, 2006).

The quinpirole-induced afterdepolarization is absent from Type B neurons

We also applied (±)quinpirole (20 μM) to type B neurons (n=7), and measured their responses to depolarizing current pulses (350 pA, 250 msec). As in the experiments with type A neurons, depolarizing current pulses either occurred immediately following optogenetic stimulation of excitatory synapses in layer V (n=3), or with 4 μM NMDA in the bath (n=4). None of these experiments elicited a quinpirole-induced afterdepolarization in type B neurons. This is quantified in Fig. 5B, which shows how various conditions affect the time for the

membrane potential to return to baseline following a depolarizing current pulse in type B neurons.

The quinpirole-induced afterdepolarization occurs in perforated-patch recordings

To rule out the possibility that the afterdepolarization only occurs after dialyzing neurons with our intracellular solution, we verified that we could observe this effect during gramicidin perforated-patch recordings (Methods). Indeed, during perforated-patch recordings from type A neurons, co-application of (±)quinpirole (20 μM) and NMDA (6 μM) elicited an afterdepolarization that was reversed by adding the D2R antagonist (-)sulpiride (5 μM) (Fig. 6A,C; n=5). Two additional details of this experiment were notable. First, in this experiment, we identified type A neurons by injecting retrobeads into MD thalamus to label CT neurons. 5/5 labeled CT neurons exhibited the quinpirole-induced afterdepolarization, providing additional evidence that CT neurons express D2Rs. Second, although we monitored the bridge balance for sudden changes indicative of a shift from a perforated-patch to whole cell recording (compare top 3 vs. bottom panels of Fig. 6A), in some cases we also included fluorescent dye in the pipette (0.05% Lucifer Yellow; n=2). As shown in Fig. 6B, this fluorescent dye was excluded from the neuron while in the perforated-patch configuration (top image), but entered the neuron after breaking in and shifting to a whole cell configuration (bottom image).

Quinpirole prolongs Ca^{2+}-mediated plateau potentials

We next sought to characterize the ion channels that contribute to the quinpirole-induced afterdepolarization. Similar afterdepolarizations have been observed in response to 5-HT in turtle motoneurons (Hounsgaard and Kiehn, 1989), in response to D1R stimulation and/or synaptic stimulation in striatal projection neurons (Hernandez-Lopez et al., 1997; Vergara et al., 2003), in frog olfactory bulb neurons (Hall and Delaney, 2002), and in nigral GABAergic neurons (Lee and Tepper, 2007). Notably, these other afterdepolarizations also caused spike height rundown very similar to what we observed with quinpirole (e.g. Fig. 4-6). Each of these other afterdepolarizations were generated by combinations of Ca^{2+} influx via L-type Ca^{2+} channels and/or NMDA receptors (NMDA-Rs), and the Ca^{2+}-activated nonselective cationic conductance (I_{CAN}). Our experiments suggest that a similar mechanism mediates the quinpirole-induced afterdepolarization, since it can be eliminated by antagonizing either L-type Ca^{2+} channels or NMDA-Rs.

An ideal experiment would be to measure how quinpirole affects L-type Ca^{2+} currents. However, none of these previous studies of similar afterdepolarizations measured L-type Ca^{2+} currents directly (Hounsgaard and Kiehn, 1989; Hernandez-Lopez et al., 1997; Hall and Delaney, 2002; Vergara et al., 2003; Lee and Tepper, 2007), because poor space clamp make it notoriously difficult to isolate and measure regenerative voltage-dependent currents in intact pyramidal neurons. In fact, attempting to do so can lead to spurious results (Maurice et al.,

2001). Measuring Ca^{2+} currents associated with the quinpirole-induced afterdepolarization would be particularly difficult because, as is the case for other afterdepolarizations (Vergara et al., 2003), the quinpirole-induced afterdepolarization likely originates in the distal dendrites, where D2Rs are located (Negyessy and Goldman-Rakic, 2005). Indeed, we attempted to directly measure the effects of quinpirole on voltage-dependent Ca^{2+} currents, but these recordings suffered from poor space clamp. Similarly, it is extremely challenging to directly measure Ca^{2+}-dependent currents such as I_{CAN}, because the intracellular Ca^{2+} concentration varies during current clamp or voltage clamp recordings. Because of these issues, numerous studies indirectly measured these Ca^{2+} and Ca^{2+}-dependent currents by studying plateau potentials which occur after blocking voltage-dependent Na^{+} and/or K^{+} currents (Forscher and Oxford, 1985; Hounsgaard and Kiehn, 1989; Hernandez-Lopez et al., 1997; Young and Yang, 2004; Lee and Tepper, 2007).

We followed this well-established approach and confirmed that quinpirole enhances Ca^{2+} and/or Ca^{2+}-dependent currents that produce the quinpirole-induced afterdepolarization, by recordeding plateau potentials that occur after application of TTX (0.5 μM) and TEA (30 mM) to block Na^{+} and K^{+} currents (Fig. 7A; Methods). In these experiments, a brief, strong depolarizing current pulse (300 pA, 100 msec) triggers a high-threshold Ca^{2+} spike that is followed by a long plateau potential. These plateau potentials last several seconds. As a result, although they may contribute to the initial Ca^{2+} spike, T-type Ca^{2+} channels will

be inactivated during the plateau potential. Furthermore, a previous study of layer V-VI pyramidal neurons in PFC found that under these conditions, evoked Ca^{2+} spikes are driven primarily by L-type Ca^{2+} channels (Young and Yang, 2004). Based on our earlier experiments, we recorded these plateau potentials in the presence of 4 μM NMDA. Thus, these plateau potentials are driven primarily by a combination of L-type Ca^{2+} currents, NMDA-R mediated currents, and Ca^{2+}-dependent currents such as the Ca^{2+}-activated nonselective cationic current, I_{CAN}. Other slowly or non-inactivating high-threshold Ca^{2+} currents, e.g. N-type, may also contribute, but likely play a much smaller role (Young and Yang, 2004). We observed a clear increase in these plateau potentials after applying (±)quinpirole (20 μM) for 20 min (Fig. 7B,C). This effect was partially reversed by adding (-)sulpiride (5 μM) for 20 min (Fig. 7B,C; n = 4 cells; $p < 0.001$ control vs. quinpirole, $p < 0.05$ quinpirole vs. quinpirole + sulpiride by repeated measures ANOVA using cell and condition as factors and after correcting for multiple comparisons). There was usually a slight increase in the plateau potential over time, so we also measured the size of the plateau potential in control ACSF after 20 min (corresponding to the time of quinpirole application) and 40 min (corresponding to the time of sulpiride application). The increase in the size of the plateau potential was much larger in cells for which we applied quinpirole (n = 4), compared to cells maintained in control ACSF (n = 4) ($p < 0.001$ by ANOVA using cell and condition as factors and after correcting for multiple comparisons). Thus, although it was not possible to directly measure L-type Ca^{2+} currents or Ca^{2+}-dependent currents, we did confirm that quinpirole enhances Ca^{2+} and/or

Ca^{2+}-dependent currents that produce plateau potentials when Na^+ and K^+ channels are blocked. This, together with our experiments using nimodipine, NMDA, and AP5, strongly suggest that like other similar afterdepolarizations, the quinpirole-induced depolarization is mediated by a combination of Ca^{2+} currents mediated by L-type channels and NMDA-Rs, as well as depolarizing Ca^{2+}-dependent currents, e.g. I_{CAN}.

Intracellular BAPTA eliminates the quinpirole-induced afterdepolarization

The experiments described above leave open whether the quinpirole-induced afterdepolarization results simply from Ca^{2+} currents themselves, or whether the activation of Ca^{2+}-dependent currents, e.g. I_{CAN}, is also required. To provide additional evidence that Ca^{2+} influx is specifically required for the quinpirole-induced afterdepolarization, we tested whether the afterdepolarization is blocked by the Ca^{2+} chelator BAPTA, which blocks or attenuates downstream effects of Ca^{2+} but not Ca^{2+} currents themselves. We made perforated patch recordings and included BAPTA (5 mM) in the intracellular solution. As in previous experiments, we made perforated patch recordings from type A neurons, and observed an afterdepolarization after applying quinpirole and NMDA (Fig. 8A). However, immediately after breaking in and switching to a whole-cell recording configuration, the afterdepolarization and other effects of quinpirole (e.g. decreasing spike heights) disappeared (Fig 8A,B; n = 3/3 cells). In 5 other neurons, we broke in and switched to a whole-cell configuration (with BAPTA in the pipette) while applying quinpirole. In all of these cases, BAPTA prevented quinpirole from inducing an afterdepolarization (Fig. 8B). Note that the

intracellular solution we used in previous experiments contained another Ca2+ chelator – EGTA. However, it is known that BAPTA but not EGTA prevents Ca^{2+} from activating I_{CAN} (Forscher and Oxford, 1985; Hall and Delaney, 2002). In particular, the fact that BAPTA, but not EGTA, blocks the quinpirole-induced afterdepolarization suggests that this phenomenon depends on I_{CAN} (which is blocked by BAPTA but not EGTA) but not intracellular Ca^{2+} acting as a second messenger (which would be blocked equally well by EGTA and BAPTA) (Forscher and Oxford, 1985).

Blocking SK channels can also unmask a quinpirole-induced afterdepolarization

A previous study of thick-tufted layer V pyramidal neurons in the mPFC (Wang and Goldman-Rakic, 2004) found that D2R activation reduces the threshold for bursts evoked by synaptic stimulation in the presence of bicuculline and AP5. This study focused on synaptically evoked bursts lasting ~ 50 msec instead of afterdepolarizations lasting for hundreds of msec or seconds, and the results of that study were obtained under conditions of $GABA_A$ and NMDA receptor blockade. Moreover, that study left open whether D2R-mediated increases in synaptically-evoked bursting result from pre- or post-synaptic effects. Nevertheless, that study, like ours, suggests that D2Rs can enhance the excitability of thick-tufted layer V pyramidal neurons in the mPFC. Thus, the increased bursting observed in that study may result from the same mechanisms which we have found produce the quinpirole-induced afterdepolarization. If this

is true, application of bicuculline and AP5 may suffice to unmask the quinpirole-induced afterdepolarization, even in the absence of synaptic stimulation. Indeed, after applying (±)quinpirole (20 μM), bicuculline (10 μM), and AP5 (50 μM), we observed an afterdepolarization in type A neurons very similar to the quinpirole-induced afterdepolarization seen in previous experiments (Fig. 9A,C; n = 3/3 neurons). Moreover, this afterdepolarization was blocked by nimodipine (1 μM; n = 3 cells). Thus, even when NMDA-Rs are blocked, quinpirole can still elicit an afterdepolarization, and this afterdepolarization depends on L-type Ca^{2+} channels. This suggests that L-type Ca^{2+} channels play a major role in quinpirole-induced afterdepolarizations, whereas NMDA-Rs may facilitate this afterdepolarization, but are not required under all conditions.

In addition to blocking $GABA_A$ receptors, bicuculline also blocks SK-type Ca^{2+} dependent K^+ channels (Johnson and Seutin, 1997; Debarbieux et al., 1998). Therefore, we tested whether the afterdepolarization observed in type A neurons after applying quinpirole, bicuculline, and AP5, depends on the blockade of $GABA_A$ receptors and/or SK channels. We found that co-application of quinpirole and the $GABA_A$ antagonist gabazine (10 μM) did not elicit an afterdepolarization (Fig. 9C; n = 3 cells), whereas co-application of quinpirole and the selective SK channel antagonist apamin (10 μM) did elicit an afterdepolarization in type A neurons (Fig. 9B,C; n = 3 cells). These results suggest that (1) the mechanism of the quinpirole-induced afterdepolarization may be relevant to the effects of D2Rs on synaptically evoked bursting observed in a

previous study, (2) SK channel blockade can unmask quinpirole-induced afterdepolarizations in the absence of synaptic stimulation, and (3) like the quinpirole-induced afterdepolarization which occurs in the presence of synaptic stimulation, the mechanism through which quinpirole increases type A neuron excitability when bicuculline is present also depends on L-type Ca^{2+} channels.

DISCUSSION

We have characterized a novel afterdepolarization elicited by D2Rs in the mPFC. This afterdepolarization depends on L-type Ca^{2+} channels and NMDA-Rs. The afterdepolarization and D2R expression both occur within a specific subpopulation of layer V pyramidal neurons that have a characteristic morphology (thick-tufted), projection targets (thalamus), and electrophysiological signature (prominent h-current). This suggests that as in striatum, prefrontal D2Rs are restricted to specific cell populations.

As described below, the quinpirole-induced afterdepolarization may underlie numerous functional and pathological effects of prefrontal D2Rs including enhancing firing during memory-guided saccades (Wang et al., 2004), generating persistent reward-related firing (Histed et al., 2009; Bernacchia et al., 2011), or increasing the variability of activity (Winterer and Weinberger, 2004; Durstewitz and Seamans, 2008). In addition, this afterdepolarization may alter prefrontal output to structures including the mediodorsal thalamus, which is important for processes such as corollary discharge (Sommer and Wurtz, 2006). Notably, the quinpirole-induced afterdepolarization may represent a mechanism for the long-standing observation that dopamine application to frontal cortical neurons *in vivo* produces a depolarization accompanied by reduced spike heights (Bernardi et al., 1982).

The dose-dependence of the quinpirole-induced afterdepolarization

Many studies have activated D2Rs using 10 μM quinpirole (Wang and Goldman-Rakic, 2004; Kreitzer and Malenka, 2005; Ramanathan et al., 2008; Sidiropoulou et al., 2009), similar to the doses used here (5 or 20 μM). In particular, Sidiropoulou et al. applied 10 μM quinpirole to layer V pyramidal neurons in PFC without activating D1Rs. Thus, we are confident that the quinpirole-induced afterdepolarization requires D2Rs, given that it selectively occurs in D2R-expressing neurons, can be elicited by 5 μM quinpirole, and is eliminated by 5 μM (-)sulpiride, which selectively antagonizes D2Rs (Seeman and Van Tol, 1994).

So why is this afterdepolarization most prominent using 20 μM quinpirole, whereas other studies have found distinct effects of quinpirole at lower doses, e.g. 1-2 μM (Tseng and O'Donnell, 2004; Tseng et al., 2008)? D2Rs couple to numerous signaling pathways, mediated by G_{bg}, b-arrestins, and scaffolding proteins (Bonci and Hopf, 2005). D2R ligands possess functional selectivity for these pathways (Mailman, 2007), and the dose-dependence of quinpirole likely varies across these pathways (Urban et al., 2007). Notably, effects mediated by b-arrestin have a timecourse ~10 min (Ahn et al., 2004), similar to what we observed. Thus, although quinpirole may bind D2Rs at concentrations <1 μM, concentrations ~1-2 μM might recruit certain signaling pathways, while concentrations ~5-20 μM elicit distinct effects. The latter effects may reflect non-canonical signaling mediated by scaffolding proteins or receptor internalization, and it will be important for future studies to elucidate these pathways.

Why haven't previous studies observed the quinpirole-induced afterdepolarization?

The quinpirole-induced afterdepolarization is masked in quiescent slices, and could be unmasked via physiologic levels of synaptic stimulation or NMDA application (4-6 μM). This makes sense since most D2Rs on layer V pyramidal neurons in the PFC are located on distal dendrites (Negyessy and Goldman-Rakic, 2005). Thus, somatic current injection might not reveal D2R effects until dendritic excitability has been sufficiently enhanced by synaptic stimulation or NMDA. Indeed, while dopamine receptor effects have been extensively studied (Seamans and Yang, 2004), stimulating synaptic inputs using optogenetics might produce a more physiological state, thereby revealing phenomena as illustrated here.

Other studies have described other effects of quinpirole on layer V pyramidal neurons. In particular, lower doses of quinpirole inhibit increases in pyramidal neuron excitability caused by AMPA or NMDA (Tseng and O'Donnell, 2004). The effects of quinpirole on responses to NMDA were mediated by D2R activation in presynaptic inhibitory interneurons, rather than direct effects of D2Rs on pyramidal neurons. It is unclear whether this effect occurs under the same conditions or in the same layer V pyramidal neurons as the quinpirole-induced afterdepolarization, but this could be an important mechanism for regulating activity driven by the quinpirole-induced afterdepolarization. Indeed,

inhibition might normally suppress this afterdepolarization, but pathological afterdepolarizations may emerge when prefrontal inhibition is compromised in schizophrenia or other conditions (Lewis et al., 2005).

Another study (Wang and Goldman-Rakic, 2004) found that doses of quinpirole similar to those used here (10 μM) promote bursting by thick-tufted layer V neurons in response to synaptic input when bicuculline and AP5 are present. We found that co-applying quinpirole, bicuculline, and AP5 also elicits an afterdepolarization that is blocked by nimodipine. Thus, the mechanism of the quinpirole-induced afterdepolarization may also underlie D2R-induced increases in bursting observed in that study.

The quinpirole-induced afterdepolarization depends on L-type Ca^{2+} channels and NMDA-Rs.

We have shown that (1) D2R activation enhances plateau potentials mediated by Ca^{2+} and Ca^{2+}-dependent currents, (2) the quinpirole-induced afterdepolarization involves both L-type channels and NMDA-Rs, and (3) chelating intracellular Ca^{2+} blocks the afterdepolarization. Thus, although D2Rs must enhance Ca^{2+} currents and/or Ca^{2+} dependent currents underlying the quinpirole-induced afterdepolarization, we cannot pinpoint the exact location of D2R action. Specifically, D2Rs might directly or indirectly enhance L-type currents, the accumulation of intracellular Ca^{2+}, and/or I_{CAN}. Our finding that in the presence of bicuculline, quinpirole-induced afterdepolarizations occur even

after NMDA-Rs are blocked, suggests that NMDA-Rs facilitate, but are not absolutely necessary for these afterdepolarizations. Thus, D2Rs are unlikely to elicit afterdepolarizations via direct actions on NMDA receptor-mediated currents. Of note, a previous study found that D1Rs in layer V pyramidal neurons in PFC can suppress L-type Ca^{2+} channel mediated potentials (Young and Yang, 2004). Since D1Rs and D2Rs often have opposing effects on overlapping signaling pathways, this suggests that D2Rs may enhance L-type Ca^{2+} channel mediated phenomena, contributing to the quinpirole-induced afterdepolarization we have found.

L-type Ca^{2+} channels and NMDA-Rs produce other afterdepolarizations similar to what we have found (Hounsgaard and Kiehn, 1989; Hernandez-Lopez et al., 1997; Hall and Delaney, 2002; Vergara et al., 2003; Lee and Tepper, 2007). Specifically, muscarinic receptors elicit similar afterdepolarizations in layer V of PFC (Haj-Dahmane and Andrade, 1998, 1999). Many of these afterdepolarizations also cause spike height rundown. Synergistic interactions between L-type Ca^{2+} channels and NMDA-Rs also produce regenerative depolarizations in pyramidal neuron dendrites (Schiller et al., 2000; Branco and Hausser, 2011). D2R activation could further amplify these interactions between NMDA-R mediated currents and L-type Ca^{2+} currents, by enhancing one or both currents, and/or the recruitment of I_{CAN}. In this way, D2R activation could profoundly enhance synaptic integration (Branco and Hausser, 2011).

L-type Ca^{2+} channels in PFC function and mental illness

L-type Ca^{2+} channels have been implicated in schizophrenia by genome-wide association (Nyegaard et al., 2010; Ripke et al., 2011) and other studies (Green et al., 2009; Bigos et al., 2010). A genetic polymorphism that increases L-type Ca^{2+} channel expression and schizophrenia risk also reduces prefrontal efficiency (Bigos et al., 2010), and L-type Ca^{2+} channel antagonists have shown promise for schizophrenia (Yamada et al., 1995; Yamada et al., 1996; Schwartz et al., 1997). L-type Ca^{2+} channels are also implicated in autism (Splawski et al., 2004) and bipolar disorder (Ferreira et al., 2008; Sklar et al., 2011). Despite this data, specific mechanisms by which L-type Ca^{2+} channels modulate prefrontal function are lacking. Our results demonstrate an afterdepolarization through which L-type Ca^{2+} channels powerfully modulate prefrontal neurons. This may have consequences as described below.

The quinpirole-induced afterdepolarization in PFC function and mental illness

On a circuit level, layer V neurons exhibiting the quinpirole-induced afterdepolarization are well poised to affect the cognitive domains disrupted in schizophrenia. As we have shown, layer V pyramidal neurons that express D2Rs and exhibit the quinpirole-induced afterdepolarization correspond to a subpopulation (“type A”) that projects subcortically, e.g. to thalamus, but not to contralateral PFC. In particular, our finding that D2Rs are restricted to type A neurons while D1Rs are expressed in type B neurons (which project to other

cortical regions) as well, could explain the recent observation that blocking D1Rs in the frontal eyes fields modulates firing in visual cortex and brainstem, whereas activating D2Rs modulates activity in brainstem but not visual cortex (Noudoost and Moore, 2011). D2Rs might specifically enhance spiking in prefrontal neurons that trigger motor responses or corollary discharges (Robbins, 1990; Frith, 1995; Wang et al., 2004; Wang, 2004) – processes that are believed to depend on D2Rs and be abnormal in schizophrenia.

The quinpirole-induced afterdepolarization may also contribute to persistent reward related activity or the modulation of neural activity by the past history of reward (Histed et al., 2009; Bernacchia et al., 2011). Although the timescales of reward-related persistent activity or modulation may exceed those shown for the quinpirole-induced afterdepolarization, we have shown that synaptic input interacts powerfully with the afterdepolarization. Thus, *in vivo* the quinpirole-induced afterdepolarization may amplify responses to weak synaptic input, producing additional firing and Ca^{2+} influx that sustain this afterdepolarization over longer timescales.

Finally, the quinpirole-induced afterdepolarization might increase the variability of PFC activity, facilitating adaptation to a changing environment (Durstewitz and Seamans, 2008; Durstewitz et al., 2010). Excessive D2R activation could produce noisy firing that is disconnected from external input and contributes to psychosis.

In summary, these findings define a novel mechanism, involving Ca^{2+} channels, through which D2Rs can powerfully regulate output from a defined subpopulation of prefrontal neurons. This mechanism is well positioned to modulate prefrontal-dependent behaviors, including those disrupted in mental illness.

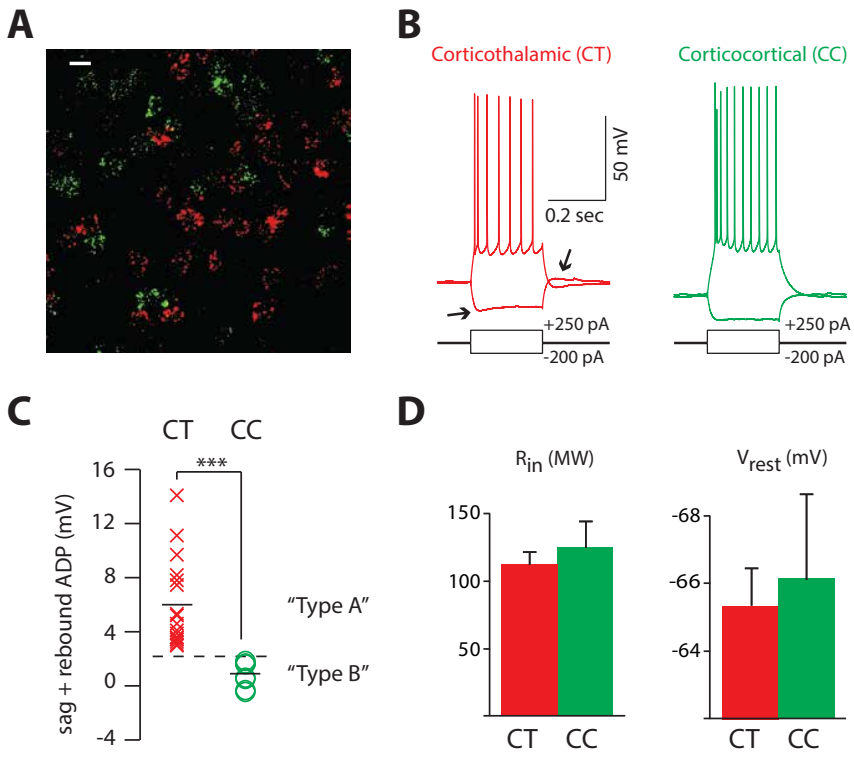

FIGURE 1. H-current distinguishes two populations of layer V pyramidal neurons that differ in their projection targets. (A) High power confocal image of layer V of mPFC showing the distribution of fluorescently labeled retrogradely transported microspheres within individual neurons. Microspheres were injected into MD thalamus (red) or the contralateral PFC (green). Bar = 10 mm. **(B)** Sample recordings from corticothalamic (CT) or corticocortical (CC) pyramidal neurons identified using retogradely transported microspheres showing responses to hyperpolarizing or depolarizing current injection. Note the voltage sag and rebound afterdepolarization in response to hyperpolarizing current injection that is visible in the CT neuron but not the CC neuron (arrows). **(C)** The amount of h-current, measured as the sum of the voltage sag and rebound afterdepolarization in response to hyperpolarizing

current pulses, in CT (n = 18) and CC neurons (n = 8). Thick horizontal bars indicate the means of each distribution, and the dotted line indicates a threshold that unambiguously separates the two nonoverlapping distributions. **(D)** Input resistances (R_{in}) and resting membrane potentials (V_{rest}) for CT and CC neurons.

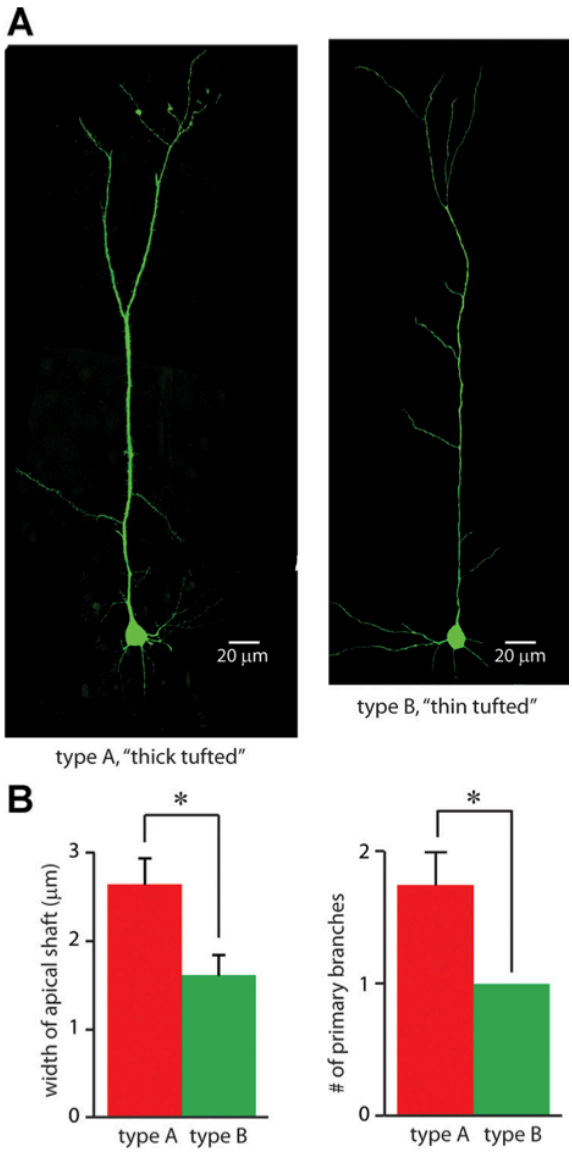

FIGURE 2. Type A and B pyramidal neurons have different morphologies. **(A)** Confocal images of representative neurons in which the amount of h-current falls either above ("type A," left image) or below ("type B," right image) the threshold in panel C. (B) Type A and B neurons differ in the widths of the shafts of their apical dendrites (left) and in the number of primary branches of their apical dendrites (right) (n = 4 neurons in each group).

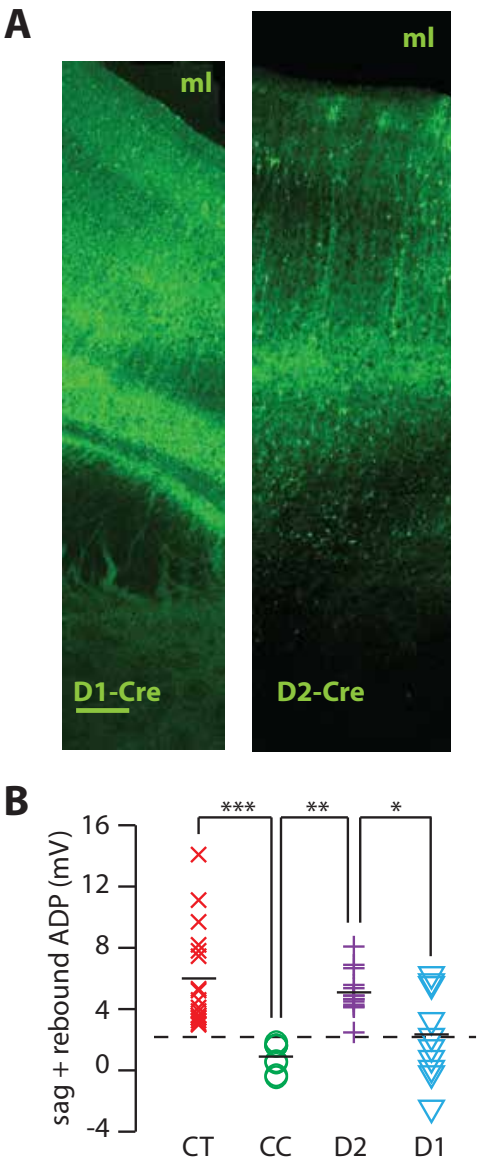

FIGURE 3. D2Rs are selectively expressed in Type A pyramidal neurons which can be distinguished using the h-current. (A) Low-power confocal images of infralimbic cortex showing the pattern of fluorescence in Drd1-Cre (D1-Cre) and Drd2-Cre (D2-Cre) transgenic mice injected with virus to drive Cre-dependent expression of ChR2-YFP. The corpus callosum and midline lie below and above both images, respectively. *ml*, midline. Bar = 0.1 mm (both images

are to the same scale). **(B)** The amount of h-current (measured as above) in identified corticothalamic (CT, n = 18), corticocortical (CC, n = 8), D2R expressing (D2, n = 14), or D1R expressing (D1, n = 10) pyramidal neurons in layer V of mPFC. The dotted line indicates the threshold that separates the distributions of h-current from CT and CC neurons. * = $p < 0.05$, ** = $p < 0.01$.

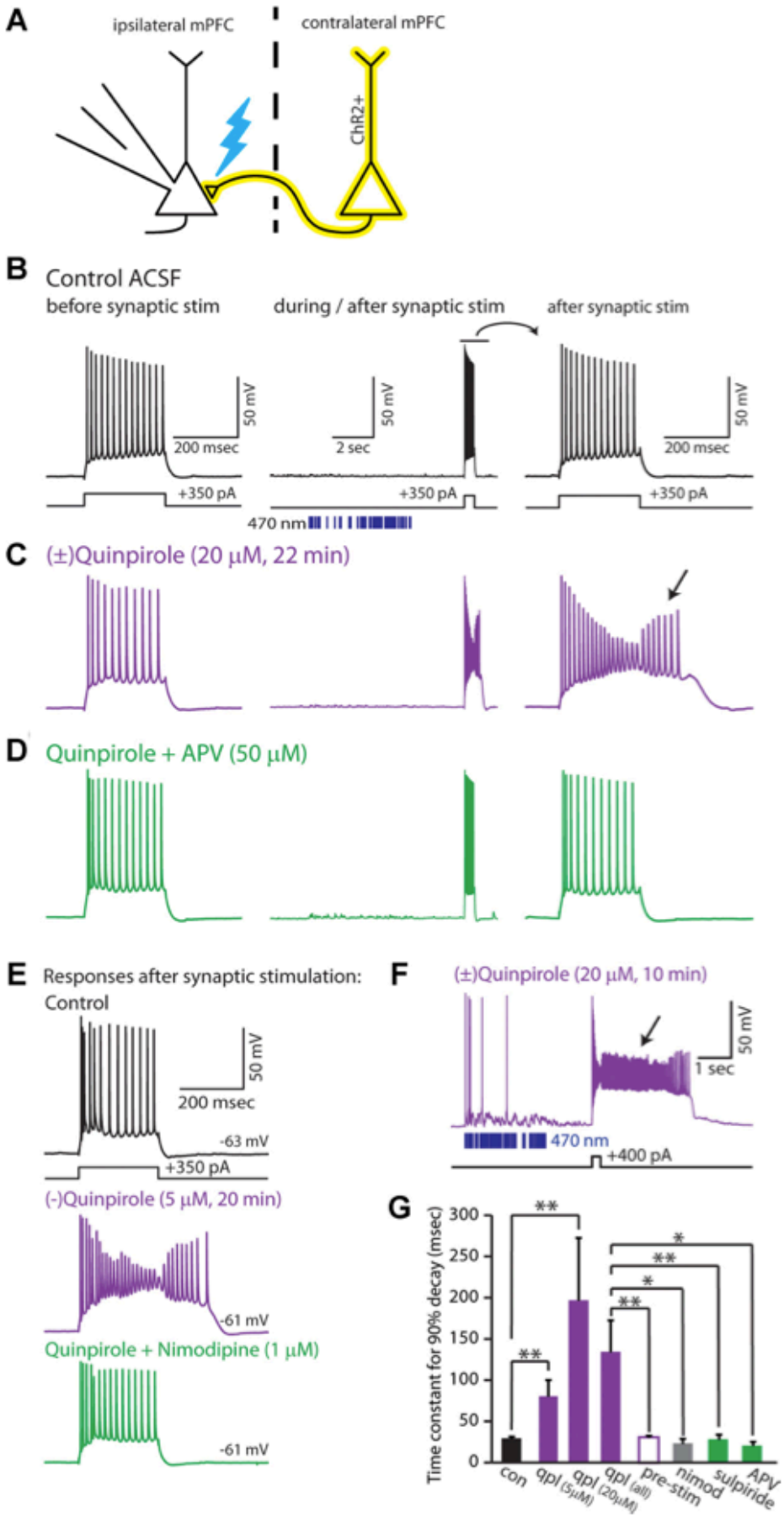
A
ipsilateral mPFC
contralateral mPFC
ChR2+
B
Control ACSF
before synaptic stim
during / after synaptic stim
after synaptic stim
50 mV
200 msec
2 sec
+350 pA
470 nm
C
(±)Quinpirole (20 μM, 22 min)
D
Quinpirole + APV (50 μM)
E
Responses after synaptic stimulation:
Control
-63 mV
(-)Quinpirole (5 μM, 20 min)
-61 mV
Quinpirole + Nimodipine (1 μM)
-61 mV
F
(±)Quinpirole (20 μM, 10 min)
1 sec
470 nm
+400 pA
G
Time constant for 90% decay (msec)
300
250
200
150
100
50
0
con
qpl (5μM)
qpl (20μM)
qpl (all)
pre-stim
nimod
sulpiride
APV

FIGURE 4. Synaptic stimulation unmakes a novel D2R-mediated afterdepolarization in specific layer V pyramidal neurons. (A) Experimental design: We recorded from ChR2 negative layer V neurons while stimulating ChR2 positive axons from the contralateral mPFC with trains of light flashes (470 nm, 2.5 msec, ~2 mW). **(B)** Responses of a type A layer V pyramidal neuron to current injection before (left panel) and immediately following (middle and right panels) optogenetic stimulation of synaptic inputs. Blue bars indicate the times of light flashes. **(C)** Prior to synaptic stimulation, no quinpirole-induced afterdepolarization is observed, however the same current injection elicits a marked afterdepolarization (along with spike height rundown) following weak synaptic stimulation. **(D)** The quinpirole-induced afterdepolarization is eliminated by the addition of AP5. **(E)** Lower doses of quinpirole (5 μM) also induce an afterdepolarization following synaptic stimulation, which can be blocked by nimodipine (1 μM). **(F)** Recording from a type A neuron showing a prolonged quinpirole-induced afterdepolarization following synaptic stimulation. **(G)** Average time constants for the membrane potential to return to baseline following a depolarizing current pulse (300-400 pA, 250-500 msec) delivered immediately following the pattern of synaptic stimulation shown above. Data is shown for control conditions (black; n=12), quinpirole (purple; 5 μM, n=7; 20 μM, n=6), quinpirole in the absence of synaptic stimulation (hollow purple bar; 5 mM, n=6), nimodipine (gray; 1 μM, n=3), sulpiride (green; 5 μM, n=4), or AP5 (green; 50 μM, n=3). * = $p < 0.05$, ** = $p < 0.01$.

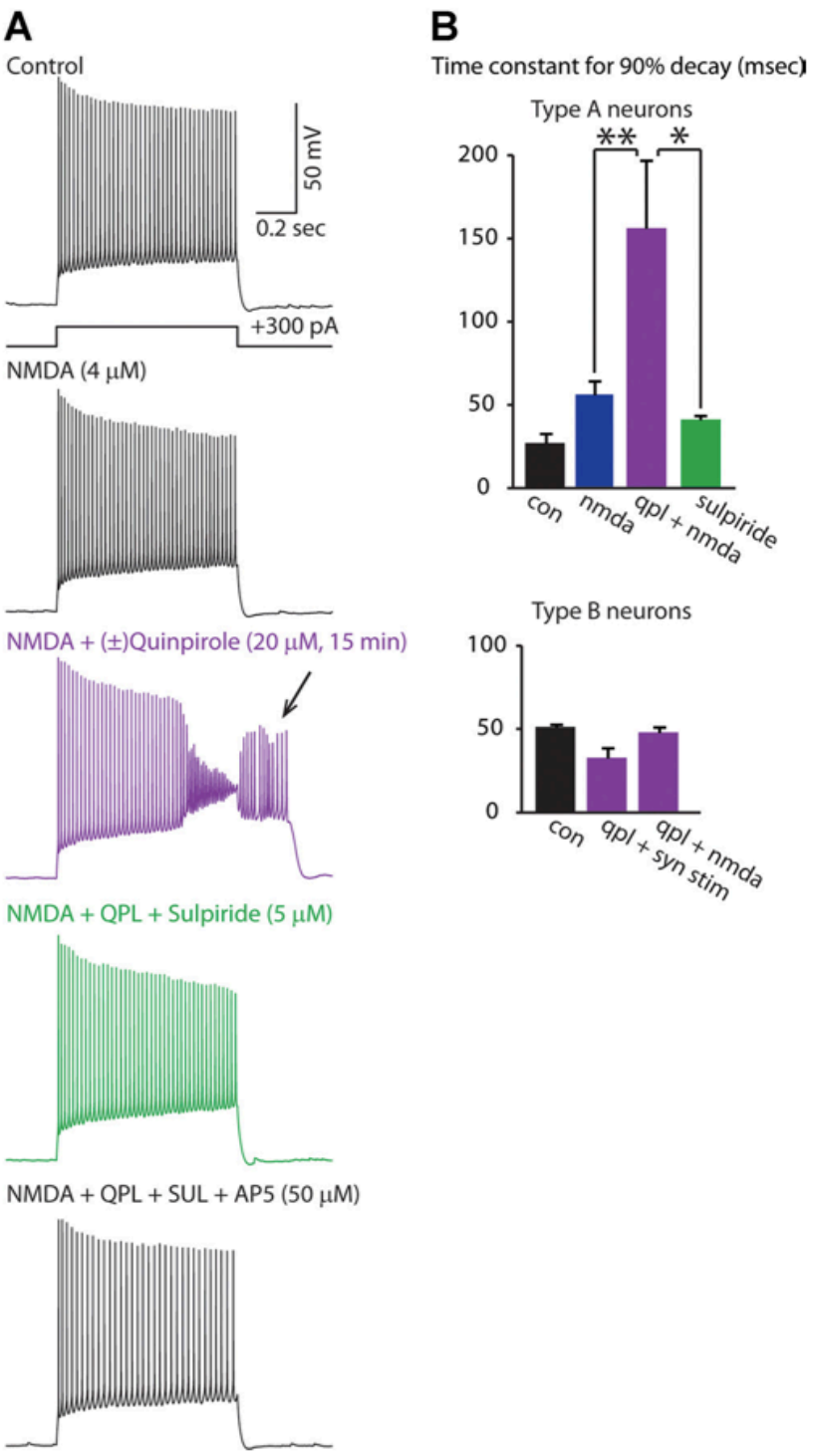

FIGURE 5. NMDA can unmask the quinpirole-induced afterdepolarization in type A neurons. (A) Responses of a type A neuron to depolarizing current

pulses in various pharmacologic conditions showing that bath application of quinpirole and NMDA, but not NMDA alone, induces an afterdepolarization (arrow) that is reversed by sulpiride. **(B, top)** Summary data showing the effect of quinpirole, NMDA, and sulpiride on the time constant for the membrane potential to return to baseline following depolarizing current pulses (350 pA, 250 msec) in type A neurons (n=4 for each condition): control (black), NMDA (4 μM, blue), (±)quinpirole (20 μM) + NMDA (purple), or sulpiride (5 μM) + quinpirole + NMDA (green). **(B, bottom)** Quinpirole does not elicit a similar afterdepolarization in type B neurons. The time constant for the membrane potential to return to baseline following depolarization current pulses (350 pA, 250 msec) in Type B neurons is shown for various conditions: control (black, n=3), (±)quinpirole (20 μM) following optogenetic synaptic stimulation (n=3; purple), (±)quinpirole (20 μM) plus NMDA (4 μM) (n=4; purple).

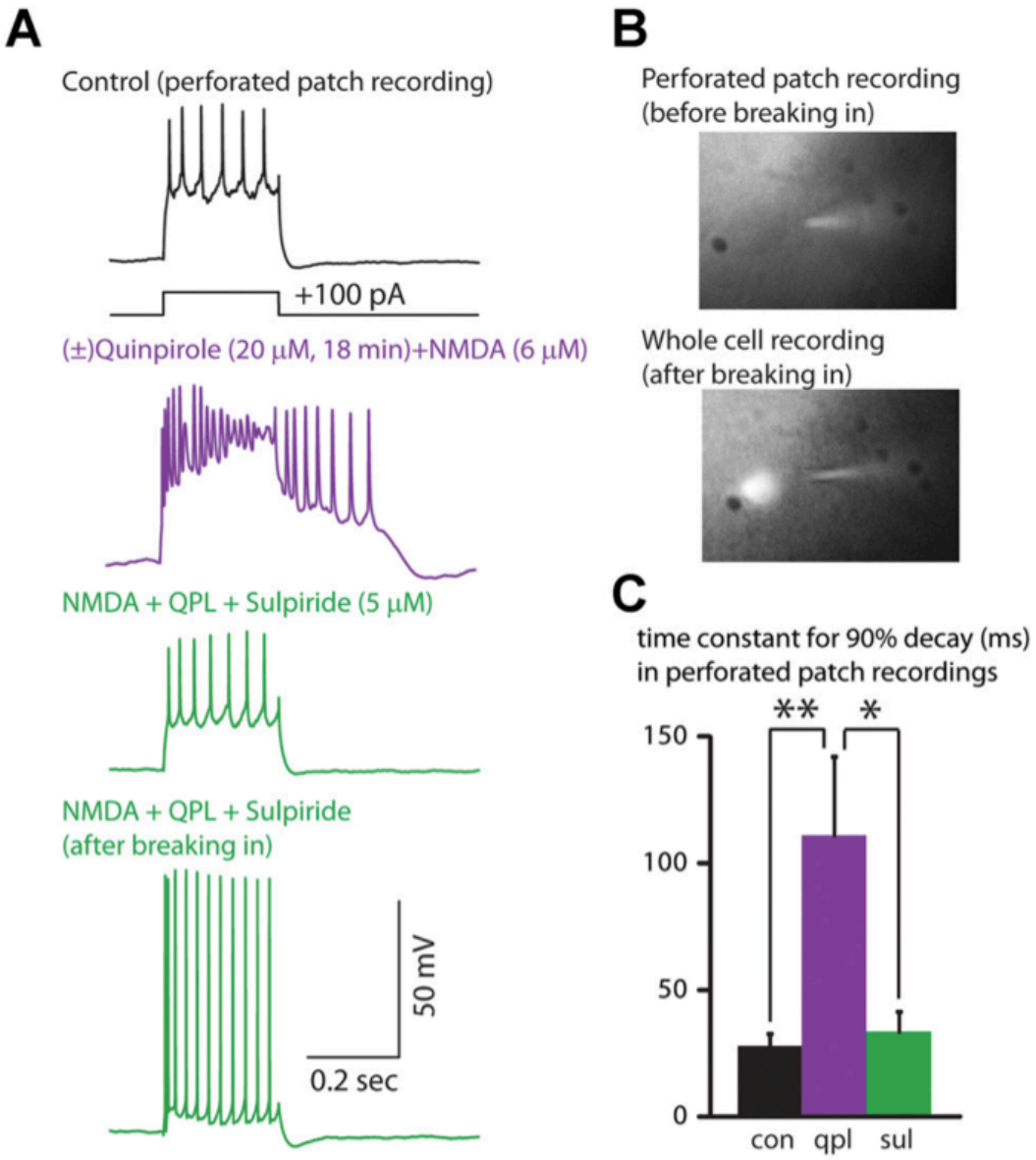

FIGURE 6. Quinpirole also induces an afterdepolarization during perforated-patch recordings from type A neurons. (A) Recordings from a type A neuron in perforated-patch configuration (top three panels) showing the quinpirole-induced afterdepolarization that occurs in the presence of NMDA, and is reversed by sulpiride. The bottom panel shows a recording from the same neuron after breaking in and shifting to a whole cell recording. **(B)** Fluorescent

dye in the recording pipette was excluded from the neuron while in the perforated-patch configuration (top image), but entered the neuron after breaking in and shifting to a whole cell configuration (bottom image). **(C)** Summary data showing that (±)quinpirole (20 μM) plus NMDA (4 μM) prolongs the time constant for the membrane potential to return to baseline following depolarizing current pulses (350 pA, 250 msec), and that this is reversed by the addition of sulpiride (5 μM) (n=5). * = $p < 0.05$, ** = $p < 0.01$.

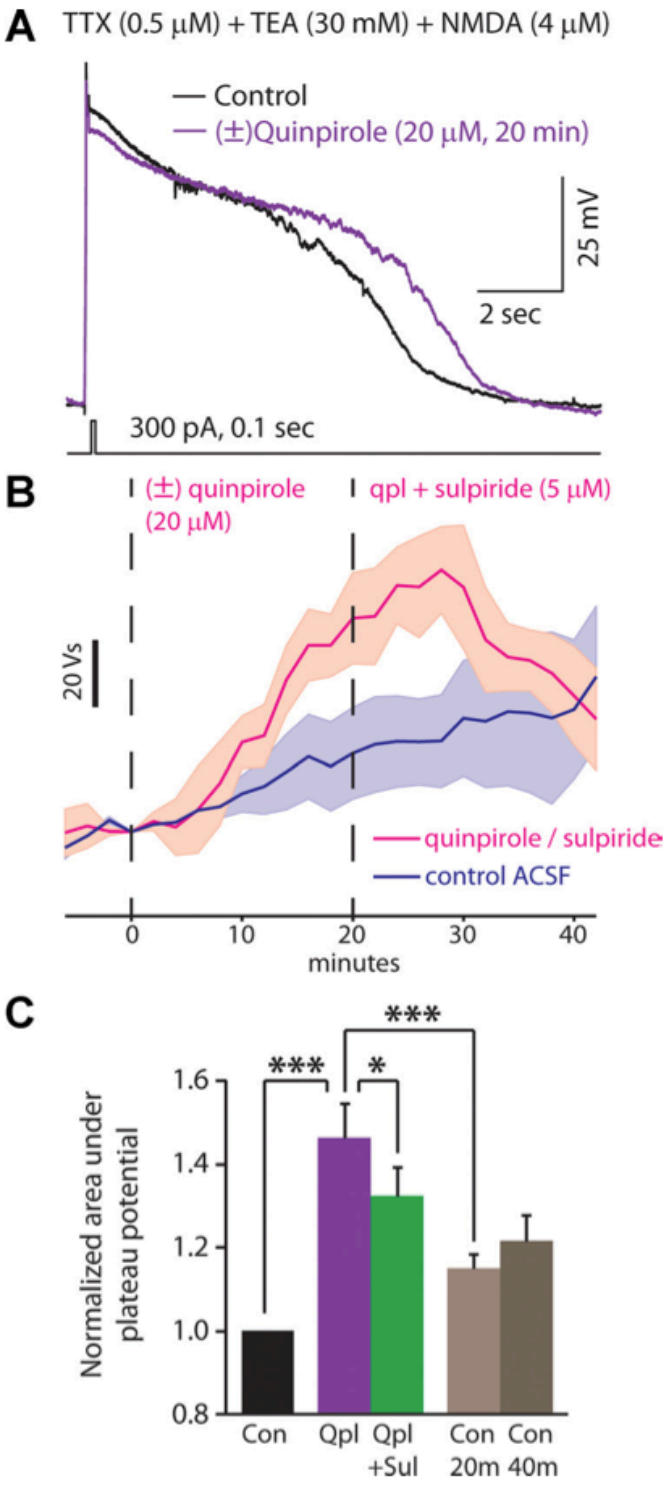

FIGURE 7. Quinpirole reversibly prolongs calcium-dependent plateau potentials. (A) A short current pulse elicits a brief Ca^{2+} spike that is followed by a prolonged plateau potential in a type A neurons after application of TTX and

TEA. Each experiment recorded plateau potentials in control conditions, then while applying (±)quinpirole (20 μM), and finally while applying quinpirole + sulpiride (5 μM). **(B)** We quantified the size of plateau potentials by measuring the area under the voltage trace. The average size of the plateau potentials are shown as a function of time (n=4 cells in each condition). For the magenta trace, t=0 represents the beginning of quinpirole application, and quinpirole and sulpiride were both applied after t=20 min. The dark blue trace represents recordings in control ACSF. Shaded regions represent ± 1 S.E.M. **(C)** Summary data for the size of plateau potentials in each condition. Each bar represents data collected from 5 min before until 5 min after the end of drug application, or corresponding timepoints during recordings in control ACSF. We measured plateau potentials every 5 min during this period and used repeated measures ANOVA and corrections for multiple comparisons to assess statistical significance. * = $p < 0.05$, *** = $p < 0.001$.

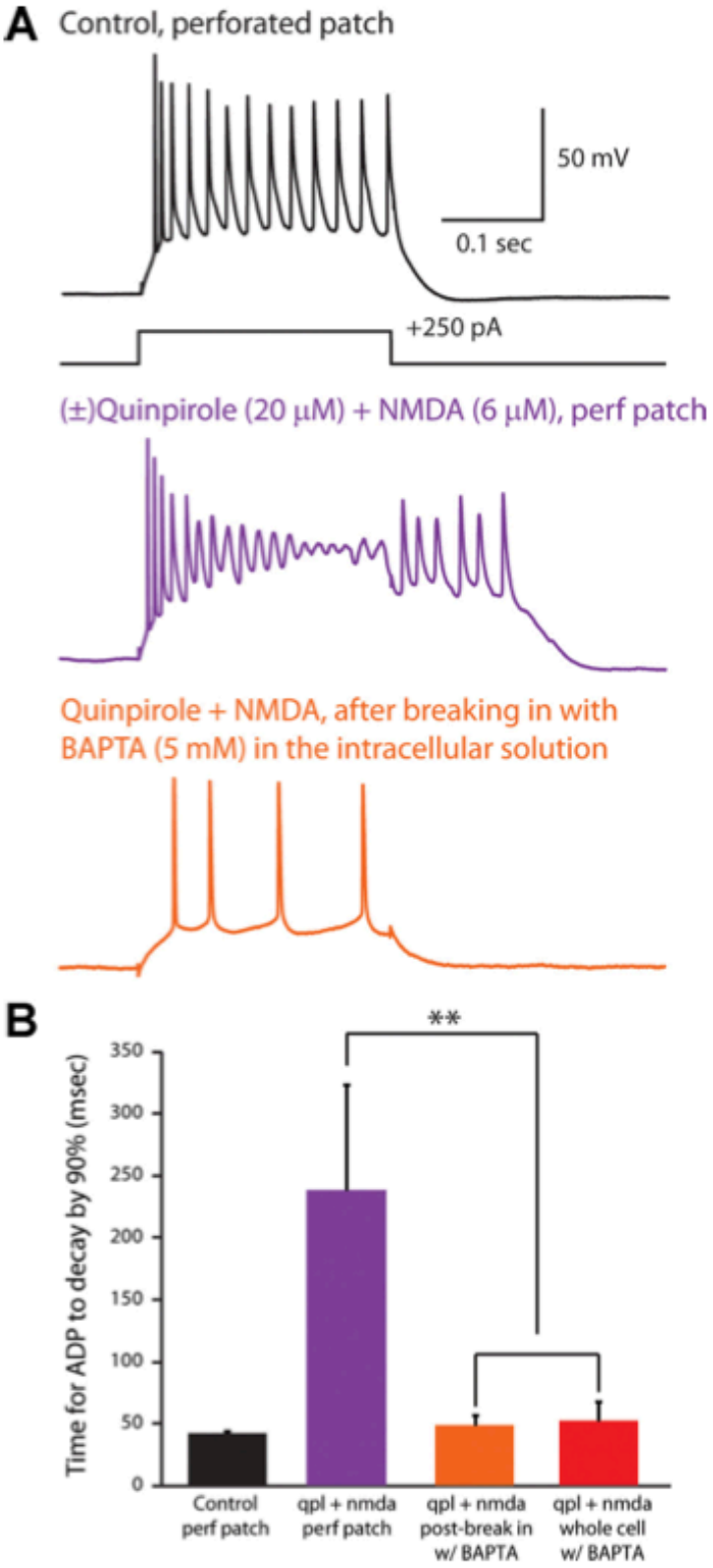

FIGURE 8. The Ca^{2+} chelator BAPTA eliminates the quinpirole-induced afterdepolarization. (A) Perforated patch recording from a type A pyramidal

neuron in control conditions (top) and after application of quinpirole + NMDA elicits an afterdepolarization (middle). Bottom panel: in the same neuron, after breaking in and switching to a whole cell recording configuration, the quinpirole-induced afterdepolarization is abolished. BAPTA (5 mM) is present in the pipette solution. **(B)** Summary data showing time constants for the membrane potential to return to baseline following depolarizing current pulses (50-150 pA, 250 msec) under various conditions. "Control" = perforated patch recordings in control ACSF (black; n = 3), "qpl + NMDA, perf patch" = the same perforated patch recordings after applying quinpirole and NMDA (orange; n = 3), "qpl + NMDA, post-break in w/ BAPTA" = whole cell recordings from the same cells that were initially recorded in perforated patch configuration (in quinpirole and NMDA) (purple; n = 3), "qpl + NMDA, whole cell w/ BAPTA" = recordings from cells that broke in and switched to whole cell configuration during the application of quinpirole + NMDA (red; n = 5). ** = $p < 0.01$.

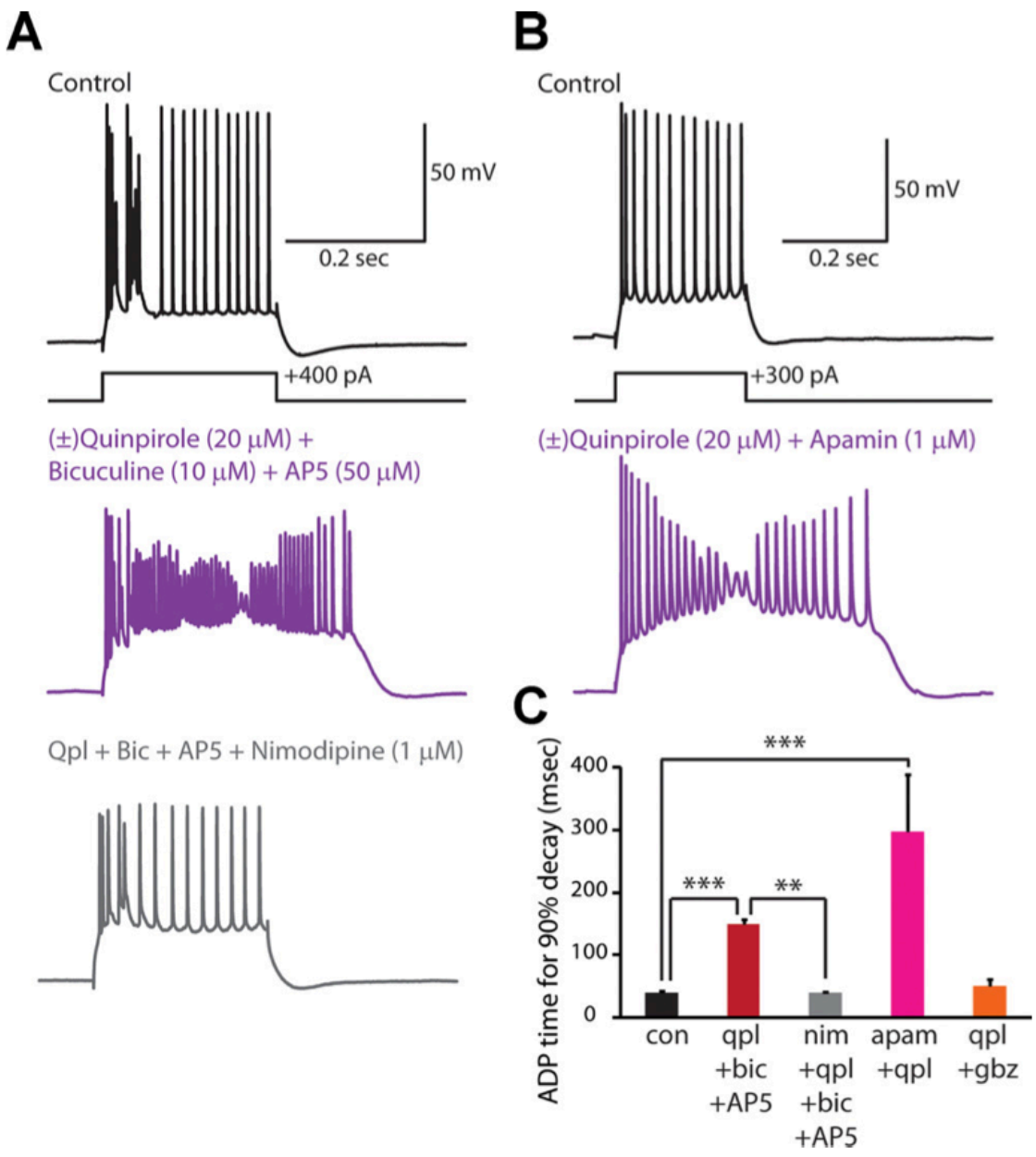

FIGURE 9. Blocking SK channels and applying quinpirole produces an afterdepolarization that requires L-type Ca^{2+} channels. (A) Responses of a type A neuron to depolarizing current pulses in various pharmacologic conditions showing that bath application of quinpirole, bicuculine, and AP5 induces an afterdepolarization (middle panel of A) that is reversed by nimodipine (bottom panel of A). **(B)** Responses of another type A neuron showing that application of

quinpirole and apamin induces a similar afterdepolarization (middle panel of B). **(C)** Summary data showing the effect of various conditions on the time constant for the membrane potential to return to baseline following depolarizing current pulses (350 pA, 250 msec) in type A neurons: control (black, n = 10), quinpirole + bicuculline + AP5 (red, n = 3), quinpirole + bicuculline + AP5 + nimodipine (gray, n = 3), apamin + quinpirole (magenta, n = 3), quinpirole + gabazine (10 μM, orange, n = 4).

REFERENCES

Ahn S, Shenoy SK, Wei H, Lefkowitz RJ (2004) Differential kinetic and spatial patterns of beta-arrestin and G protein-mediated ERK activation by the angiotensin II receptor. J Biol Chem 279:35518-35525.

Arnsten AF, Goldman-Rakic PS (1998) Noise stress impairs prefrontal cortical cognitive function in monkeys: evidence for a hyperdopaminergic mechanism. Arch Gen Psychiatry 55:362-368.

Arnsten AF, Cai JX, Steere JC, Goldman-Rakic PS (1995) Dopamine D2 receptor mechanisms contribute to age-related cognitive decline: the effects of quinpirole on memory and motor performance in monkeys. The Journal of neuroscience : the official journal of the Society for Neuroscience 15:3429-3439.

Bernacchia A, Seo H, Lee D, Wang XJ (2011) A reservoir of time constants for memory traces in cortical neurons. Nat Neurosci 14:366-372.

Bernardi G, Cherubini E, Marciani MG, Mercuri N, Stanzione P (1982) Responses of intracellularly recorded cortical neurons to the iontophoretic application of dopamine. Brain Res 245:267-274.

Bigos KL, Mattay VS, Callicott JH, Straub RE, Vakkalanka R, Kolachana B, Hyde TM, Lipska BK, Kleinman JE, Weinberger DR (2010) Genetic Variation in CACNA1C Affects Brain Circuitries Related to Mental Illness. Archives of General Psychiatry 67:939-945.

Bonci A, Hopf FW (2005) The dopamine D2 receptor: new surprises from an old friend. Neuron 47:335-338.

Branco T, Hausser M (2011) Synaptic integration gradients in single cortical pyramidal cell dendrites. Neuron 69:885-892.

Brown SP, Hestrin S (2009) Intracortical circuits of pyramidal neurons reflect their long-range axonal targets. Nature 457:1133-1136.

Brozoski TJ, Brown RM, Rosvold HE, Goldman PS (1979) Cognitive deficit caused by regional depletion of dopamine in prefrontal cortex of rhesus monkey. Science 205:929-932.

Debarbieux F, Brunton J, Charpak S (1998) Effect of bicuculline on thalamic activity: a direct blockade of IAHP in reticularis neurons. J Neurophysiol 79:2911-2918.

Dembrow NC, Chitwood RA, Johnston D (2010) Projection-specific neuromodulation of medial prefrontal cortex neurons. J Neurosci 30:16922-16937.

Ding JB, Guzman JN, Peterson JD, Goldberg JA, Surmeier DJ (2010) Thalamic gating of corticostriatal signaling by cholinergic interneurons. Neuron 67:294-307.

Druzin MY, Kurzina NP, Malinina EP, Kozlov AP (2000) The effects of local application of D2 selective dopaminergic drugs into the medial prefrontal cortex of rats in a delayed spatial choice task. Behav Brain Res 109:99-111.

Durstewitz D, Seamans JK (2008) The dual-state theory of prefrontal cortex dopamine function with relevance to catechol-o-methyltransferase genotypes and schizophrenia. Biol Psychiatry 64:739-749.

Durstewitz D, Vittoz NM, Floresco SB, Seamans JK (2010) Abrupt transitions between prefrontal neural ensemble states accompany behavioral transitions during rule learning. Neuron 66:438-448.

Egan MF, Goldberg TE, Kolachana BS, Callicott JH, Mazzanti CM, Straub RE, Goldman D, Weinberger DR (2001) Effect of COMT Val108/158 Met genotype on frontal lobe function and risk for schizophrenia. Proceedings of the National Academy of Sciences of the United States of America 98:6917-6922.

Ferreira MAR et al. (2008) Collaborative genome-wide association analysis supports a role for ANK3 and CACNA1C in bipolar disorder. Nature genetics 40:1056-1058.

Floresco SB, Magyar O, Ghods-Sharifi S, Vexelman C, Tse MTL (2006) Multiple dopamine receptor subtypes in the medial prefrontal cortex of the rat regulate set-shifting. Neuropsychopharmacology : official publication of the American College of Neuropsychopharmacology 31:297-309.

Forscher P, Oxford GS (1985) Modulation of calcium channels by norepinephrine in internally dialyzed avian sensory neurons. J Gen Physiol 85:743-763.

Frith C (1995) Functional imaging and cognitive abnormalities. Lancet 346:615-620.

Gong S, Zheng C, Doughty ML, Losos K, Didkovsky N, Schambra UB, Nowak NJ, Joyner A, Leblanc G, Hatten ME, Heintz N (2003) A gene expression atlas of the central nervous system based on bacterial artificial chromosomes. Nature 425:917-925.

Green EK, Grozeva D, Jones I, Jones L, Kirov G, Caesar S, Gordon-Smith K, Fraser C, Forty L, Russell E, Hamshere ML, Moskvina V, Nikolov I, Farmer A, McGuffin P, Holmans PA, Owen MJ, O'Donovan MC, Craddock N (2009) The bipolar disorder risk allele at CACNA1C also confers risk of recurrent major depression and of schizophrenia. Molecular psychiatry 15:1016-1022.

Gulledge AT, Jaffe DB (1998) Dopamine decreases the excitability of layer V pyramidal cells in the rat prefrontal cortex. J Neurosci 18:9139-9151.

Haj-Dahmane S, Andrade R (1998) Ionic mechanism of the slow afterdepolarization induced by muscarinic receptor activation in rat prefrontal cortex. J Neurophysiol 80:1197-1210.

Haj-Dahmane S, Andrade R (1999) Muscarinic receptors regulate two different calcium-dependent non-selective cation currents in rat prefrontal cortex. Eur J Neurosci 11:1973-1980.

Hall BJ, Delaney KR (2002) Contribution of a calcium-activated non-specific conductance to NMDA receptor-mediated synaptic potentials in granule cells of the frog olfactory bulb. J Physiol 543:819-834.

Hattox AM, Nelson SB (2007) Layer V neurons in mouse cortex projecting to different targets have distinct physiological properties. J Neurophysiol 98:3330-3340.

Hernandez-Lopez S, Bargas J, Surmeier DJ, Reyes A, Galarraga E (1997) D1 receptor activation enhances evoked discharge in neostriatal medium spiny neurons by modulating an L-type Ca2+ conductance. J Neurosci 17:3334-3342.

Histed MH, Pasupathy A, Miller EK (2009) Learning substrates in the primate prefrontal cortex and striatum: sustained activity related to successful actions. Neuron 63:244-253.

Hounsgaard J, Kiehn O (1989) Serotonin-induced bistability of turtle motoneurones caused by a nifedipine-sensitive calcium plateau potential. J Physiol 414:265-282.

Johnson SW, Seutin V (1997) Bicuculline methiodide potentiates NMDA-dependent burst firing in rat dopamine neurons by blocking apamin-sensitive Ca2+-activated K+ currents. Neurosci Lett 231:13-16.

Kellendonk C, Simpson EH, Polan HJ, Malleret G, Vronskaya S, Winiger V, Moore H, Kandel ER (2006) Transient and selective overexpression of

dopamine D2 receptors in the striatum causes persistent abnormalities in prefrontal cortex functioning. Neuron 49:603-615.

Kravitz AV, Freeze BS, Parker PR, Kay K, Thwin MT, Deisseroth K, Kreitzer AC (2010) Regulation of parkinsonian motor behaviours by optogenetic control of basal ganglia circuitry. Nature 466:622-626.

Kreitzer AC, Malenka RC (2005) Dopamine modulation of state-dependent endocannabinoid release and long-term depression in the striatum. J Neurosci 25:10537-10545.

Lee CR, Tepper JM (2007) A calcium-activated nonselective cation conductance underlies the plateau potential in rat substantia nigra GABAergic neurons. J Neurosci 27:6531-6541.

Lewis DA, Hashimoto T, Volk DW (2005) Cortical inhibitory neurons and schizophrenia. Nat Rev Neurosci 6:312-324.

Lidow MS, Wang F, Cao Y, Goldman-Rakic PS (1998) Layer V neurons bear the majority of mRNAs encoding the five distinct dopamine receptor subtypes in the primate prefrontal cortex. Synapse 28:10-20.

Lobo MK, Karsten SL, Gray M, Geschwind DH, Yang XW (2006) FACS-array profiling of striatal projection neuron subtypes in juvenile and adult mouse brains. Nat Neurosci 9:443-452.

Mailman RB (2007) GPCR functional selectivity has therapeutic impact. Trends Pharmacol Sci 28:390-396.

Maurice N, Tkatch T, Meisler M, Sprunger LK, Surmeier DJ (2001) D1/D5 dopamine receptor activation differentially modulates rapidly inactivating and persistent sodium currents in prefrontal cortex pyramidal neurons. J Neurosci 21:2268-2277.

Minton GO, Young AH, McQuade R, Fairchild G, Ingram CD, Gartside SE (2009) Profound changes in dopaminergic neurotransmission in the prefrontal cortex in response to flattening of the diurnal glucocorticoid rhythm: implications for bipolar disorder. Neuropsychopharmacology 34:2265-2274.

Minzer K, Lee O, Hong JJ, Singer HS (2004) Increased prefrontal D2 protein in Tourette syndrome: a postmortem analysis of frontal cortex and striatum. J Neurol Sci 219:55-61.

Morishima M, Kawaguchi Y (2006) Recurrent connection patterns of corticostriatal pyramidal cells in frontal cortex. J Neurosci 26:4394-4405.

Negyessy L, Goldman-Rakic PS (2005) Subcellular localization of the dopamine D2 receptor and coexistence with the calcium-binding protein neuronal calcium sensor-1 in the primate prefrontal cortex. J Comp Neurol 488:464-475.

Noudoost B, Moore T (2011) Control of visual cortical signals by prefrontal dopamine. Nature 474:372-375.

Nyegaard M, Demontis D, Foldager L, Hedemand A, Flint TJ, Sorensen KM, Andersen PS, Nordentoft M, Werge T, Pedersen CB, Hougaard DM, Mortensen PB, Mors O, Borglum AD (2010) CACNA1C (rs1006737) is associated with schizophrenia. Mol Psychiatry 15:119-121.

Otsuka T, Kawaguchi Y (2008) Firing-pattern-dependent specificity of cortical excitatory feed-forward subnetworks. J Neurosci 28:11186-11195.

Ramanathan S, Tkatch T, Atherton JF, Wilson CJ, Bevan MD (2008) D2-like dopamine receptors modulate SKCa channel function in subthalamic nucleus neurons through inhibition of Cav2.2 channels. J Neurophysiol 99:442-459.

Ripke S et al. (2011) Genome-wide association study identifies five new schizophrenia loci. Nat Genet 43:969-976.

Robbins TW (1990) The case of frontostriatal dysfunction in schizophrenia. Schizophr Bull 16:391-402.

Santana N, Mengod G, Artigas F (2009) Quantitative analysis of the expression of dopamine D1 and D2 receptors in pyramidal and GABAergic neurons of the rat prefrontal cortex. Cereb Cortex 19:849-860.

Schiller J, Major G, Koester HJ, Schiller Y (2000) NMDA spikes in basal dendrites of cortical pyramidal neurons. Nature 404:285-289.

Schultz W (2007) Multiple dopamine functions at different time courses. Annu Rev Neurosci 30:259-288.

Schwartz BL, Fay-McCarthy M, Kendrick K, Rosse RB, Deutsch SI (1997) Effects of nifedipine, a calcium channel antagonist, on cognitive function in schizophrenic patients with tardive dyskinesia. Clin Neuropharmacol 20:364-370.

Seamans JK, Yang CR (2004) The principal features and mechanisms of dopamine modulation in the prefrontal cortex. Prog Neurobiol 74:1-58.

Seeman P, Van Tol HH (1994) Dopamine receptor pharmacology. Trends Pharmacol Sci 15:264-270.

Sheets PL, Suter BA, Kiritani T, Chan CS, Surmeier DJ, Shepherd GM (2011) Corticospinal-specific HCN expression in mouse motor cortex: Ih-dependent synaptic integration as a candidate microcircuit mechanism involved in motor control. J Neurophysiol.

Sidiropoulou K, Lu FM, Fowler MA, Xiao R, Phillips C, Ozkan ED, Zhu MX, White FJ, Cooper DC (2009) Dopamine modulates an mGluR5-mediated depolarization underlying prefrontal persistent activity. Nat Neurosci 12:190-199.

Simonic I, Gericke GS, Ott J, Weber JL (1998) Identification of genetic markers associated with Gilles de la Tourette syndrome in an Afrikaner population. Am J Hum Genet 63:839-846.

Sklar P et al. (2011) Large-scale genome-wide association analysis of bipolar disorder identifies a new susceptibility locus near ODZ4. Nat Genet 43:977-983.

Sohal VS, Huguenard JR (2005) Inhibitory coupling specifically generates emergent gamma oscillations in diverse cell types. Proc Natl Acad Sci U S A 102:18638-18643.

Sohal VS, Zhang F, Yizhar O, Deisseroth K (2009) Parvalbumin neurons and gamma rhythms enhance cortical circuit performance. Nature 459:698-702.

Sommer MA, Wurtz RH (2006) Influence of the thalamus on spatial visual processing in frontal cortex. Nature 444:374-377.

Splawski I, Timothy KW, Sharpe LM, Decher N, Kumar P, Bloise R, Napolitano C, Schwartz PJ, Joseph RM, Condouris K, Tager-Flusberg H, Priori SG, Sanguinetti MC, Keating MT (2004) Ca(V)1.2 calcium channel dysfunction causes a multisystem disorder including arrhythmia and autism. Cell 119:19-31.

St Onge JR, Abhari H, Floresco SB (2011) Dissociable contributions by prefrontal D1 and D2 receptors to risk-based decision making. J Neurosci 31:8625-8633.

Steeves TD, Ko JH, Kideckel DM, Rusjan P, Houle S, Sandor P, Lang AE, Strafella AP (2010) Extrastriatal dopaminergic dysfunction in tourette syndrome. Ann Neurol 67:170-181.

Stewart CV, Plenz D (2006) Inverted-U profile of dopamine-NMDA-mediated spontaneous avalanche recurrence in superficial layers of rat prefrontal cortex. J Neurosci 26:8148-8159.

Tseng KY, O'Donnell P (2004) Dopamine-glutamate interactions controlling prefrontal cortical pyramidal cell excitability involve multiple signaling mechanisms. J Neurosci 24:5131-5139.

Tseng KY, O'Donnell P (2005) Post-pubertal emergence of prefrontal cortical up states induced by D1-NMDA co-activation. Cereb Cortex 15:49-57.

Tseng KY, O'Donnell P (2007) D2 dopamine receptors recruit a GABA component for their attenuation of excitatory synaptic transmission in the adult rat prefrontal cortex. Synapse 61:843-850.

Tseng KY, Lewis BL, Hashimoto T, Sesack SR, Kloc M, Lewis DA, O'Donnell P (2008) A neonatal ventral hippocampal lesion causes functional deficits in adult prefrontal cortical interneurons. J Neurosci 28:12691-12699.

Urban JD, Clarke WP, von Zastrow M, Nichols DE, Kobilka B, Weinstein H, Javitch JA, Roth BL, Christopoulos A, Sexton PM, Miller KJ, Spedding M, Mailman RB (2007) Functional selectivity and classical concepts of quantitative pharmacology. J Pharmacol Exp Ther 320:1-13.

Vergara R, Rick C, Hernandez-Lopez S, Laville JA, Guzman JN, Galarraga E, Surmeier DJ, Bargas J (2003) Spontaneous voltage oscillations in striatal projection neurons in a rat corticostriatal slice. J Physiol 553:169-182.

Wang M, Vijayraghavan S, Goldman-Rakic PS (2004) Selective D2 receptor actions on the functional circuitry of working memory. Science 303:853-856.

Wang Y (2004) D2 receptor regulation of synaptic burst firing in prefrontal cortical pyramidal neurons. Proceedings of the National Academy of Sciences 101:5093-5098.

Wang Y, Goldman-Rakic PS (2004) D2 receptor regulation of synaptic burst firing in prefrontal cortical pyramidal neurons. Proc Natl Acad Sci U S A 101:5093-5098.

Wang Y, Markram H, Goodman PH, Berger TK, Ma J, Goldman-Rakic PS (2006) Heterogeneity in the pyramidal network of the medial prefrontal cortex. Nat Neurosci 9:534-542.

Winterer G, Weinberger DR (2004) Genes, dopamine and cortical signal-to-noise ratio in schizophrenia. Trends Neurosci 27:683-690.

Yamada K, Ashikari I, Onishi K, Kanba S, Yagi G, Asai M (1995) Effectiveness of nilvadipine in two cases of chronic schizophrenia. Psychiatry Clin Neurosci 49:237-238.

Yamada K, Kanba S, Ashikari I, Ohnishi K, Yagi G, Asai M (1996) Nilvadipine is effective for chronic schizophrenia in a double-blind placebo-controlled study. off. J Clin Psychopharmacol 16:437-439.

Yizhar O, Fenno LE, Prigge M, Schneider F, Davidson TJ, O'Shea DJ, Sohal VS, Goshen I, Finkelstein J, Paz JT, Stehfest K, Fudim R, Ramakrishnan C, Huguenard JR, Hegemann P, Deisseroth K (2011) Neocortical excitation/inhibition balance in information processing and social dysfunction. Nature 477:171-178.

Yoon DY, Gause CD, Leckman JF, Singer HS (2007) Frontal dopaminergic abnormality in Tourette syndrome: a postmortem analysis. J Neurol Sci 255:50-56.

Young CE, Yang CR (2004) Dopamine D1/D5 receptor modulates state-dependent switching of soma-dendritic Ca2+ potentials via differential protein kinase A and C activation in rat prefrontal cortical neurons. J Neurosci 24:8-23.

Zhang Y, Bertolino A, Fazio L, Blasi G, Rampino A, Romano R, Lee ML, Xiao T, Papp A, Wang D, Sadee W (2007) Polymorphisms in human dopamine D2 receptor gene affect gene expression, splicing, and neuronal activity during working memory. Proc Natl Acad Sci U S A 104:20552-20557.

CHAPTER 3

Pyramidal Neurons in Prefrontal Cortex Receive Subtype-specific Forms of Excitation and Inhibition

ABSTRACT

Layer 5 pyramidal neurons comprise at least two subtypes: thick-tufted, subcortically-projecting Type A neurons, with prominent h-current, and thin-tufted, callosally-projecting Type B neurons, which lack prominent h-current. Using optogenetic stimulation, we find that these subtypes receive distinct forms of input that could subserve divergent functions. Repeatedly stimulating callosal inputs evokes progressively smaller excitatory responses in Type B but not Type A neurons. Callosal inputs also elicit more spikes in Type A neurons. Surprisingly, these effects arise via distinct mechanisms. Differences in the dynamics of excitatory responses reflect differences in presynaptic input, whereas differences in spiking depend on postsynaptic mechanisms. We also find that fast-spiking parvalbumin interneurons, but not somatostatin interneurons, preferentially inhibit Type A neurons, which leads to greater feedforward inhibition in this subtype. These differences may enable Type A neurons to detect salient inputs that are focused in space and time, while Type B neurons integrate across these dimensions.

INTRODUCTION

Patterns of network activity emerge from the organization of connections in neural circuits. Thus, it is critically important to determine whether these connections follow a specific wiring diagram, and if so, to identify possible computational functions that emerge as a result. Many studies have shown that across multiple neocortical regions, layer 5 (L5) pyramidal neurons can be divided into at least two subtypes (Brown and Hestrin, 2009; Dembrow et al., 2010; Gee et al., 2012; Hattox and Nelson, 2007; Morishima and Kawaguchi, 2006; Sheets et al., 2011; Wang et al., 2006). One subtype, which we call “Type A” neurons, has thick-tufted apical dendrites, projects subcortically, and has a prominent h-current (I_h). The other subtype – “Type B neurons” – projects to the contralateral cortex or striatum, has thin tufted apical dendrites, and lacks prominent I_h.

Several groups have studied differences in local connections between these two subtypes (Brown and Hestrin, 2009; Morishima and Kawaguchi, 2006; Morishima et al., 2011; Wang et al., 2006). However, it remains unknown whether long-range excitatory inputs or local inhibitory connections also differ between these subtypes. Two recent studies found that neocortical interneurons nonspecifically target nearby pyramidal neurons (Fino and Yuste, 2011; Packer and Yuste, 2011) but these studies did not examine subtypes of L5 pyramidal neurons. By contrast, studies in other regions suggest that inhibitory interneurons can selectively innervate pyramidal neurons that project to specific targets, while

sparing neighboring pyramidal neurons that project elsewhere (Krook-Magnuson et al., 2012; Varga et al., 2010).

We addressed these issues by studying excitatory connections from the contralateral mPFC and inhibitory connections from fast-spiking parvalbumin interneurons (FSINs) onto Type A and B neurons in mPFC. We find that optogenetic stimulation of callosal inputs elicits distinct patterns of responses in Type A and B neurons and that FSINs preferentially innervate Type A neurons. These findings have important implications for the normal and pathological function of prefrontal microcircuits.

METHODS

All experiments were conducted in accordance with procedures established by the Administrative Panels on Laboratory Animal Care at the University of California, San Francisco.

Slice Preparation

We cut 250 μm coronal slices from 8- to 11-week-old mice of either sex (Gee et al., 2012). Slices were cut in a chilled slicing solution in which Na^+ was replaced by sucrose, then incubated in warmed artificial cerebrospinal fluid (ACSF) at 30° C–31° C for ~1 hr before being used for recordings. ACSF contained 126 mM NaCl, 26 mM $NaHCO_3$, 2.5 mM KCl, 1.25 mM NaH_2PO_4, 1 mM $MgCl_2$, 2 mM CaCl, and 10 mM glucose. We used the following mouse lines: wild-type C57BL/6 mice (Charles River), B6;129P2-*Pvalbtm1(cre)Arbr*/J (Jackson Laboratory) and B6N.Cg-$Sst^{tm2.1(cre)Zjh}$/J (Jackson Laboratory). We secured the slice via a harp along the midline.

Intracellular Recording

We obtained somatic whole-cell patch recordings from visually identified pyramidal cells in layer 5 infralimbic or prelimbic cortex using differential contrast video microscopy on an upright microscope (BX51WI; Olympus). Recordings were made using a Multiclamp 700A (Molecular Devices). Patch electrodes (tip resistance = 2–6 MOhms) were filled with the following: 130 mM K-gluconate, 10 mM KCl, 10 mM HEPES, 10 mM EGTA, 2 mM MgCl, 2 mM MgATP, and

0.3 mM NaGTP (pH adjusted to 7.3 with KOH). All recordings were at 32.5° C ± 1° C. Series resistance was usually 10–20 MΩ, and experiments were discontinued above 30 MΩ.

Injection of Virus for ChR2 Expression

For Cre-dependent expression of ChR2 or EFYP, we used a previously described adeno- associated virus (AAV) vector that drives Cre-dependent expression of a ChR2-EFYP fusion protein (Sohal et al., 2009). In other cases, we expressed ChR2-EFYP in pyramidal neurons using a previously described AAV vector that contains a gene encoding ChR2-EYFP under control of the promoter for CaMKIIα (Sohal et al., 2009). In each case, we injected 0.5–0.75 μl of virus following previously described procedures (Sohal et al., 2009). For experiments in which we recorded from ChR2-negative neurons while stimulating ChR2-positive axons, we injected virus into the contralateral medial PFC (mPFC) and verified that we observed fluorescent soma on the injected side but not on the contralateral side (which was the location for recording). For experiments in which we recorded optogenetically evoked inhibition from pyramidal neurons, we injected Cre-dependent ChR2-EYFP virus into ipsilateral mPFC. We waited at least 4 weeks after virus injection before preparing brain slices. Coordinates for injection into mPFC were (in millimeters relative to bregma): 1.7 anterior-posterior (AP), 0.3 mediolateral (ML), and −2.75 dorsoventral (DV).

Injection of Retrogradely Transported Microspheres for Projection-Targeting Experiments

Procedures for injection of these microspheres were similar to those for virus injection. We waited at least 48 hr after each injection before preparing brain slices. Coordinates for mPFC injections were the same as for virus injections. For injections into mediodorsal (MD) thalamus, coordinates were (in millimeters relative to bregma): +1.7 AP, 0.3 ML, and −3.5 DV. For each experiment, we verified that microspheres were present in the correct target (MD thalamus or mPFC). For injections into MD thalamus, we also verified that microspheres were not present in neighboring structures, e.g., striatum.

Electrophysiological Identification of Type A Neurons

Type A neurons were distinguished by their voltage sag and rebound afterdepolarization (ADP) following hyperpolarizing current pulses (−200 pA, 250 ms) and afterhyperolarization (AHP) following depolarizing current pulses (250 pA, 250 ms): type A neurons were defined based on a combined sag, rebound ADP, and AHP > 6.5 mV.

Electrophysiologic Identification of Fast-Spiking Interneurons

Fast-spiking interneurons were first preliminarily identified through an AAV-Dlxi12b enhancer-mCherry, which marks a diverse population of interneurons (Potter et al., 2009). Putative interneurons were then identified as fast spiking based on electrophysiological properties. Specifically, the action

potential width at half-maximal amplitude was ≤0.5 ms, and during responses to a depolarizing current pulse (400 pA, 250 ms), the adaptation ratio, i.e., the ratio between the first and last interspike interval, was <2.

Drug Application

For electrophysiology, all drugs were dissolved in water (DL-AP5, 4AP, bicuculline methiodide, ZD7288) or dimethylsulfoxide (mibefradil, nimodipine, nickel, picrotoxin) before being diluted in ACSF, except for TTX, which was dissolved in a pH 4.8 citrate buffer.

ChR2 Stimulation

We stimulated ChR2 using flashes of light (~2 mW/mm^2 measured at the sample) generated by a Lambda DG-4 high-speed optical switch with a 300 W Xenon lamp (Sutter Instruments) and an excitation filter set centered around 470 nm, delivered to the slice through a 40× objective (Olympus). Illumination was delivered across a full high-power (40×) field. We delivered 5 Hz trains of light flashes first, followed by 10 Hz and 20 Hz trains. The interval between each train was at least 8 s.

Statistical Analysis

We used Student's t tests to compare pairs of groups, unless there were repeated-measurements or more than two groups, in which case we used ANOVA. In one case, as noted in the text, we used Fisher's exact test to

compare the frequency of connections between two groups. Error bars indicate ±1 SEM unless otherwise specified.

RESULTS

To compare responses of Type A and B neurons to callosal inputs, we performed dual whole cell recordings in pairs of Type A and B neurons while optogenetically stimulating inputs from the contralateral mPFC (n=11 pairs; Fig. 1A). We differentiated Type A and B neurons by the prominence of the I_h induced sag and rebound in response to hyperpolarizing current pulses and the presence of an afterhyperpolarization following depolarizing current pulses (Methods; Fig. S1A) (Gee et al., 2012). We expressed ChR2 in pyramidal neurons in the mPFC in one hemisphere (Methods; Fig. 1A), then stimulated the terminals of their callosal projections via rhythmic trains of light flashes (470nm; ~2 mW/mm^2, 5ms; 5 or 10 Hz, 10 flashes/train). Some studies optogenetically stimulate terminals in TTX + 4-AP to block polysynaptic activity (Petreanu et al., 2007). However, in TTX + 4-AP, synaptic release is triggered by the ChR2-driven depolarization of terminals rather than by spiking. This would not be suitable for studying the short-term dynamics of synaptic responses, therefore, by design, we did not use TTX + 4-AP to block polysynaptic activity. This also enabled us to measure how callosal inputs recruit different levels of spiking in Type A and B neurons and how feedforward inhibition, recruited by callosal inputs, contribute to this and other effects. We did attempt additional experiments using TTX + 4-AP, but found that optogenetically-evoked synaptic release was completely abolished (3/3 pairs of Type A and B neurons; Fig. S1B), indicating that, in our preparation, optogenetically-evoked synaptic release is mediated by spiking. Although we were not able to use TTX + 4-AP to isolate monosynaptic excitatory responses,

several observations described below suggest that monosynaptic callosal input dominated the responses we recorded.

Callosal stimulation elicits subtype-specific excitatory responses in pyramidal cells

Trains of optogenetic stimulation delivered to callosal inputs elicited EPSPs in Type A/B pairs. In 3/11 pairs, at least one cell spiked. In the remainder, all EPSPs were subthreshold. Notably, the pattern of subthreshold EPSPs differed in Type A and B neurons (Fig. 1B). We observed marked depression of EPSP responses to successive light flashes in Type B neurons, i.e. the responses to light flashes 2-10 were consistently weaker than the first response ($p<0.001$ for an effect of response number on response amplitude by ANOVA; responses 2-10 were each weaker than the first response, $p<0.05$ by t-test; n=8 cells). No such depression occurred in Type A neurons, and normalized EPSP responses to light flashes 2-10 were significantly greater in Type A than Type B neurons ($p<0.0001$ for 5 Hz, $p<0.01$ for 10 Hz via ANOVA using cell subtype, recording pair, and flash number as factors; n=8 pairs) (Fig. 1C). In fact, in some Type A neurons, the first few responses to light flashes at 5 Hz were facilitating, i.e. they grew progressively larger, (gray traces in Fig. 1B). The average amplitude of the first EPSP was not significantly different for Type A and B neurons, respectively ($p=0.18$ for 5 Hz; $p=0.41$ for 10 Hz; n=8 pairs). To confirm that Type A and B neurons have different projection targets, we also made recordings after injecting red and green fluorescent retrogradely transported

microspheres (Lumafluor) into MD thalamus and contralateral mPFC. In 3/3 pairs consisting of one corticothalamic (CT) and one corticocortical (CC) neuron, we observed the same pattern – strong depression of EPSPs in CC (Type B) neurons but not in CT (Type A) neurons (Fig. S1D-F).

Subtype-specific patterns of EPSPs could reflect differences in monosynaptic callosal inputs, or the effects of polysynaptic circuit activity. In all of the recordings used to analyze EPSPs, callosal stimulation failed to evoke spikes in either of the simultaneously recorded neurons, suggesting that when present, polysynaptic activity was limited. Two additional observations suggest that differences in EPSP dynamics reflect monosynaptic callosal inputs to Type A and B neurons. First, in 3 recordings from A/B pairs, light stimulation failed to evoke appreciable inhibitory currents (measured in voltage clamp at +10 mV). ChR2 expression varied across slices, and these recordings presumably represent cases with the least expression and minimal network activity. These recordings continue to show EPSP depression in Type B but not Type A neurons (Fig S1C).

Second, when we did observe spiking in current clamp recordings, these spikes occurred several milliseconds *after* the peak of the EPSC response (measured in voltage clamp). Specifically, in voltage clamp, the EPSC peak occurred 7.3 ± 0.5 msec after the beginning of the light flash. By contrast, in current clamp, spikes occurred an average of 11.3 ± 1.7 msec after the beginning of the light flash (n=6 cells). Thus, peak responses almost certainly reflect predominately monosynaptic input. For these reasons, we believe that differences in EPSP dynamics originate at the level of monosynaptic callosal

inputs. Regardless, we have found that callosal inputs recruit distinct patterns of excitation in Type A and B neurons.

Differences in presynaptic input explain subtype-specific differences in EPSPs

We next asked whether the different EPSP dynamics in Type A and B neurons reflect pre- or postsynaptic mechanisms. When dual-patching onto A/B pairs in voltage clamp at -70 mV (Fig 2A, top), we did not find significant differences in peak excitatory currents or charge transfer (Fig 2B). Normalized, averaged excitatory currents elicited by light stimulation show that Type A or B neurons receive slightly facilitating or depressing currents, respectively (Fig 2C). We asked whether these facilitating and depressing currents suffice to reproduce the subtype-specific EPSP patterns in Fig. 1. This would suggest that subtype-specific patterns of presynaptic input account for differences in EPSP dynamics. Alternatively, different postsynaptic properties of Type A and B neurons, e.g. resonance properties (Dembrow et al., 2010), may contribute to different EPSP responses to callosal stimulation. To address this, we averaged the input waveform recorded in voltage clamp from Type A neurons, and the waveform recorded from Type B neurons (Fig. 2C). Then we played back each waveform to both Type A and B neurons in current clamp (Fig. 2D). If cell-intrinsic properties contribute to differences in EPSP dynamics, voltage responses to the injected inputs should depend on the identity of the patched neuron (A or B). However, the response of Type A and B cells depended only on the identity of the injected

current waveform (Fig 2E). Both Type A and B pyramidal neurons showed EPSP depression in response to the “Type B” input waveform but not the Type A waveform (Fig 2F).

Of course, the current waveforms we recorded in voltage clamp may not accurately reflect the pattern of synaptic input. These waveforms could be contaminated by unclamped dendritic currents in Type A and B neurons, and such voltage-dependent Ca^{2+} currents in the dendrites might enhance temporal summation between EPSPs in Type A neurons, masking the sort of EPSP depression observed in Type B neurons (Branco and Hausser, 2011; Schiller et al., 2000). To rule this out, we recorded Type A neuron responses to callosal stimulation before and after blocking T-type Ca^{2+} channels, L-type Ca^{2+} channels, and NMDARs with mibefradil (5 μM) + nimodipine (5 μM) + AP5 (50 μM). We found no alteration in the paired-pulse ratio after blocking these postsynaptic voltage-dependent Ca^{2+} channels ($p=0.19$, $n=4$, Fig S2), i.e. even after blocking these channels, EPSPs in Type A neurons were still non-depressing. This suggests that differences between the pattern of callosally-evoked EPSPs in Type A and B neurons reflect differences in their presynaptic input, not postsynaptic factors.

Differences in callosally-evoked spiking depend on postsynaptic Ca^{2+} currents

During paired-recordings of callosal stimulation (described above), we observed more spikes in Type A neurons than Type B neurons (Fig 3A; spiking

occurred in 3/11 pairs). We next asked whether this was the result of differences in presynaptic inputs or postsynaptic excitability. To test this, we injected the same current waveforms as in Fig 2C, but scaled these up by a factor of 2 to elicit spiking. Note that the waveforms in Fig. 2C reflect averages across all experiments, whereas EPSPs were larger in recordings that elicited spiking. Thus the “scaled up” waveforms were consistent with the EPSP amplitudes associated with spiking. We also injected tonic current to maintain all resting membrane potentials near -65 mV (average resulting resting potentials were -65.0 mV for both type A and B neurons; average current, Type A: 8.7 ± 4.1; Type B: 15 ± 6.1; $p=0.4$). Type A neurons spiked more than Type B neurons, regardless of whether we injected input waveforms derived from Type A or B neurons, suggesting that postsynaptic differences between Type A and B neurons contribute to differences in spiking (Fig 3B,C).

We have previously found that Ca^{2+} and Ca^{2+}-dependent currents profoundly influence the excitability of Type A neurons (Gee et al., 2012). To test whether similar mechanisms might enhance Type A neuron spiking here, we recorded the voltage responses of Type A neurons to input waveforms derived from both Type A and B neurons before and after applying Ni^{2+} (0.5 mM) to block voltage-gated Ca^{2+} channels. The increased firing observed in Type A neurons was significantly reduced when voltage-gated calcium channels were blocked ($p<0.01$; Fig 3C, D), suggesting that voltage-gated Ca^{2+}channels contribute to increased spiking in Type A neurons.

We also tested whether the more prominent I_h in Type A neurons affects their responses to these input wavforms, but found minimal changes in spiking and EPSP dynamics after blocking I_h with ZD7288 (25 μM; Fig. S3).

Callosal stimulation elicits more circuit inhibition in Type A neurons

Excitatory callosal inputs recruit local feedforward inhibitory circuits. Although previous studies suggested that interneurons (INs) make indiscriminate connections onto neighboring pyramidal neurons, they did not account for pyramidal subtypes (Fino and Yuste, 2011; Packer and Yuste, 2011). Thus we tested if Type A and B neurons receive different levels of inhibition. In the previously described experiments, in which we excited ChR2-expressing callosal projections while dual-patching Type A and B neurons, we also recorded IPSCs in voltage-clamp at +10mV. Surprisingly, Type A neurons received significantly more inhibitory current than Type B neurons (Fig 4A,B). Both the peak IPSC amplitude (Type A: 1.0 ± 0.3 nA, Type B: 0.4 ± 0.2 nA; $p<0.01$) and inhibitory charge transfer (Type A: 18.9 ± 6.0 pC, Type B: 10.5 ± 5.5 pC; $p<0.05$) were significantly greater in Type A than B neurons (n=11 pairs). Fast outward currents were completely blocked by picrotoxin (10 μM; n=3; Fig. S4A). The latency from the beginning of each light flash to the peak IPSC was ~2 msec longer than the EPSC latency (9.7 ± 0.8 msec vs. 7.3 ± 0.5 ms; Fig S4D), consistent with primarily feedforward (as opposed to feedback) inhibition.

Fast-spiking parvalbumin interneurons preferentially inhibit Type A neurons

Differences in inhibition might reflect different connectivity between INs and these two pyramidal neuron subtypes. To explore this possibility, we recorded from fast-spiking parvalbumin interneurons (FSINs) in current clamp while simultaneously recording from either Type A or B neurons in voltage clamp at +10mV (Fig 4C). We initially selected putative INs for patching based on expression of mCherry driven by an AAV with the DlxI12b enhancer (Methods) (Potter et al., 2009), then confirmed FSIN identity based on electrophysiological properties (Methods). FSINs had significantly greater probabilities of connecting onto Type A than Type B neurons (6/11 vs 1/12, p=0.027, Fisher's exact test). Importantly, the average distance between FSINs and Type A or B neurons was not significantly different (Fig. S4E).

To further investigate inhibitory output from FSINs onto different L5 pyramidal neuron subtypes, we optogenetically activated FSINs while simultaneously recording from a pair of Type A and B neurons. We injected AAV to drive Cre-dependent expression of ChR2 into the mPFC of parvalbumin (PV)::Cre mice (Sohal et al., 2009) (Fig 4E), in which Cre expression is limited to PV-positive INs, which in neocortex are FSINs. Optogenetic stimulation of PV INs elicited significantly greater peak inhibitory current (Type A: 2.6 ± 0.7 nA; Type B: 1.3 ± 0.5 nA, $p<0.05$) and charge transfer (Type A: 60 ± 16 pC; Type B: 36 ± 13 pC, $p<0.01$) in Type A compared to Type B neurons. Again, we confirmed that

this pattern of greater inhibition in Type A neurons was also present in pairs of retrogradely-labeled CT/CC pyramidal neurons (data not shown; n=2 pairs).

Finally, to determine whether this preferential inhibition of Type A neurons was specific to PV INs, we also recorded from pairs of Type A and B neurons (n=7 pairs) in somatostatin (SOM)::Cre mice injected with the same AAV (Fig. 4G). In this case, ChR2 was expressed in SOM INs, and optogenetic stimulation elicited similar levels of peak inhibitory current (Type A: 1.1 ± 0.3 nA; Type B: 0.9 ± 0.3 nA, p=0.5) and charge transfer in Type A and B neurons (Type A: 34 ± 11 pC; Type B: 30 ± 9 pC, p=0.7) (Fig. S4F-G).

Inhibition sharpens Type A neuron responses to callosal input

If callosal inputs preferentially recruit feedforward inhibition in Type A neurons, this may accelerate the return to baseline following EPSPs in Type A neurons. We revisited our current clamp traces (Fig 1B) and calculated the decay time constant for the falling phase of EPSPs (Fig 4G). Indeed, Type A cells had sharper responses to callosal inputs as indicated by their significantly shorter decay time constant (Fig 4H, Type A: 41 ± 7 ms; Type B: 92 ± 19 ms, $p<0.05$).

Feedforward inhibition might also influence the facilitation or depression of EPSPs in Type A neurons. To test this possibility, we recorded EPSPs in Type A neurons before and after applying picrotoxin (PTX) to block $GABA_A$ currents. To avoid epileptiform discharges we applied 10 μM PTX for 10-16 min; this was sufficient to eliminate most feedforward IPSCs (Fig. S4A), but had minimal effects on the short term dynamics of EPSPs in Type A cells (Fig. S4B-C).

DISCUSSION

These results build on earlier studies that divided L5 pyramidal neurons in the mPFC into two subtypes. We found that callosal inputs elicit depressing EPSPs in Type B neurons while EPSPs both fail to depress and evoke more spikes in Type A neurons. Differences in the dynamics of EPSPs can be explained by differences in presynaptic inputs to Type A and B neurons whereas postsynaptic differences, including voltage-dependent Ca^{2+} currents in Type A neurons, drive the higher level of spiking in these neurons. Several observations suggest these differences derive primarily from monosynaptic callosal inputs. Regardless, callosal input elicits excitatory circuit activity that manifests differently in Type A and B neurons. Callosal inputs also elicit approximately twice as much circuit inhibition in Type A neurons compared to Type B neurons. We found that FSINs (but not SOM INs) preferentially innervate Type A neurons, which may explain this difference.

Relationship to previous studies

This study builds on previous work that has found differences in the local connectivity between subtypes of L5 pyramidal neurons (Brown and Hestrin, 2009; Morishima and Kawaguchi, 2006; Morishima et al., 2011; Wang et al., 2006). Our findings suggest that similar differences are also present for long-range inputs, in this case, from the contralateral mPFC. Notably, our finding that callosal stimulation elicits EPSPs which depress in Type B neurons but not in Type A is consistent with previous studies suggesting that local excitatory

connections between neurons having the characteristics of either Type A or B neurons, exhibit facilitation and depression, respectively (Morishima et al., 2011; Wang et al., 2006).

Our result that FSINs preferentially inhibit Type A neurons may explain an earlier observation that disynaptic inhibition occurs more frequently between pairs of thick-tufted L5 pyramidal neurons than between pairs of callosally projecting L5 pyramidal neurons in the somatosensory cortex of juvenile rats (Le Be et al., 2007). However, our result contrasts with an older anatomical study in cat visual cortex, showing that corticocortical neurons receive more inhibitory synapses onto their somata and axon initial segments than do corticothalamic neurons (Farinas and DeFelipe, 1991). It will be important to determine whether this reflects species or regional differences, or differences between anatomical and physiologic measurements.

Our finding of differential FSIN output onto neighboring subtypes of L5 pyramidal neurons also parallels similar findings in the entorhinal cortex (Varga et al., 2010), but contrasts with another study of FSINs in neocortex (Packer and Yuste, 2011). There are several differences between the latter study and this one, including different methods for measuring interneuron connectivity (glutamate uncaging vs. paired recording), different ages of mice (P12-17 vs. adult), and different neocortical regions (primarily somatosensory vs. prefrontal) and layers (primarily L2/3 vs. L5) that were studied. It will be important to determine which factors explain the differences between the two studies.

Implications for normal and pathological prefrontal microcircuit function

As described above, increased circuit inhibition in Type A neurons, likely mediated in large part by increased FSIN innervation, sharpens Type A neuron responses to callosal input. By contrast, the relative absence of such inhibition results in an approximate doubling of EPSP duration in Type B neurons. These differences could make Type A and B neurons maximally sensitive to distinct spatial patterns of input. If inputs facilitate even weakly, then postsynaptic neurons will respond more when input pulses are concentrated on a single fiber, eliciting facilitation, than when input pulses are distributed across many fibers, in which case no facilitation occurs. Depressing inputs elicit the opposite pattern: input concentrated on a single fiber cause depression, and as a consequence, postsynaptic neurons respond more strongly when inputs are distributed across many fibers. Based on this logic, Type A and B neurons should be maximally responsive to focal and distributed patterns of input, respectively. These differences may endow these two pyramidal neuron subtypes with distinct computational properties. Specifically, Type B neurons, which project callosally, may integrate intracortical inputs over space to accumulate evidence as part of decision making (Curtis and Lee, 2010), or maintain persistent activity that stores items in working memory (Funahashi et al., 1989). By contrast, Type A neurons may be sensitive to strong, focal inputs in both the spatial and temporal domains. This may enable Type A neurons to transmit signals about particularly salient events to downstream subcortical structures, e.g. MD thalamus, as part of

corollary discharge (Wang et al., 2004). Activation of dopamine D2 receptors may further amplify Type A neuron responses to salient inputs (Gee et al., 2012).

Greater FSIN innervation of Type A neurons suggests that FSIN dysfunction, hypothesized to play a major roles in schizophrenia (Lewis et al., 2005), may cause relatively more severe disruptions in Type A neuron function. Within prefrontal cortex, Type A neurons could represent a point of convergence for FSIN-mediated inhibition, L-type Ca^{2+} channels, outputs to MD thalamus, and D2 receptors, all of which have been strongly linked to schizophrenia (Marenco et al., 2012; Ripke et al., 2011). Thus our findings suggest that abnormal Type A neuron excitability may represent a specific physiological substrate that contributes to prefrontal dysfunction in schizophrenia.

Limitations and future directions

Although we recorded simultaneous responses of Type A and B neurons to stimulation of callosal inputs, we do not know whether the same callosal fibers synapsed onto both Type A and B neurons, or whether subpopulations of callosal fibers, perhaps originating from different neurons in the contralateral mPFC innervate these two subtypes. Future experiments might selectively stimulate various subpopulations of callosally-projecting pyramidal neurons in the mPFC , and measure the responses of Type A and B neurons to disambiguate these two possibilities.

Conclusions

Callosal inputs elicit circuit excitation and inhibition that manifest differently in two subtypes of L5 pyramidal neurons within the mPFC, possibly contributing to distinct computational functions. It will be important for future studies to determine whether other sources of long-range input also differentially innervate these and other subtypes of prefrontal neurons.

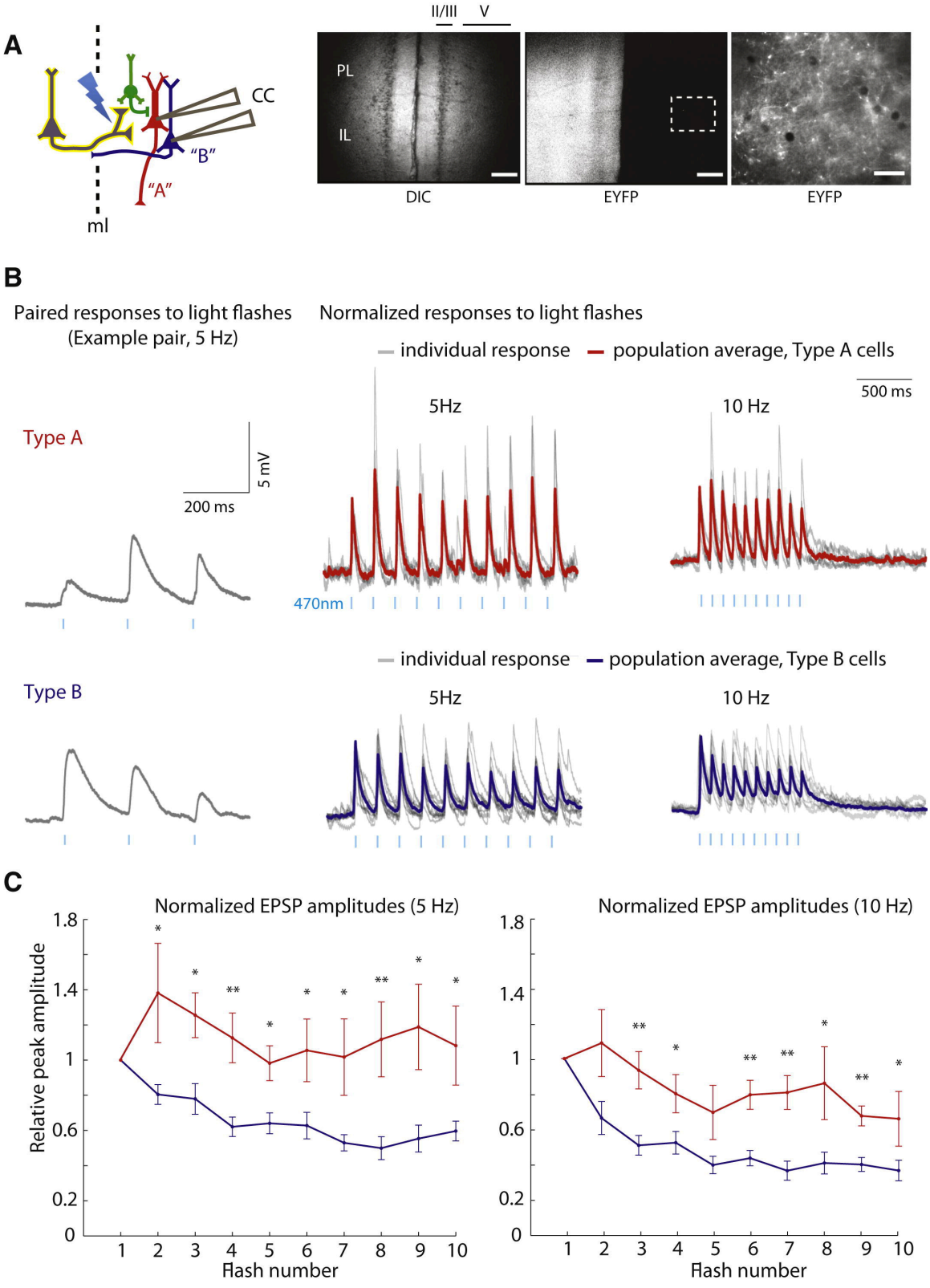

FIGURE 1. EPSP dynamics differ across subtypes of L5 pyramidal neurons.

(A) Experimental design: we simultaneously recorded from a Type A (red) and

Type B (blue) pyramidal neuron while activating ChR2-expressing inputs (yellow) from the contralateral mPFC. Low-power images of mPFC, including the prelimbic and infralimbic cortices (PL and IL), showing a DIC image (left) and ChR2-EYFP expression (middle) (scale bar=50 μm). Right: High-power image of the dotted region in the middle panel, showing ChR2-EYFP expression in axon terminals from the contralateral mPFC (scale bar=12.5 mm). **(B)** Paired responses of Type A and B neurons to 5 Hz light stimulation in current clamp (left). Population average (bold) and individual (grey) current clamp responses to 5 Hz (middle) and 10 Hz (right) stimulation. **(C)** Normalized EPSP amplitudes during trains of light flashes in Type A and B neurons with subthreshold responses (n=8/11 pairs). *=$p<0.05$, **=$p<0.01$.

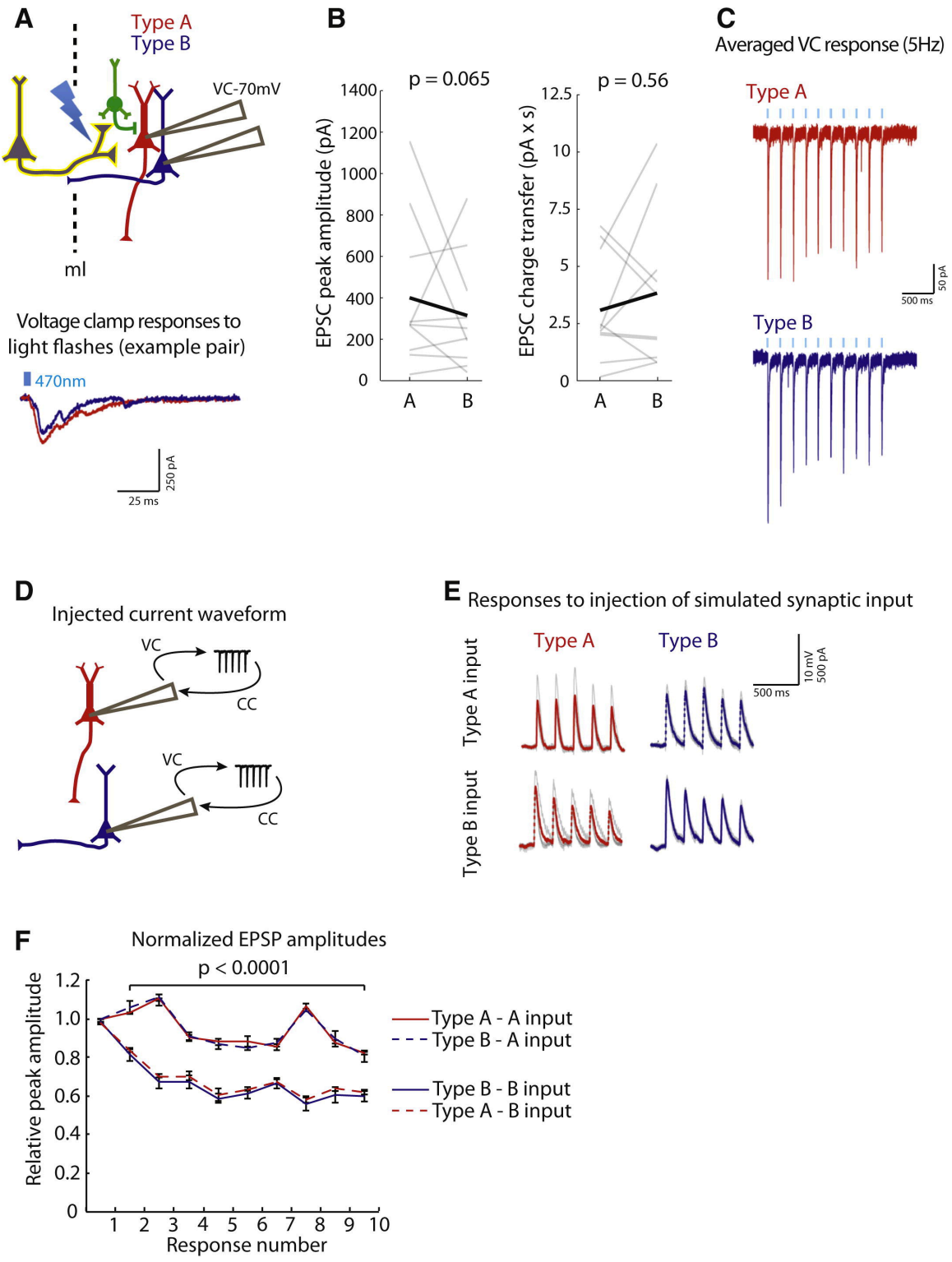

FIGURE 2. Subtype-specific synaptic responses in L5 pyramidal cells depend on presynaptic inputs. (A) Left: simultaneous recordings were made

from Type A (red) and B (blue) neurons in voltage clamp at -70 mV while optogenetically stimulating callosal inputs (yellow). Example voltage traces from a Type A/B pair (bottom). **(B)** EPSC peak amplitude (left) and charge transfer (right) for each cell type**. (C)** Normalized, averaged voltage clamp responses to 5 Hz light stimulation in Type A (red) and B (blue) neurons (n=11 pairs). **(D)** Normalized, averaged voltage clamp responses of Type A and B neurons to callosal input were played back in current clamp to Type A or B neurons. **(E)** Population (bold) and individual (grey) current clamp responses to these averaged waveforms representing callosal inputs to either Type A or B neurons. **(F)** Normalized EPSP amplitudes in response to injection of Type A or B waveforms. (n=4 for each condition)

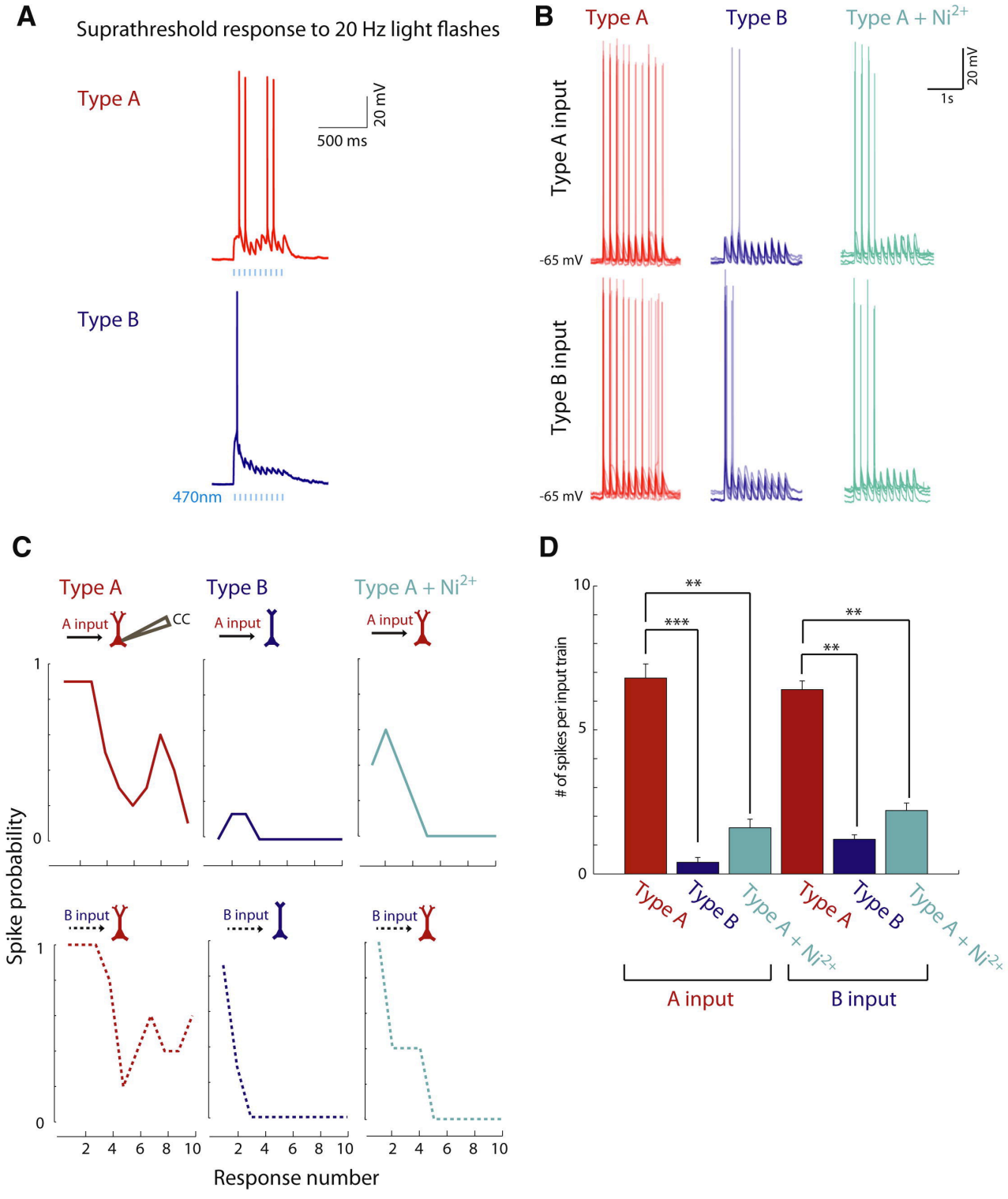

FIGURE 3. Postsynaptic Ca^{2+} currents contribute to increased spiking in Type A neurons.

(A) Example of paired Type A/B responses illustrating greater spiking in Type A neurons. **(B)** Population overlay of responses of either Type A (red) or B (blue) neurons to Type A or B current waveforms. Type A neuron responses in Ni^{2+} are in green. Steady current was injected to maintain all resting membrane potentials at -65 ± 2 mV. **(C)** Spike probability for each simulated light pulse during injection of Type A or B current waveforms into postsynaptic Type A or B neurons. Type A neurons spiked more, regardless of the type of input waveform (A vs. B). Ni^{2+} dramatically reduces spiking in Type A neurons. **(D)** Number of spikes per train of ten simulated inputs. **=$p<0.01$, ***=$p<0.001$, n=5 for each condition.

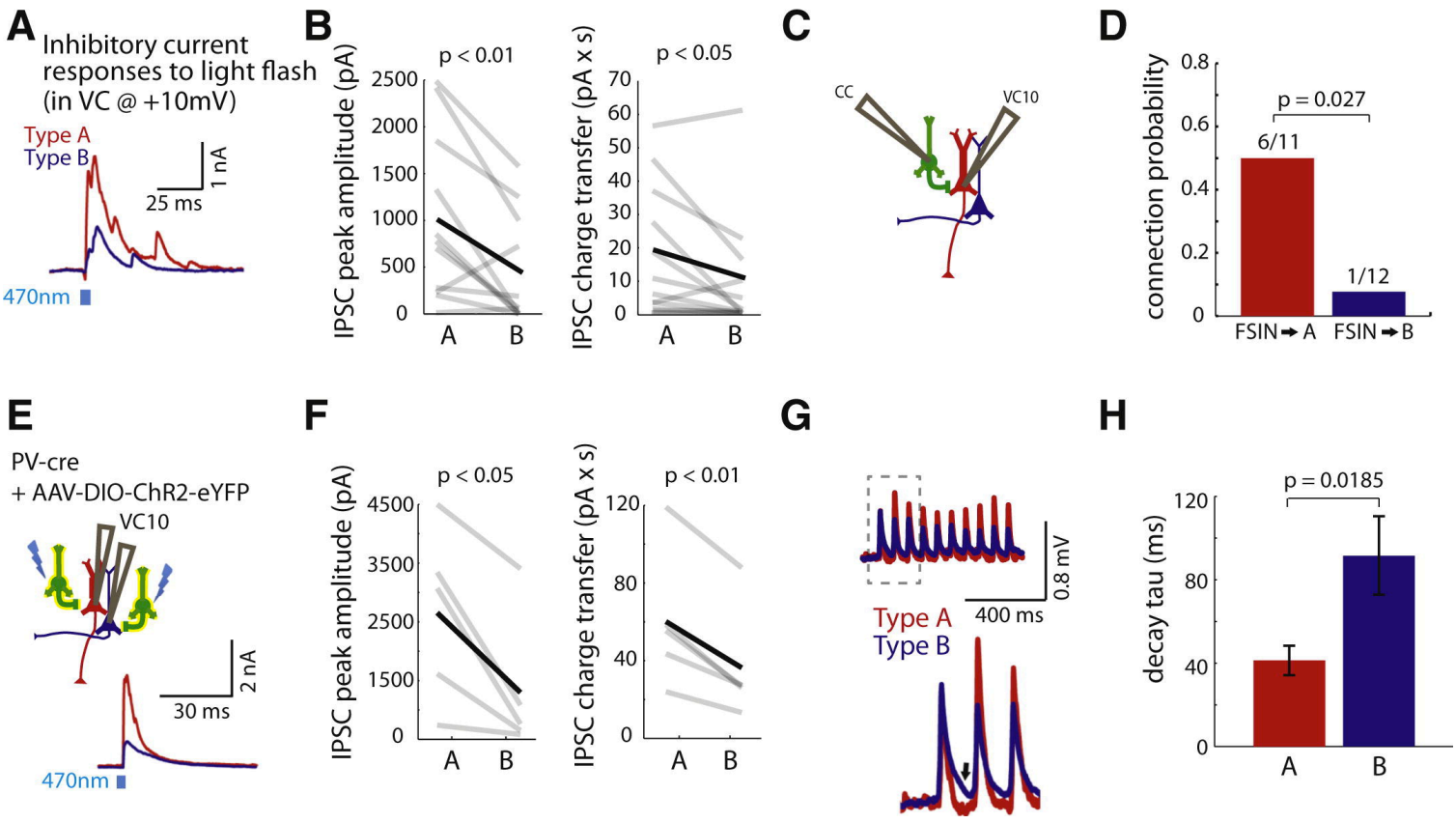

FIGURE 4. Fast-spiking parvalbumin interneurons preferentially inhibit Type A neurons. (A) Simultaneous recordings of IPSCs in a Type A and B neuron during optogenetic stimulation of callosal inputs. Cells were voltage clamped at +10mV. **(B)** Peak IPSC amplitude (left) and inhibitory charge transfer (right) were larger in Type A neurons compared to simultaneously recorded Type B neurons (respectively, n=11 pairs). **(C)** We made simultaneous current clamp (CC) recordings from a fast-spiking interneuron (FSIN, green) and voltage clamp recordings from either a Type A or B neuron. Current was injected to elicit FSIN spiking while recording from the pyramidal neuron in voltage clamp at +10mV (VC10). **(D)** The connection probability from FSINs was greater onto Type A neurons than Type B neurons (n=23 pairs). **(E)** Experimental design: We

recorded simultaneously from a Type A and B neuron in PV::Cre mice injected with virus to drive Cre-dependent ChR2-EYFP expression (yellow, left). During optogenetic stimulation of ChR2-expressing PV interneurons, we recorded simultaneous IPSCs in Type A and B neurons (bottom right). **(F)** PV interneuron-mediated IPSC peak amplitude (left) and inhibitory charge transfer (right) were greater in Type A than Type B neurons (n=5 pairs). **(G)** Normalized, averaged EPSPs in Type A and B neurons following optogenetic stimulation of callosal inputs. Type A neurons (red) repolarize faster (arrow marks repolarization). **(H)** The decay time constant of callosally-evoked EPSPs is faster in Type A neurons (n=11 pairs).

FIGURE S1

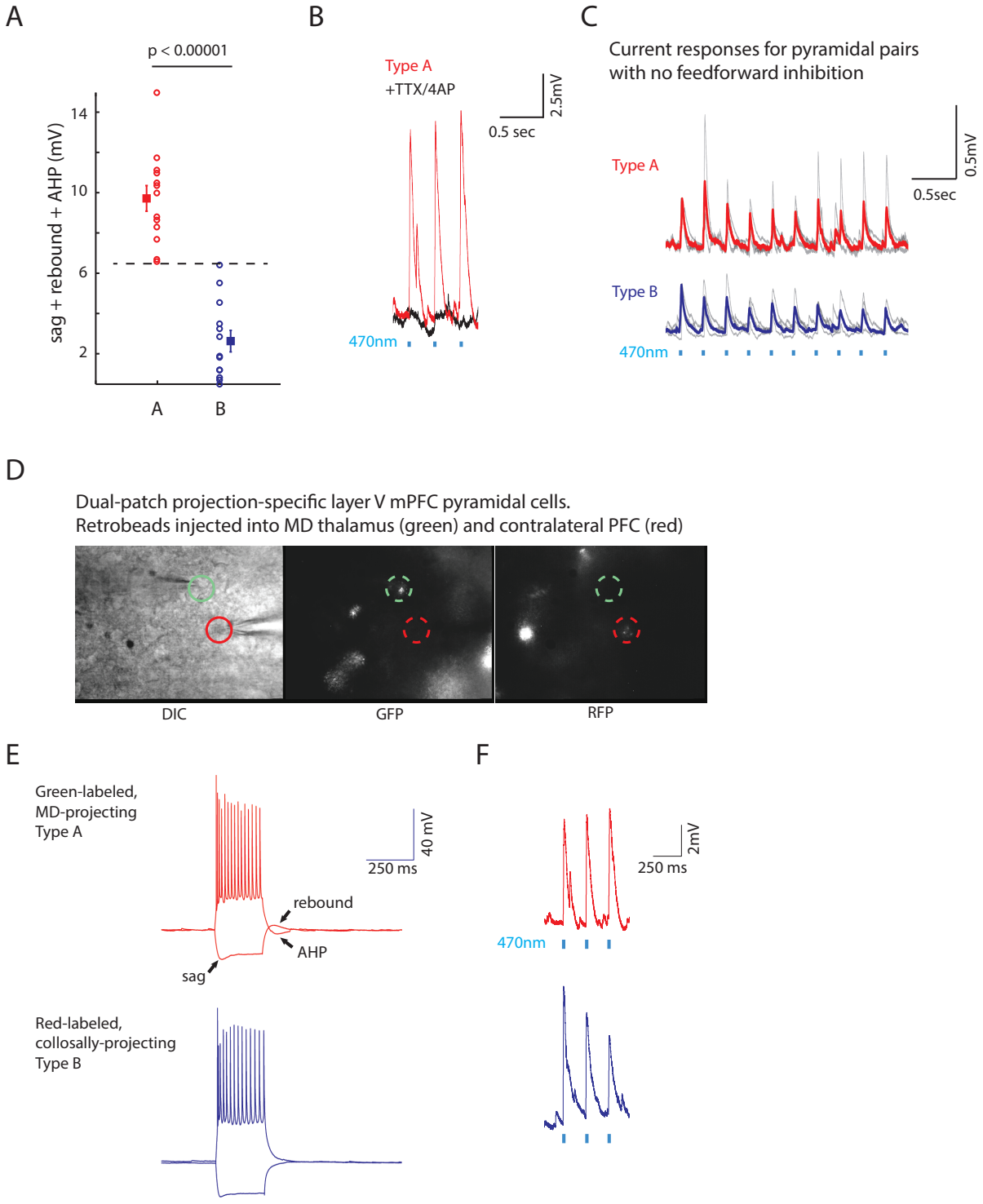

FIGURE S1. Classification of Type A and B neurons, and differences between callosal EPSPs in Type A and B neurons, Related to Fig. 1. (A)

Classification of Type A and Type B neurons based on a combination of the sag and rebound in response to a -250 pA pulse, and the afterhyperolarization (AHP) following a +250pA current pulse. Type A neurons were classified as cells with combined values >6.5 mV (dotted line). (B) Application of TTX and 4-AP eliminates excitatory responses to optogenetic stimulation of callosal projections. (C) EPSP dynamics in simultaneously recorded Type A and B neurons in cases that failed to evoke circuit inhibition (n = 3 pairs). These experiments have a similar latency to EPSP peak as our other experiments (15.4 ± 2.1 msec in these experiments, compared to 13.8 ± 1.8 msec in our complete dataset; p = 0.64). In these experiments, the difference between the pattern of EPSPs in Type A and B neurons was also similar to our other experiments. Specifically, the ratio between the second and first response was 1.57 ± 0.57 in Type A cells, and 0.77 ± 0.13 and in Type B cells, compared to 1.25 ± 0.18 and 0.78 ± 0.15 respectively in our complete dataset. (D) Representative image of Type A (green) and Type B (red) neurons labeled with retrogradely transported fluorescent microspheres injected into the MD thalamus (red) and contralateral mPFC (green), respectively. (E) Current clamp responses of labeled Type A (coticothalamic, CT) and B (cortiocallosal, CC) neurons to injection of -250pA. (F) Optogenetic stimulation of callosal inputs elicit depressing EPSPs in labeled Type B (CC) neurons, but not in labeled Type A (CT) neurons.

FIGURE S2

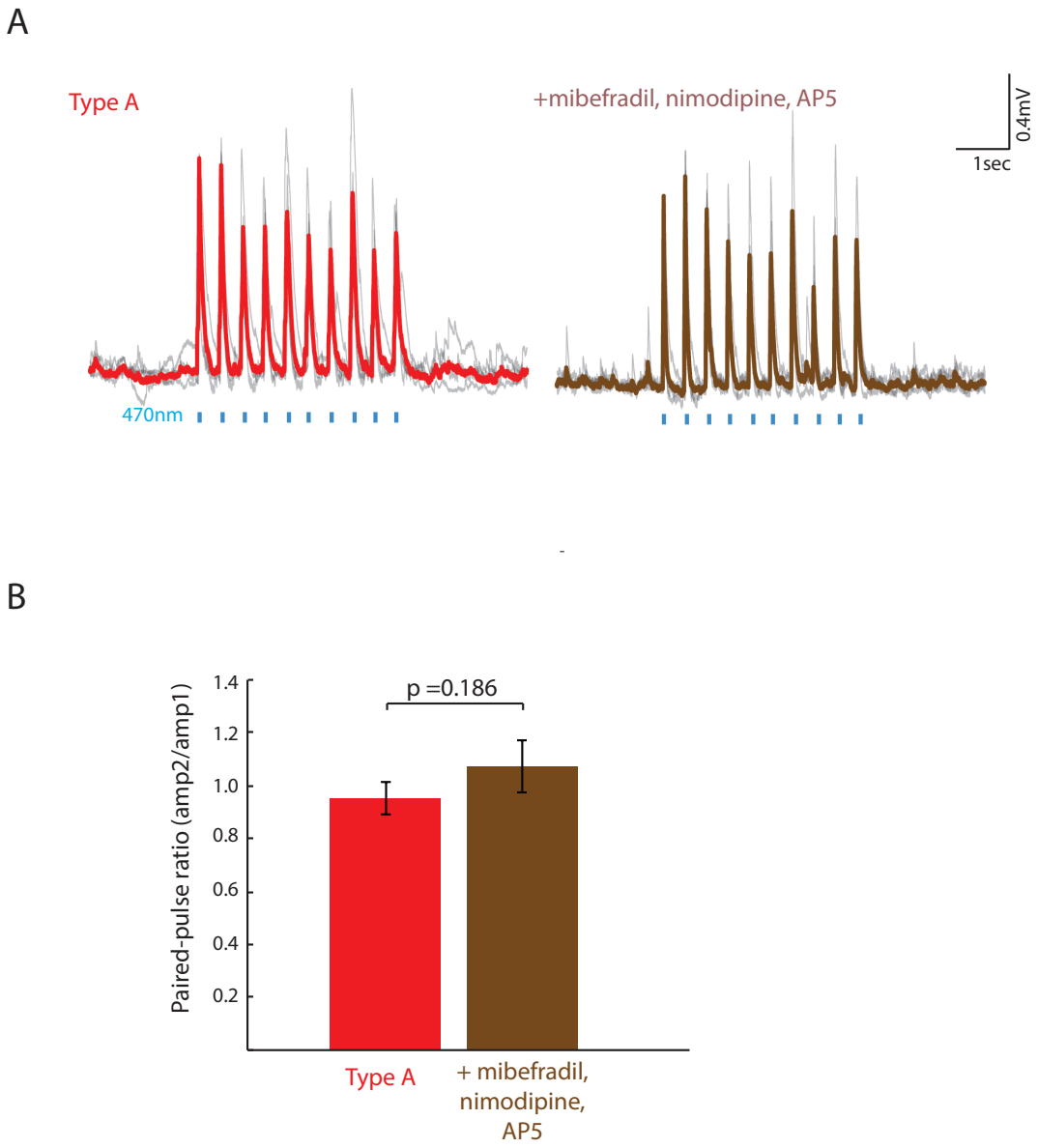

FIGURE S2. Blocking post-synaptic voltage-dependent Ca^{2+} channels and NMDARs does not alter EPSP dynamics in Type A neurons, Related to Fig.

2. (A) Application of mibefradil (5 μM) + nimodipine (5 μM) + AP5 (50 μM) does not alter EPSP dynamics in Type A during optogenetic stimulation of callosal inputs (n = 4). (B) The paired-pulse ratio is not significantly different after applying these Ca^{2+}channel blockers (p = 0.19, n = 4).

FIGURE S3

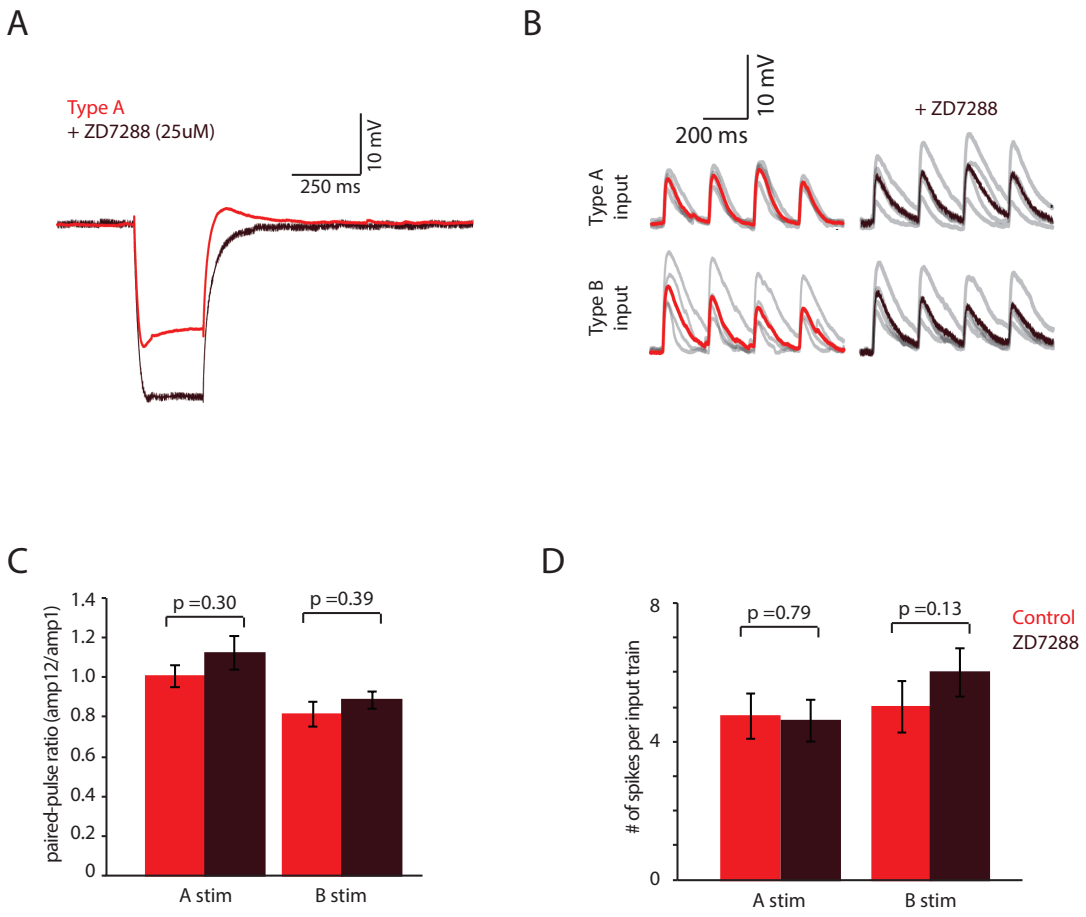

FIGURE S3. Blocking h-current has minimal effects on simulated EPSPs and spiking in Type A neurons, Related to Fig. 3. (A) ZD7288 (25 μM) blocks Ih in Type A neurons. (B) ZD7288 (brown) has minimal effects on the current clamp responses of Type A neurons to injection of Type A or B current waveforms (averaged response shown in black, individual responses shown in gray). (C) The paired-pulse ratio during responses of Type A neurons to simulated EPSCs in these current waveforms is not significantly altered by blocking Ih current (p = 0.30 and 0.39 for Type A and B waveforms, respectively;

n=4 cells). (D) Blocking Ih with ZD7288 also fails to significantly alter the amount of spiking in Type A neurons in response to scaled up, suprathreshold current waveforms (p = 0.79 and 0.13 for Type A and B waveforms, respectively; n=4 cells).

FIGURE S4

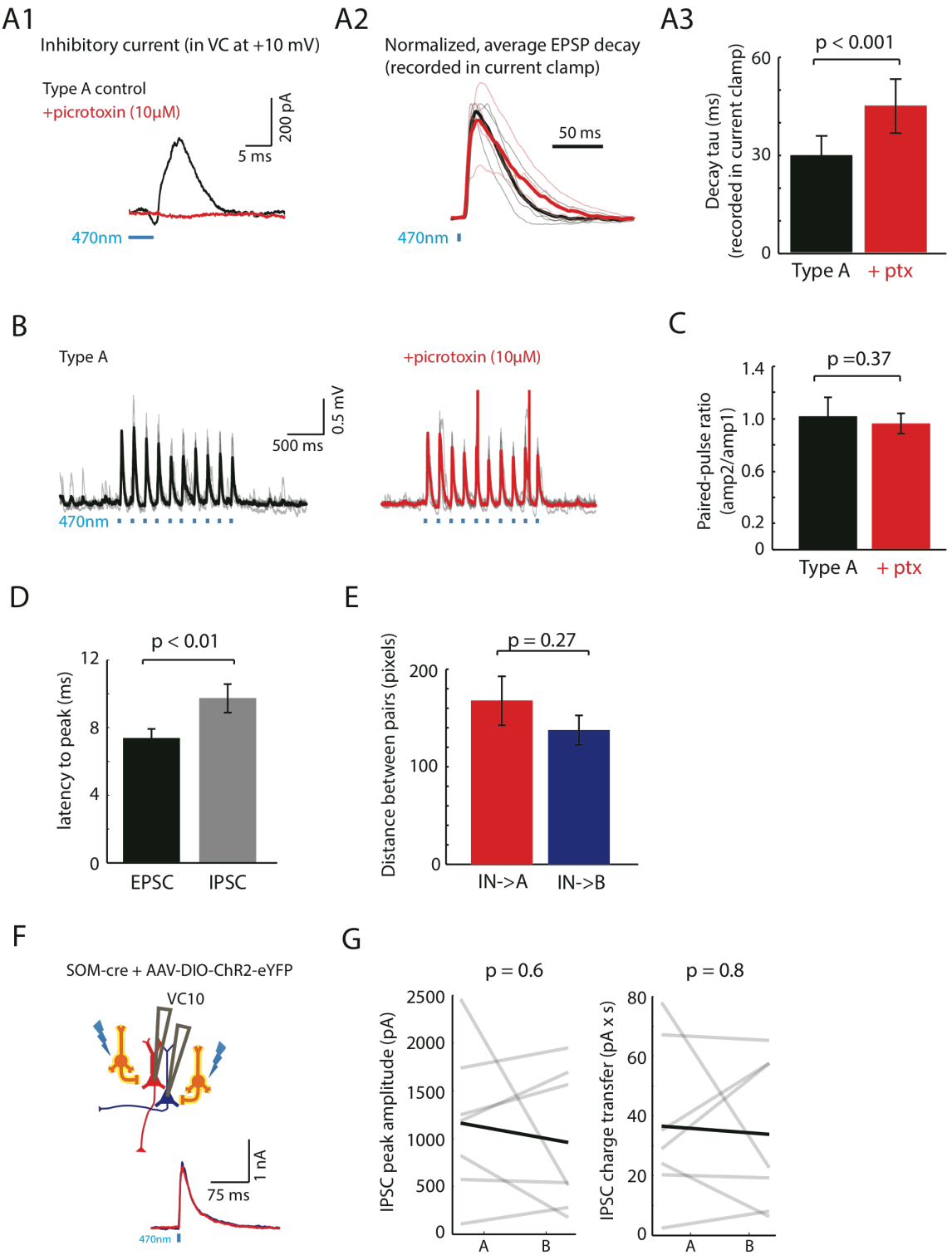

FIGURE S4. Effects of blocking GABAARs on EPSPs, and measuring inhibitory inputs to Type A and B neurons, Related to Fig. 4. (A) A1:

Picrotoxin (ptx; 10 μM) blocks outward currents that follow optogenetic stimulation of callosal inputs and represent feedforward inhibition in Type A neurons. A2: Ptx application prolongs EPSPs in Type A neurons evoked by optogenetic stimulation of callosal inputs. Thick lines represent the averaged EPSPs before (black) and after (red) ptx application. Before averaging, each EPSP trace was normalized by the average amplitude of control EPSPs in that cell. Thin lines show individual normalized responses. A3: Ptx significantly prolongs the decay time constant for callosal EPSPs in Type A neurons (n=4 cells; $p<0.001$ by repeated measures ANOVA). (B) The dynamics of callosal EPSPs in Type A neurons are not significantly altered by application of ptx (black). To avoid epileptiform discharges, the light power was reduced to ~0.2 mW/mm2, i.e. 10% of the typical power, for some of these experiments. Spikes during responses in ptx have been truncated. (C) Ptx does not significantly alter the paired-pulse ratio for Type A neuron responses to optogenetic stimulation of callosal inputs ($p = 0.37$, n=4 cells). (D) Inhibitory currents peak ~2 msec after excitatory currents during optogenetic stimulation of callosal inputs ($p < 0.01$). (E) The average distance between FSINs and Type A or B neurons during experiments to measure connectivity from FSIN to these two subtypes ($p = 0.271$). (F) Experimental design: We simultaneously recorded from a pair of Type A (red) and B (blue) neurons in SOM::Cre mice injected with virus to drive Cre-dependent ChR2-EYFP expression (orange). During optogenetic stimulation of ChR2-expressing SOM interneurons, we recorded simultaneous IPSCs in Type A and B neurons in voltage clamp at +10 mV (bottom). (G) The peak amplitude of

SOM interneuron-mediated IPSCs (left) and the corresponding inhibitory charge transfer (right) were similar in Type A and B neurons ($p = 0.6$ and $p = 0.8$, respectively; $n=7$ pairs).

REFERENCES

Branco, T., and Hausser, M. (2011). Synaptic integration gradients in single cortical pyramidal cell dendrites. Neuron *69*, 885-892.

Brown, S.P., and Hestrin, S. (2009). Intracortical circuits of pyramidal neurons reflect their long-range axonal targets. Nature *457*, 1133-1136.

Curtis, C.E., and Lee, D. (2010). Beyond working memory: the role of persistent activity in decision making. Trends Cogn Sci *14*, 216-222.

Dembrow, N.C., Chitwood, R.A., and Johnston, D. (2010). Projection-specific neuromodulation of medial prefrontal cortex neurons. J Neurosci *30*, 16922-16937.

Farinas, I., and DeFelipe, J. (1991). Patterns of synaptic input on corticocortical and corticothalamic cells in the cat visual cortex. I. The cell body. J Comp Neurol *304*, 53-69.

Fino, E., and Yuste, R. (2011). Dense inhibitory connectivity in neocortex. Neuron *69*, 1188-1203.

Funahashi, S., Bruce, C.J., and Goldman-Rakic, P.S. (1989). Mnemonic coding of visual space in the monkey's dorsolateral prefrontal cortex. J Neurophysiol *61*, 331-349.

Gee, S., Ellwood, I., Patel, T., Luongo, F., Deisseroth, K., and Sohal, V.S. (2012). Synaptic activity unmasks dopamine D2 receptor modulation of a specific class of layer V pyramidal neurons in prefrontal cortex. J Neurosci *32*, 4959-4971.

Hattox, A.M., and Nelson, S.B. (2007). Layer V neurons in mouse cortex projecting to different targets have distinct physiological properties. J Neurophysiol *98*, 3330-3340.

Krook-Magnuson, E., Varga, C., Lee, S.H., and Soltesz, I. (2012). New dimensions of interneuronal specialization unmasked by principal cell heterogeneity. Trends Neurosci *35*, 175-184.

Le Be, J.V., Silberberg, G., Wang, Y., and Markram, H. (2007). Morphological, electrophysiological, and synaptic properties of corticocallosal pyramidal cells in the neonatal rat neocortex. Cereb Cortex *17*, 2204-2213.

Lewis, D.A., Hashimoto, T., and Volk, D.W. (2005). Cortical inhibitory neurons and schizophrenia. Nat Rev Neurosci *6*, 312-324.

Marenco, S., Stein, J.L., Savostyanova, A.A., Sambataro, F., Tan, H.Y., Goldman, A.L., Verchinski, B.A., Barnett, A.S., Dickinson, D., Apud, J.A.*, et al.* (2012). Investigation of anatomical thalamo-cortical connectivity and FMRI activation in schizophrenia. Neuropsychopharmacology *37*, 499-507.

Morishima, M., and Kawaguchi, Y. (2006). Recurrent connection patterns of corticostriatal pyramidal cells in frontal cortex. J Neurosci *26*, 4394-4405.

Morishima, M., Morita, K., Kubota, Y., and Kawaguchi, Y. (2011). Highly differentiated projection-specific cortical subnetworks. J Neurosci *31*, 10380-10391.

Packer, A.M., and Yuste, R. (2011). Dense, unspecific connectivity of neocortical parvalbumin-positive interneurons: a canonical microcircuit for inhibition? J Neurosci *31*, 13260-13271.

Petreanu, L., Huber, D., Sobczyk, A., and Svoboda, K. (2007). Channelrhodopsin-2-assisted circuit mapping of long-range callosal projections. Nat Neurosci *10*, 663-668.

Potter, G.B., Petryniak, M.A., Shevchenko, E., McKinsey, G.L., Ekker, M., and Rubenstein, J.L. (2009). Generation of Cre-transgenic mice using Dlx1/Dlx2 enhancers and their characterization in GABAergic interneurons. Mol Cell Neurosci *40*, 167-186.

Ripke, S., Sanders, A.R., Kendler, K.S., Levinson, D.F., Sklar, P., Holmans, P.A., Lin, D.Y., Duan, J., Ophoff, R.A., Andreassen, O.A.*, et al.* (2011). Genome-wide association study identifies five new schizophrenia loci. Nat Genet *43*, 969-976.

Schiller, J., Major, G., Koester, H.J., and Schiller, Y. (2000). NMDA spikes in basal dendrites of cortical pyramidal neurons. Nature *404*, 285-289.

Sheets, P.L., Suter, B.A., Kiritani, T., Chan, C.S., Surmeier, D.J., and Shepherd, G.M. (2011). Corticospinal-specific HCN expression in mouse motor cortex: Ih-dependent synaptic integration as a candidate microcircuit mechanism involved in motor control. J Neurophysiol.

Sohal, V.S., Zhang, F., Yizhar, O., and Deisseroth, K. (2009). Parvalbumin neurons and gamma rhythms enhance cortical circuit performance. Nature *459*, 698-702.

Varga, C., Lee, S.Y., and Soltesz, I. (2010). Target-selective GABAergic control of entorhinal cortex output. Nat Neurosci *13*, 822-824.

Wang, M., Vijayraghavan, S., and Goldman-Rakic, P.S. (2004). Selective D2 receptor actions on the functional circuitry of working memory. Science *303*, 853-856.

Wang, Y., Markram, H., Goodman, P.H., Berger, T.K., Ma, J., and Goldman-Rakic, P.S. (2006). Heterogeneity in the pyramidal network of the medial prefrontal cortex. Nat Neurosci *9*, 534-542.

CHAPTER 4

Dopamine D1 and D2 receptors have opposing effects on network activity in a subpopulation of prefrontal neurons

ABSTRACT

We previously showed that activating dopamine D2 receptors (D2Rs) in a specific subpopulation of L5 pyramidal neurons ("type A neurons") within the prefrontal cortex elicits afterdepolarizations that depend on Ca^{2+} influx via voltage-gated Ca^{2+} channels (VGCCs). Although these afterdepolarizations followed depolarizing current pulses, they only occurred when NMDA receptors (NMDARs) were also activated, suggesting that this D2R-mediated increase in excitability might powerfully modulate type A neuron responses to synaptic input. Here, we show that indeed, D2R activation increases responses of type A neurons to synaptic inputs, and these effects depend on NMDARs and Ca^{2+} influx via VGCCs. Specifically, we used weak optogenetic stimulation to evoke network activity in prefrontal brain slices from Thy1-ChR2 mice. This network activity led to spikes in type A neurons that were driven by synaptic input and enhanced by D2R activation. This D2R-induced increase in synaptically-driven spiking was eliminated by chelating internal Ca^{2+} or by blocking NMDARs or VGCCs. Interestingly, we also found that type A neurons integrated their inputs over tens of milliseconds; this also depends on Ca^{2+} influx via NMDARs and VGCCs and was enhanced by D2R activation. Surprisingly, D1Rs, which have previously been shown to excite a distinct subpopulation of L5 pyramidal neurons, suppressed D2R-mediated increases in type A neuron excitability. These results demonstrate (1) how a combination of synaptic and intrinsic mechanisms can facilitate temporal integration, and (2) how dopamine

might bi-directionally modulate prefrontal function via opposing D1 and D2R-mediated effects on the responses of specific L5 pyramidal neurons to network activity.

INTRODUCTION

Recurrent networks within layer 5 (L5) of the prefrontal cortex (PFC) generate activity that underlies working memory and other components of executive function (Shepherd, 2013). Dopamine acts through two classes of receptors, “D1-like” or “D2-like,” to modulate prefrontal neurons and their activity, including activity associated with cognitive tasks (Sawaguchi and Goldman-Rakic, 1994; Seamans and Durstewitz 2001; Wang and Goldman-Rakic 2004; Tseng and O’Donnell 2005). This has led to the hypothesis that prefrontal networks operate in two distinct functional states, depending on which class of dopamine receptors is activated (Seamans and Durstewitz, 2008). According to this scheme, D1 receptor (D1R) activation makes the prefrontal network relatively insensitive to incoming input, whereas D2R activation allows incoming inputs to evoke large changes in prefrontal activity. These actions are hypothesized to exert corresponding effects on PFC-dependent behavior. Indeed, intra-PFC infusion of D1 antagonists or agonists can increase or decrease the exploration of new behavioral strategies, respectively, whereas D2 antagonists and agonists have the opposite effects (St Onge et al., 2011). Alterations of this dopaminergic modulation of PFC may contribute to cognitive dysfunction in disorders including schizophrenia (Winterer and Weinberger 2004; Durstewitz and Seamans 2008). Thus, it is critical to understand the mechanisms through which dopamine modulates prefrontal network activity.

Recent studies have elucidated how subtypes of L5 pyramidal neurons within the PFC are differentially modulated by dopamine (Seong and Carter

2012; Wang and Goldman-Rakic 2004; Gee and Ellwood et al., 2012). Specifically, one subtype, which we call “type A,” consists of subcortically projecting neurons that have a prominent h-current (I_h) and express D2 receptors (D2Rs). The other subtype, “type B,” consists of intracortically projecting neurons that have a less prominent I_h, and lack D2Rs (Gee and Ellwood et al., 2012). We previously found that D2R activation elicits a Ca^{2+} dependent afterdepolarization in type A, but not type B, neurons. Another study found that D1R activation increases excitability specifically within type B neurons. While these studies describe how dopamine affects responses of prefrontal neurons to current injection, our knowledge of how dopamine receptors can modulate the responses of specific subtypes of prefrontal neurons to synaptic inputs during network activity remains limited.

Based on these previous studies, we hypothesized that D2Rs enhance the responses of type A neuron to synaptic inputs. Here, we found that D2R activation enhanced type A neuron spikes that are driven by synaptic input during optogenetically-evoked network activity in prefrontal slices. Consistent with our previous study, this phenomenon depends on NMDARs as well as Ca^{2+} influx via voltage-gated Ca^{2+} channels. Notably, this increase in type A neuron excitability also enhanced temporal summation between optogenetic inputs delivered tens of milliseconds apart. Surprisingly, activating D1Rs suppressed both D2R-induced afterdepolarizations in type A neurons, and the D2R-induced increase in type A neuron spikes driven by synaptic input during optogenetically evoked network activity. These results show how dopamine, acting through D1Rs and D2Rs, can

bi-directionally modulate a cellular phenomenon and thereby regulate prefrontal network activity that mediates critical aspects of working memory and behavioral flexibility.

METHODS

All experiments were conducted in accordance with procedures established by the Administrative Panels on Laboratory Animal Care at the University of California, San Francisco.

Slice preparation. Slice preparation and intracellular recording followed our published protocol (Sohal and Huguenard, 2005). We cut 250 mm coronal slices from 8- to 10-week-old mice of either sex. We used the Thy1-ChR2-YFP founder line 18 transgenic mouse line (Jackson Labs). We secured the slice by placing a harp along the midline between the two hemispheres.

Intracellular recording. We obtained somatic whole-cell patch recordings from visually identified pyramidal cells in layer 5 of infralimbic or prelimbic cortex using differential contrast video microscopy on an upright microscope (BX51WI; Olympus). Recordings were made using a Multiclamp 700A (Molecular Devices). Except when otherwise noted, patch electrodes (tip resistance = 2–6 MOhms) were filled with the following (in mM): 130 K-gluconate, 10 KCl, 10 HEPES, 10 EGTA, 2 MgCl, 2 MgATP, and 0.3 NaGTP (pH adjusted to 7.3 with KOH). ACSF contained the following (in mM): 126 NaCl, 26 $NaHCO_3$, 2.5 KCl, 1.25 NaH_2PO_4, 1 $MgCl_2$, 2 $CaCl_2$, and 10 glucose. In experiments that used tetraethylammonium chloride (TEA), the amount of NaCl was decreased by a corresponding amount (30 mM) to maintain the osmolarity of the extracellular solution. All recordings were at 32.5 ± 1°C. Series resistance was usually 10–20 MΩ, and experiments were discontinued above 30 MΩ.

Drug application. For electrophysiology, all drugs were dissolved in water (quinpirole, NMDA, DL-AP5, CNQX) or dimethylsulfoxide (sulpiride, mibefradil, nickel, and nimodipine) before being diluted in ACSF. Throughout the text, APV refers to DL-AP5, quinpirole refers to (-)quinpirole, and sulpiride refers to (-)sulpiride.

ChR2 stimulation. We stimulated ChR2 in pyramidal neurons using flashes of light generated by a Lambda DG-4 high-speed optical switch with a 300W Xenon lamp, and an excitation filter set centered around 470 nm, delivered to the slice through a 40X objective (Olympus). Illumination was delivered across a full high-power (40X) field. Light power was adjusted to ~0.1mW/mm^2 using neutral density filters.

Statistical analysis. We used Student's t tests to compare pairs of groups,

RESULTS

Optogenetic stimulation in prefrontal slices from Thy1-ChR2 mice elicits recurrent network activity

To study the effects of D2R modulation on network activity, we performed whole cell recordings in type A neurons within L5 of the mPFC using acute brain slices from Thy1-ChR2-EYFP founder line 18 transgenic mice (Thy1-ChR2 mice; Jackson Labs), in which cortical expression of ChR2 is limited to L5 (Arenkiel et al., 2007). We identified type A neurons by the promnince of the I_h-induced sag and rebound in response to hyperpolarizing current injection (Gee and Ellwood et al, 2012). In current clamp, we measured responses to random trains of light flashes (470 nm; ~0.1 mW/mm^2, 1 ms pulses, 50-500Hz, ~20 flashes/train; 20 trains/ cell; Figure 1A). Notably, these light flashes used relatively low light intensities, which minimized ChR2 desensitization. Responses were driven by a contribution of synaptic currents and direct, ChR2-mediated current (Figure 1A,E). In voltage clamp light flashes elicited excitatory responses (-306 ± 45 pA; n = 7) at a holding potential of -70mV and inhibitory responses (988 ± 251 pA) at a holding potential of +10mV (Figure 1B and 1C). The onset of excitatory and inhibitory currents occurred ~0.5 and 5 msec following each light flash, respectively, suggesting disynaptic inhibition.

In current clamp, we measured the probability of spiking in response to random light trains. At a light intensity of ~0.1mW/mm^2, approximately 10% of light flashes elicited action potentials (Figure 1A). We plotted the probability of

spiking against the normalized excitatory and inhibitory current. As expected, the probability of spiking was highest after the onset of excitatory current and prior to the onset of inhibitory current (Figure 1D). However, a surprising number of spikes, which we refer to as “late spikes,” occurred >10ms following light flashes. Because ChR2-mediated currents decay after 5-10 msec we reasoned that these spikes were likely to be driven by synaptic currents associated with network activity in L5. To test this possibility, we recorded before and after applying CNQX and APV to block excitatory synaptic currents and network activity. Indeed, late spikes were abolished when excitatory synaptic activity was blocked (Fig 1F).

D2R activation increases synaptic input-driven late spikes

We sought to determine if D2R activation modulated the late spikes we observed during optogenetically evoked network activity. In the presence of the D2R agonist quinpirole (5 μM), the probability that a light flash evoked a late spike increased from 1.7 ± 0.5% in control conditions to 4.0 ± 0.9% ($p < 0.01$; n = 23 cells) (Figure 2A,B,D). This increase was reversed by subsequent application of the selective D2R antagonist sulpiride (5 μM); (from 2.7 ± 1.8% to 0.9 ± 0.9%; $p < 0.05$; n = 5 cells; Figure 2B), confirming that this increase in late spikes was mediated by D2Rs.

We also measured the probability of spiking <10ms after each light flash. Quinpirole also increased the probability of spiking <10ms compared from 16 ± 2% in control conditions to 22 ± 4% ($p < 0.05$; n = 23 cells), demonstrating that

the increase in late spikes reflects an increase in Type A neuron excitability, not just a delay in spiking. However we focused on late spikes, as they required synaptic input and thus served as a measure of responses to network activity.

The quinpirole-mediated increase in spiking requires NMDARs and postsynaptic Ca^{2+} channels

In a previous study, we found that the quinpirole-induced afterdepolarizarion in type A neurons depended on NMDARs and voltage-gated Ca^{2+} channels (VGCCs), specifically L-type Ca^{2+} channels (Gee and Ellwood et al., 2012). We therefore wanted to test if the increase in synaptic input-driven spiking occurred via a similar mechanism. Indeed, we found that NMDA blockade by AP5 eliminated the quinpirole-induced late spikes (Figure 3). Next, we tested if Ca^{2+} channels were required for this effect by either nonspecifically blocking VGCCs with Ni^{2+} (500 μM), specifically blocking L-type channels with nimodipine (5 μM), or blocking L- and T-type channels with nimodipine plus mibefradil (5 μM). We found that Ni^{2+} (500 μM), or a combination of nimodipine (5μM) and mibefradil (5μM) were sufficient to eliminate the late spikes elicited by quinpirole (Figure 4B and 4C), suggesting that D2Rs might act through a combination of L- and T-type Ca^{2+} channels to increase spike probability. However, nimodipine alone was not sufficient to significantly reduce late spikes.

Downstream effects of Ca^{2+} influx via L- or T-type Ca^{2+} channels could mediate the D2R-mediated increase in late spikes. If this is true, then including the Ca^{2+} chelator BAPTA in the intracellular recording solution should prevent the

increase in late spikes following D2R activation. To test this, we repeated the same experiments while including BAPTA (5 mM) in the intracellular solution. In 5/5 cells, BAPTA prevented quinpirole from inducing an increase in late spikes, demonstrating that this effect is cell autonomous and requires postsynaptic Ca^{2+} influx (Fig. 4A,C). For example, an alternative explanation for the quinpirole-induced increase in late spikes would be that quinpirole increases activity throughout the network, and that this generalized increase in network activity is sufficient to enhance activity in the cell from which we are recording. However in that scenario, BAPTA would not abolish the quinpirole-induced increase in late spikes.

D2R activation enhances temporal integration

So far, we have shown that synaptic input drives late spikes, and these are enhanced by D2R activation through a mechanism that depends on Ca^{2+} influx. Next, we looked for other aspects of network activity, besides late spikes, that might be sensitive to D2R activation. Interestingly, we found that in our paradigm, type A neurons are able to integrate input over ~30-40 msec. Specifically, following a subthreshold light flash, i.e. a flash that fails to elicit a spike, the probability that the next light flash will successfully elicit a spike depends strongly on the time interval between the two flashes (Figure 5A). This probability is ~50% for interflash intervals <10 msec, and drops to <10% for intervals >40 msec. This form of temporal integration, particularly at intervals between 10 and 30 msec, depends on excitatory synaptic input. This can be

seen in Figure 5A – applying CNQX and AP5 reduces the spiking probability at intervals between 10 and 30 miliseconds, but not at very short (<10 msec) or longer (>40 msec) intervals.

Based on the ability of D2Rs to increase late spikes, we hypothesized that D2R activation might enhance temporal summation through a similar mechanism. Indeed, quinpirole enhanced spiking at short (<30ms) interflash intervals (Figure 5B), and consistent with the mechanism described earlier, this effect was not observed when BAPTA was present in the intracellular solution (Figure 5C; n = 5). Bath application of Ni^{2+} (500 μM) also reversed the quinpirole-induced increase in spiking (Figure 5D; n = 5). Taken together, these results demonstrate that type A neurons can integrate inputs over timescales ~40 msec. This integration does not occur solely at the network level (since it can be blocked by intracellular BAPTA), nor can it be observed in neurons that have been synaptically isolated by application of CNQX + AP5. Rather, it reflects interactions between excitatory synaptic input and Ca^{2+} influx via VGCCs that can be enhanced by D2R activation.

D1Rs oppose D2R-mediated effects on spiking

Prefrontal D1 and D2Rs exert opposing effects on decision-making (St. Onge et al., 2011). This made us wonder whether the D2R-induced afterdepolarization (ADP) we previously described in type A cells (Gee and Ellwood et al., 2012) might be opposed by D1R activation. To elicit the ADP, we bath applied quinpirole (5 μM) and NMDA (4 μM). Then, we added the D1R

agonist SKF38393 (SKF, 5 μM) and quantified the ADP by measuring the time for the membrane potential to return to baseline following an injection of depolarizing current (350pA, 250 msec). SKF dramatically suppressed the quinpirole-induced ADP, as indicated by a reduction in the time required for the membrane to return to within 90% of the baseline membrane potential, from 198 ± 60 ms in quinpirole + NMDA, to 60 ± 10 ms after adding SKF (this time was 35 ± 5 ms in control conditions; Figure 5A,C; n = 4 cells).

Based on the ability of D1R activation to suppress the D2R-induced ADP, we hypothesized D1Rs might also oppose effects of D2Rs on type A responses during optogenetically evoked network activity. Indeed, adding SKF after applying quinpirole reduced the probability of observing a late spike after each light flash (Figure 5B,D). Interestingly, SKF did not affect temporal integration in type A neurons, characterized by the probability of spiking as a function of the inter-flash interval (Figure 5E). This suggests that D1R activation reduces type A neuron excitability without directly suppressing Ca^{2+} influx via VGCCs and NMDARs, or the downstream effects of Ca^{2+}, since those effects would be expected to suppress temporal integration. Rather, D1Rs presumably act via some other mechanism that has the effect of reducing the ADP and late spikes.

DISCUSSION

Here we describe mechanisms through which specific L5 pyramidal neurons in the PFC ("type A neurons") process their inputs, and show how these mechanisms are modulated by D1 and D2Rs. We used weak optogenetic stimulation to elicit network activity in type A neurons, inducing spikes that occur >10ms after light flashes and depend on synaptic input. These late spikes were enhanced by D2R activation through a mechanism that depends on NMDARs, voltage-gated Ca^{2+} channels, and intracellular Ca^{2+}, and D1R activation counteracted this effect. We also found that type A neurons can integrate their inputs over tens of milliseconds via a combination of intrinsic and synaptic mechanisms. This phenomenon is also enhanced by D2R activation. As described below, these results illustrate mechanisms through which dopamine can bi-directionally modulate prefrontal function as well as general mechanisms through which neurons may integrate their inputs.

Implications for prefrontal function. Prefrontal activity can be modulated by expected rewards and/or the past history of reward (Wang and Goldman-Rakic 2004; Histed et al., 2009; Bernacchia et al., 2011). Dopamine provides reward-related signals that may drive these effects. *In vitro* studies using current injection have found that D2R activation elicits an afterdepolarization in type A neurons, while D1Rs increase spiking in a distinct population of L5 pyramidal neurons (Gee and Ellwood et al., 2012; Seong and Carter 2012). Although these studies identify cellular mechanisms through which dopamine regulates prefrontal activity, an important next step is understanding

how these changes in cellular excitability influence responses to more physiological forms of input that comprise a mix of excitatory and inhibitory currents, occur in a discrete fashion, and are distributed across time. Our results show that in type A neurons, the cellular effects of D2R activation can amplify responses to such input, resulting in increased spiking at long latencies following input, as well as the enhanced temporal summation of inputs over tens of milliseconds. In this way, dopamine may act through D2Rs to enhance firing in a manner that reflects current, anticipated, or past rewards.

Our results also demonstrate general mechanisms through which neurons can integrate their inputs over time, even when these inputs consist of a combination of excitatory and inhibitory currents. In a recurrent excitatory network, excitatory input recruits excitation as well as feedback inhibition. In general, this feedback inhibition should outlast the excitation in order to prevent runaway excitatory activity. Indeed, this is exactly what we observe (Fig. 1D). However, such long-lasting inhibition interferes with the ability of successive inputs to summate in an additive fashion. Specifically, when a second input arrives >10 msec after the first, excitatory current elicited by the first input will have decayed, while residual feedback inhibition recruited by first input will still be present. Under these conditions, the first input should exert a minimal, or possibly weakly inhibitory, effect on responses to the second input. However, we found that this residual inhibition can be overcome by cell-intrinsic mechanisms. Specifically, the first input triggers Ca^{2+} influx through voltage-gated channels

and NMDARs that enhances the probability of spiking in response to subsequent inputs (Fig. 5), presumably via Ca^{2+}-dependent currents, e.g. I_{CaN}.

These findings are also consistent with the hypothesis that D1Rs and D2Rs exert opposing effects on PFC function, by demonstrating how such opposing effects may arise in part, via opposing actions on individual L5 pyramidal neurons. Specifically, behavioral studies have found opposing effects of activating D1 or D2Rs in the PFC (St. Onge et al., 2008). In addition, an integration of many studies suggests a "dual-state" model for PFC function in which D2R activation elicits variable patterns of PFC activity that support flexible behavior, while D1R activation stabilize patterns of prefrontal activity that serve to maintain items in working memory and/or maintain stable behavioral strategies (Durstewitz and Seamans, 2008). Here we have shown that D1 and D2Rs can bi-directionally modulate cellular excitability (Fig. 6A,C) as well as responses to input (Fig. 6B,D) in type A neurons. This may represent one neural substrate for opposing effects of D1 and D2Rs on network activity and behavior. This could complement the ability of D1 and D2Rs to increase activity in distinct subpopulations of neurons (Gee and Ellwood et al., 2012; Seong and Carter 2012).

Relationship to previous studies. We previously found that activating D2Rs elicits an afterdepolarization in type A neurons that depends on Ca^{2+} influx via L-type Ca^{2+} channels and NMDARs. Here, we found that the mechanism through which D2R activation enhances spiking during optogenetically-evoked network activity also depends on Ca^{2+} influx through voltage-gated Ca^{2+} channels

and NMDARs. However, in this case, we could not abolish the D2R-induced increase in activity by blocking L-type Ca^{2+} channels alone, but only by blocking both L and T-type channels. This suggests that D2Rs are not acting directly on L-type channels, but perhaps on a downstream target, e.g. I_{CaN}.

Our finding that D1Rs can oppose D2R-induced increases in type A neuron excitability contrasts with a study showing that co-activation of NMDARs and D1Rs enhances spontaneous plateau potentials in prefrontal L5 pyramidal neurons (Tseng and O'Donnell, 2005) An important difference between that study and ours is that we measured afterdepolarizations in response to current injection and spiking in response to stereotyped levels of ChR2-evoked network activity, whereas the previous study measured plateau potentials driven by spontaneous network activity. Thus, it is possible that D1Rs suppress the cellular excitability of type A neurons, producing the effects we observed, while simultaneously enhancing spontaneous network activity (possibly via effects on type B neurons) and/or enhancing synaptic inputs to type A neurons. Because we directly activated networks of type A neurons with ChR2, we bypassed spontaneous network activity and some synaptic inputs; as a result, our measurements reflect the responsiveness of type A neurons to input, rather than levels of internally generated activity in the network as a whole. Additionally, unlike the previous study, we did not measure the effects of activating D1Rs alone – only the effects of activating D1Rs after D2Rs had already been activated for some time. Thus, it is possible that activating D1Rs alone would have led to different effects in our experiments.

Our findings also contrast with an earlier study that failed to observe either D1R expression or effects of D1R agonists in type A neurons (Seong and Carter, 2012). There are several possible explanations for this apparent difference. First, the effects we see may not be cell autonomous. Second, the experiments in Seong and Carter (2012) were done in 3-4 week old mice, whereas we studied mice that were at least 8 weeks old. Thus, D1R expression in Type A neurons, which we observed previously (Gee et al., 2012), and/or the physiological effects of D1Rs on Type A neurons described here, may only appear post-adolescence. Finally, the effects we observed may only occur when D1 and D2Rs are co-activated, and may not be evident when only D1Rs are activated.

Limitations and future directions. The brief, weak light flashes we used are likely to activate mainly prefrontal somata, but it is possible that some projections from other regions also contributed to the responses we measured. This would not change our basic finding, that D2R activation can enhance type A responses to synaptic input, but would make the source of such synaptic inputs unclear. Future experiments, using viral approaches, might selectively express ChR2 within the PFC to address this issue.

Although our results suggest a mechanism in which D2R activation enhances type A neuron excitability via a mechanism that depends on Ca^{2+} influx, the details of this mechanism, e.g. whether D2Rs act directly on I_{CaN} or a similar conductance, remain unclear. The specific mechanism that enables D1Rs to oppose effects of D2Rs on type A neurons is also unclear. D1Rs are known to act directly on several intrinsic mechanisms in L5 pyramidal neurons in the PFC

(Durstewitz and Seamans 2008). Alternatively, D1Rs may indirectly suppress type A neuron excitability by acting through another class of cells, e.g. GABAergic interneurons (Seamans and Yang, 2001). Notably, D1R activation suppressed D2R-induced afterdepolarizations and increases in late spikes, but not D2R-induced increases in temporal summation (Fig. 6E), suggesting that D1Rs do not act on exactly the same mechanism as D2Rs.

Finally, the use of ChR2 to directly activate the L5 network is both a strength and limitation. Optogenetic stimulation recruits a combination of excitatory and feedback inhibitory currents, a key feature of network activity *in vivo*. Optogenetic stimulation also evokes relatively stereotyped levels of input, making it possible to focus on how the responsiveness of a type A neuron to similar levels of inputs changes as a result of D2R activation. Thus, by design, this study has not examined how D2Rs might modulate the strength of synaptic inputs to prefrontal neurons. Integrating those effects with our findings will be an important next step.

These results clarify mechanisms through which L5 pyramidal neurons process their input, and ways in which dopamine modulates these mechanisms. This adds to our understanding of how dopaminergic modulation of prefrontal function may contribute to both normal behavior and disorders such as schizophrenia.

FIGURE 1

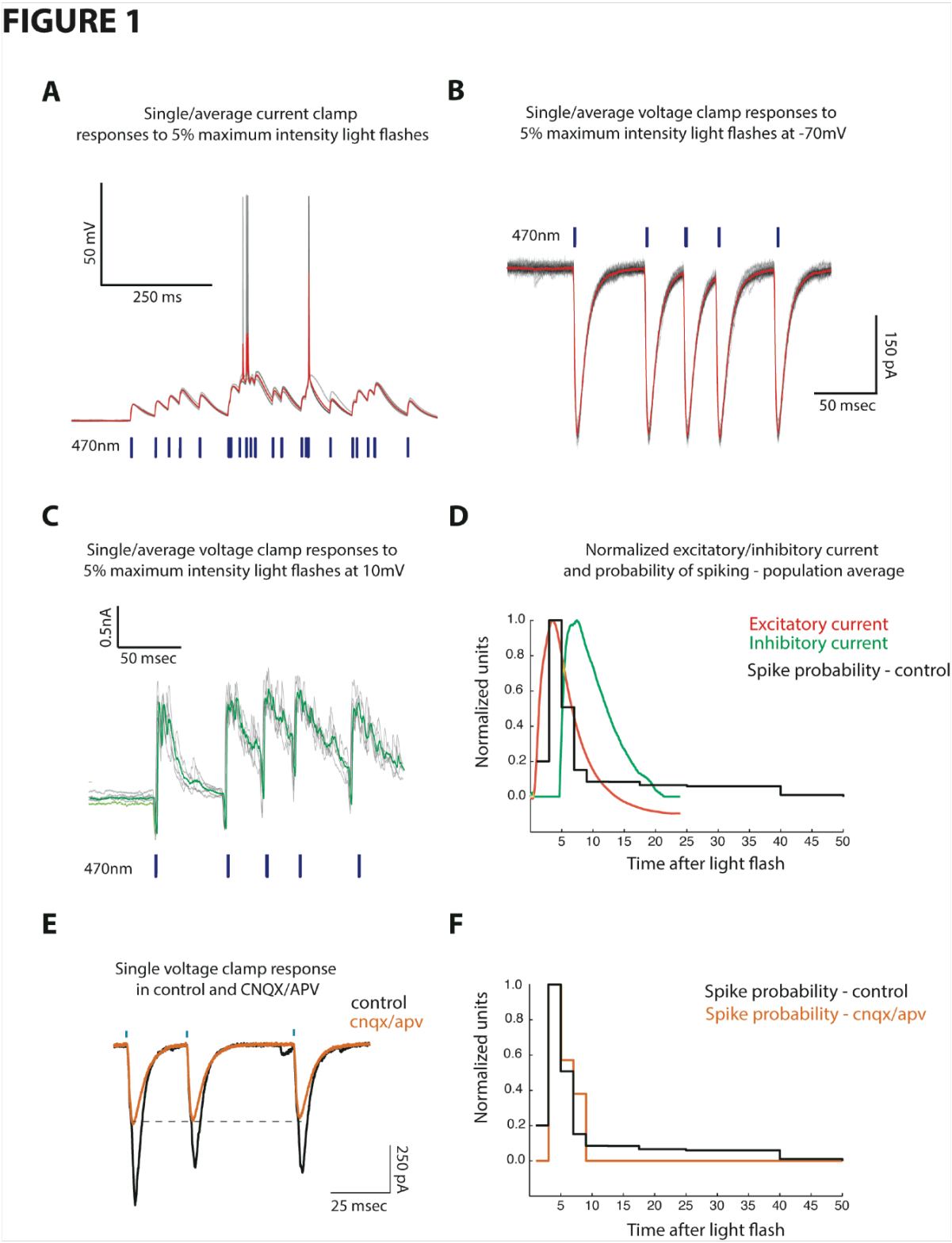

FIGURE 1. Optogenetic stimulation of L5 pyramidal neurons in Thy1-ChR2 mice elicits stereotyped excitatory and inhibitory responses. We recorded

from Type A neurons while activating ChR2-expressing cells in layer 5 of mPFC. **(A)** Current clamp responses of a Type A neuron to repeated presentations of a train of randomly arranged light flashes. Population average (red) and individual (gray) current clamp responses of a single neuron to repeated presentations of a single, random light train are both shown. **(B)** We also recorded from Type A neurons in voltage clamp at -70 mV during random light trains. Average voltage clamp responses (red; n = 12) and an individual response (gray) are shown. **(C)** Population averages (green) and an individual response (gray) are shown for voltage clamp recordings at +10 mV during responses to random light trains in type A neurons (n = 5). Note that voltage clamp recordings have been rectified. **(D)** The probability of spiking is plotted as a function of time after each light flash (averaged across 5 neurons). The normalized, averaged, and rectified excitatory and inhibitory currents are plotted in red and green respectively. The maximum spike probability occurs after the onset of excitatory current and before the onset of inhibitory current. **(E)** Light flashes elicit excitatory currents (black trace) that represent a combination of recurrent network activity, and direct ChR2-mediated currents that remain even after blocking excitatory synaptic activity with CNQX (5 μM) + APV (50 μM) (orange trace). **(F)** Same as in (D) but with synaptic activity blocked using CNQX + APV (n = 5). Blocking synaptic activity essentially eliminates “late” spikes which occur >10 ms after each light flash.

FIGURE 2

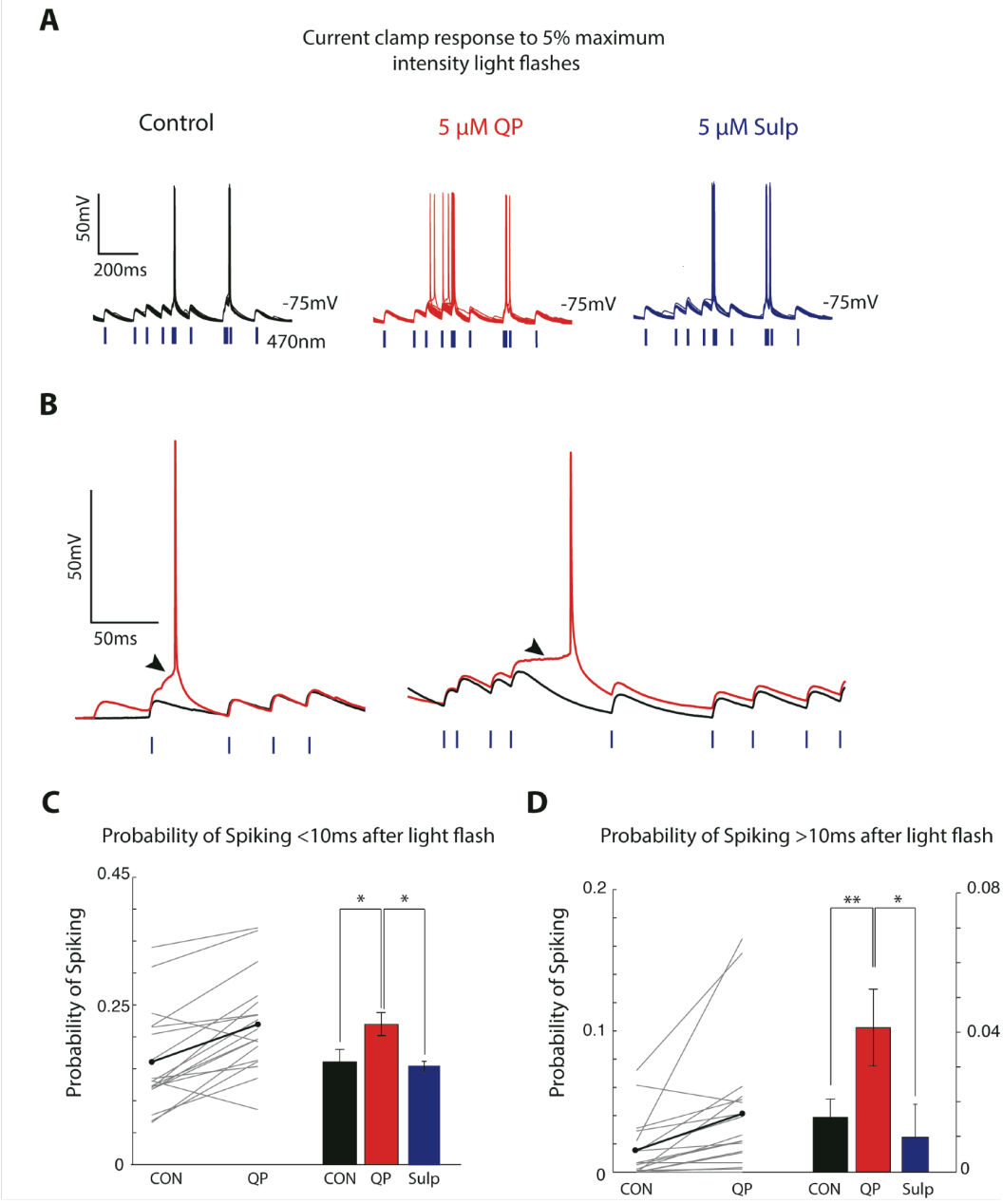

FIGURE 2. D2R activation reversibly increases the probability of spiking in response to optogenetic network activation. We recorded current clamp responses of Type A neurons during stimulation with random light trains first in control conditions, then after washing in quinpirole (5 µM), and finally after the addition of sulpiride (5 µM). **(A)** Overlaid current clamp responses of one neuron

to repeated presentations of the same random light train (using 5% of the maximum light intensity). Approximately 20% of the light flashes elicit spikes in control conditions (left). Bath application of quinpirole (5 μM) increases spiking in response to light flashes (middle), and this increase was reversed by the subsequent addition of sulpiride (5 μM, right). **(B)** Expanded view of current clamp responses before (black) and after (red) application of quinpirole. Arrows indicate EPSPs which either occur after the initial response to the light flash (left), or which grew progressively instead of decaying (right), leading to late spikes which occur >10ms after light flashes. **(C-D)** Quantification of the changes in spiking illustrated in *A* and *B*. Quinpirole increases the probability of spikes occurring either <10ms after light flashes (C) or >10ms after light flashes (D). In both cases, this increase is reversed by the subsequent application of sulpiride. n = 23 in control and quinpirole, n = 5 in sulpiride.

FIGURE 3

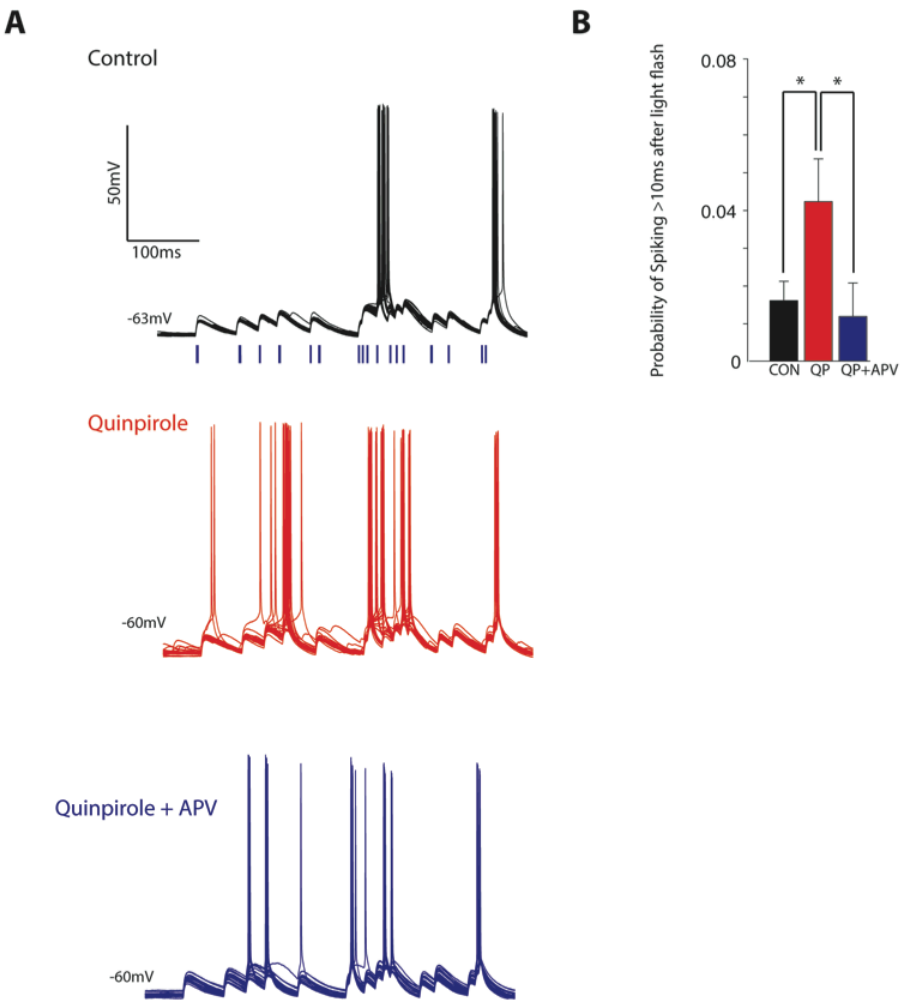

FIGURE 3. Blocking NMDARs reduce quinpirole-dependent increases in excitability. We recorded current clamp responses of Type A neurons during stimulation with random light trains in control conditions, after bath application of quinpirole, and finally after adding the NMDAR-antagonist APV. **(A)** Overlay of representative current clamp responses in various conditions. **(B)** Quantification of the change in late spikes illustrated by *A* showing that APV reverses the

quinpirole-induced increase in late spikes (spikes occurring >10ms after light flashes). n = 23, 23 and 5 for control, quinpirole, and quinpirole + APV, respectively.

FIGURE 4

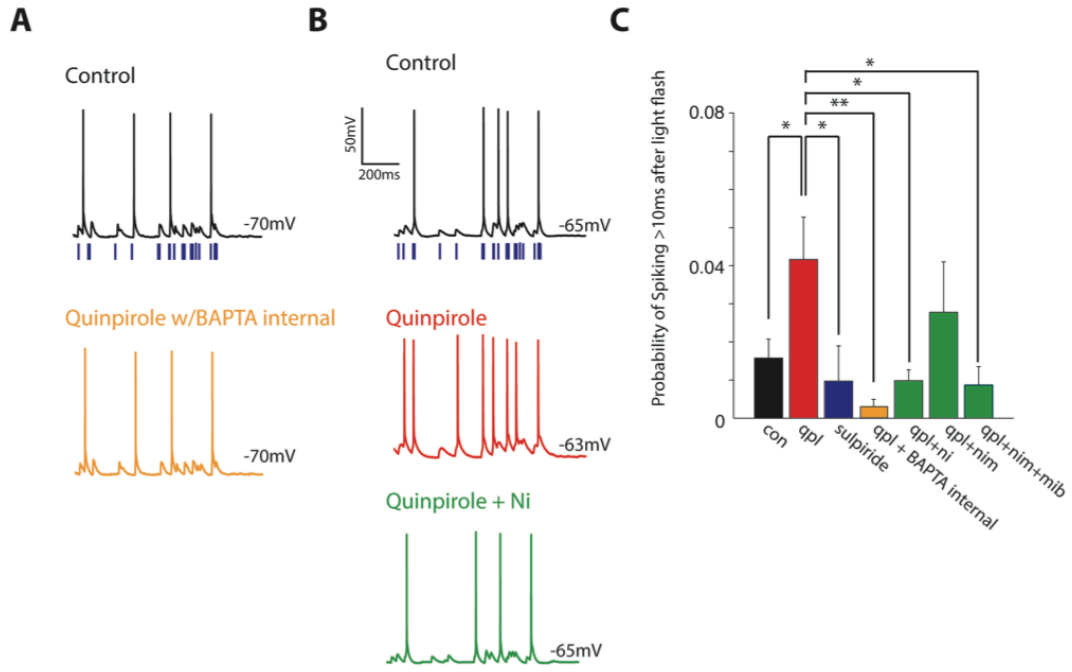

FIGURE 4. The quinpirole-induced increase in late spikes is absent in the presence of intracellular BAPTA and suppressed by blocking VGCCs. (A) Representative current clamp responses in control condition (top) and quinpirole (bottom) during in experiment with BAPTA (5 mM) in the intracellular pipette solution. **(B)** Recordings showing the quinpirole-induced increase in spike probability (middle) is suppressed after nonspecifically blocking voltage-gated Ca^{2+} channels with Ni^{2+} (0.5 mM). **(C)** Summary of how various manipulations affect the occurrence of late spikes (spikes occurring >10 msec following a late flash; qpl = quinpirole (5 mM), nim = nimodipine (5 mM), mib = mibefradil (5 mM); n = 17 in quinpirole, n = 5 in quinpirole + sulpiride, n = 5 in Ni^{2+}, n = 7 in quinpirole + nimodipine and quinpirole + nimodipine + mibefradil). Blocking both

T- and L-type Ca^{2+} channels with a combination of nimodipine and mibefradil abolishes the increase in late spikes elicited by quinpirole.

FIGURE 5

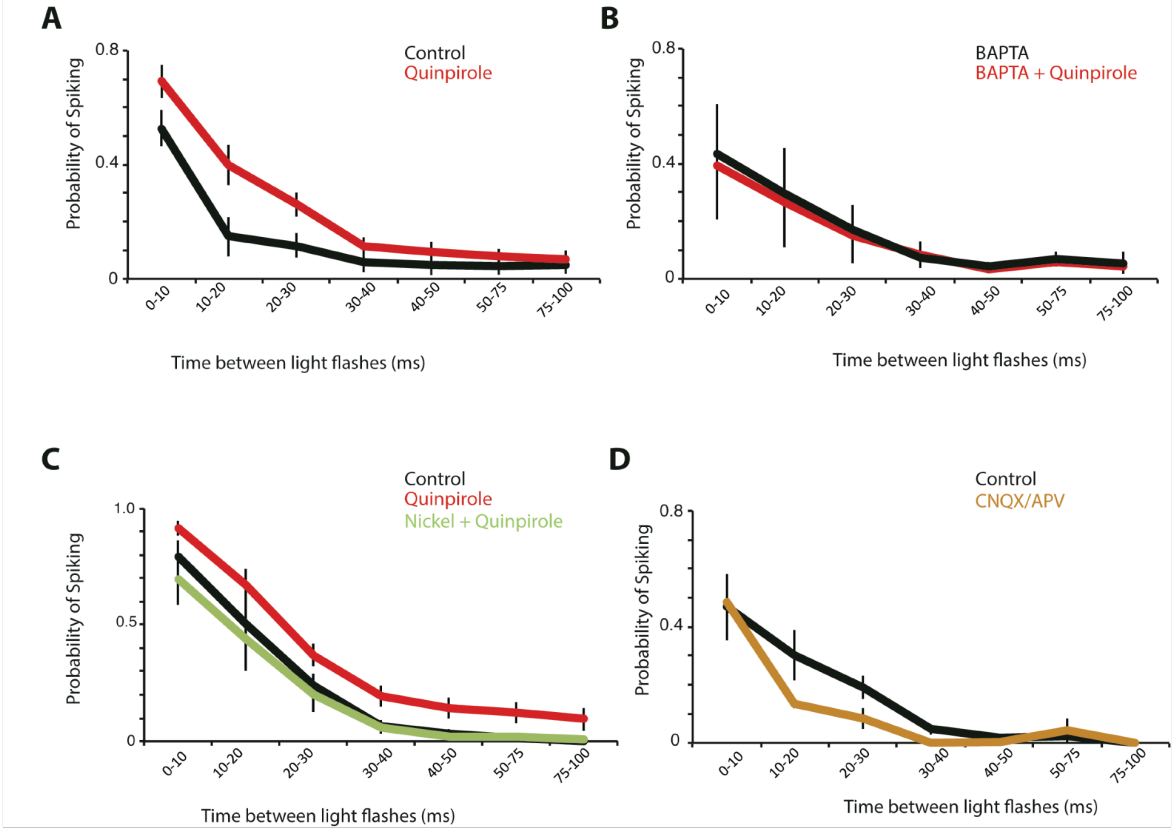

FIGURE 5. Temporal integration depends on Ca^{2+} influx via synaptic and intrinsic mechanisms and is enhanced by quinpirole. (A) We measured the probability of spiking during random light trains as a function of the most recent inter-flash interval. Quinpirole increased the probability of spiking at short interflash intervals (n = 16). **(B)** Including BAPTA in the intracellular solution prevented this quinpirole-induced increase (n = 16). **(C)** Nonspecifically blocking VGCCs with Ni^{2+} (0.5 mM) suppresses the quinpirole-induced increase in spiking at short inter-flash intervals (n = 5). **(D)** Blocking excitatory synapses with CNQX and APV also suppressed temporal integration as evidenced by reduced spiking at intermediate inter-flash intervals (10-30 msec) (n = 5).

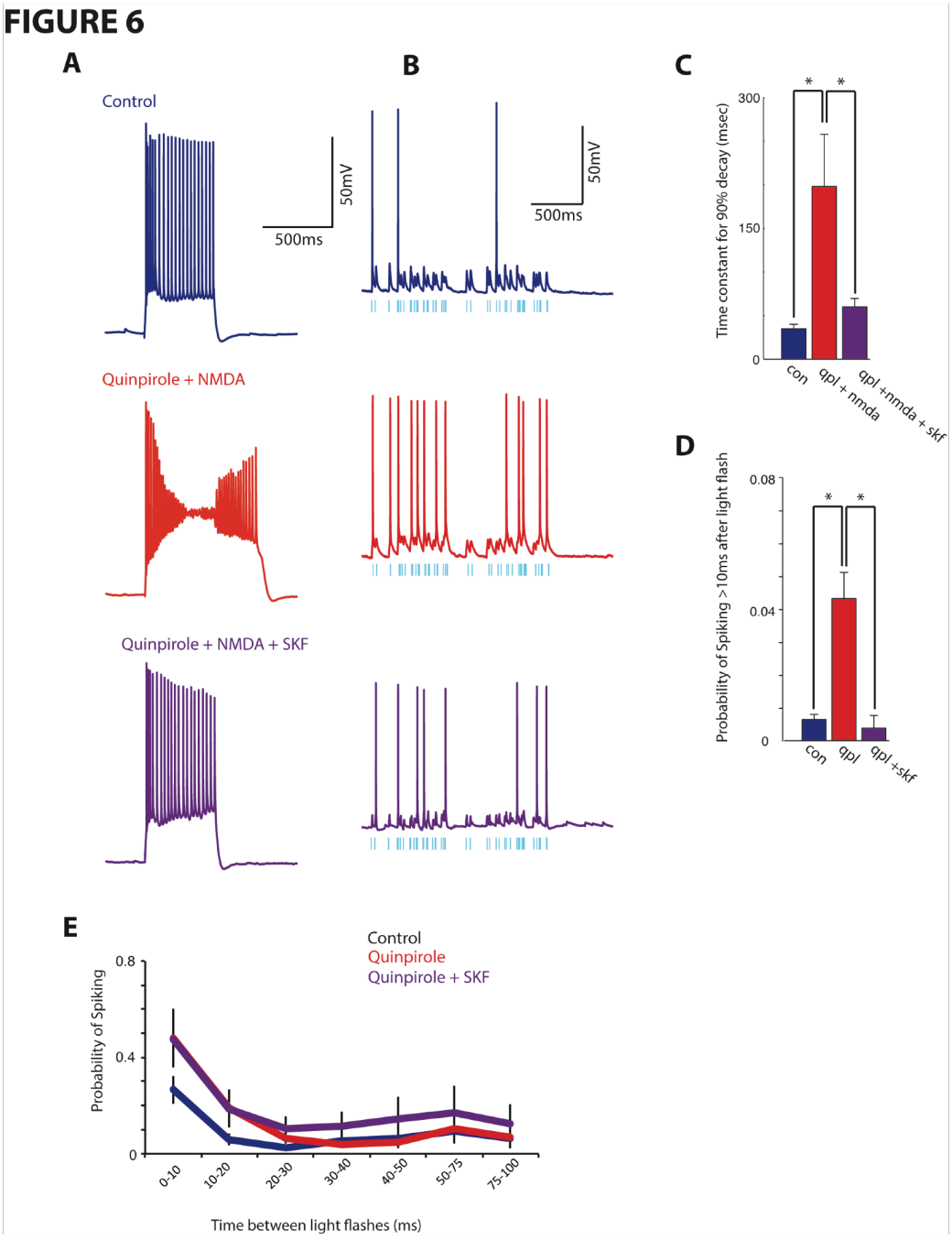

FIGURE 6. D1R activation opposes the D2R-induced afterdepolarization and increase in late spikes. (A) Activating D1Rs with SKF (10 μM) eliminates the afterdepolarization elicited by quinpirole (5 μM) + NMDA (4 μM). **(B)**

Representative current clamp responses to random light trains in control conditions (top), quinpirole + NMDA, and quinpirole + NMDA + SKF. **(C)** We quantified the duration of the afterdepolarization in control conditions, quinpirole + NMDA, and quinpirole + NMDA + SKF (n = 4) by measuring the time required for the membrane potential to return to within 90% of the baseline membrane potential after a depolarizing current pulse (400 pA, 500 ms). **(D)** The average probability of observing a late spike >10 msec after each light flash in control conditions, quinpirole + NMDA and quinpirole + NMDA + SKF (n = 5). **(E)** Activation of D1Rs with SKF does not suppress the quinpirole-induced increase in spike probability at short inter-flash intervals (n = 5).

REFERENCES

Arenkiel BR, Peca J, Davison IG, Feliciano C, Deisseroth K, Augustine GJ. et al (2007) In vivo light-induced activation of neural circuitry in transgenic mice expressing channelrhodopsin-2. Neuron 54: 205–218.

Bernacchia A, Seo H, Lee D, Wang XJ (2011) A reservoir of time constants for memory traces in cortical neurons. Nat Neurosci 14:366 –372.

Durstewitz D, Semans JK. (2008) The dual-state theory of prefrontal cortex dopamine function with relevance to catechol-o-methyltransferase genotypes and schizophrenia. Biol Psychiatry 64:739-49.

Gee S, Ellwood I, Patel T, Luongo F, Deisseroth K, Sohal VS (2012) Synaptic activity unmasks dopamine D2 receptor modulation of a specific class of layer V pyramidal neurons in prefrontal cortex. J Neurosci 32: 4959–4971.

Histed MH, Pasupathy A, Miller EK (2009) Learning Substrates in the Primate Prefrontal Cortex and Striatum: Sustained Activity Related to Successful Actions. Neuron, 63:244–253.

Sawaguchi T, Goldman-Rakic PS (1991) D1 dopamine receptors in prefrontal cortex:involvement in working memory. Science 251:947-50.

Seamans JK, Durstewitz D, Christie BR, Stevens CF, Sejnowski TJ. (2001) Dopamine D1/D5 receptor modulation of excitatory synaptic inputs to layer V prefrontal cortex neurons. Proc Natl Acad Sci USA 98:301-6

Seamans JK, Yang CR (2004) The principal features and mechanisms of dopamine modulation in the prefrontal cortex. Prog Neurobiol 74:1–58.

Seong HJ, Carter AG. (2012) D1 Receptor Modulation of Action Potential Firing in a Subpopulation of Layer 5 Pyramidal Neurons in the Prefrontal Cortex. J Neurosci 32: 10516–10521.

Shepherd GM (2013) Corticostriatal connectivity and its role in disease. Nat Rev Neurosci 14:278-291.

Sohal VS, Huguenard JR (2005) Inhibitory coupling specifically generates emergent gamma oscillations in diverse cell types. Proc Natl Acad Sci U S A 102:18638-18643.

St Onge JR., Abhari H., Floresco SB (2011). Dissociable Contributions by

Prefrontal D1 and D2 Receptors to Risk-Based Decision Making. J Neurosci 31: 8625–8633.

Tseng KY, O'Donnell P. (2005) Post-pubertal emergence of prefrontal cortical up states induced by D1-NMDA co-activation. Cereb Cortex 15:47-57.

Wang M, Vijayraghavan S, Goldman-Rakic PS. (2004) Selective D2 receptor actions on the functional circuitry of working memory. Science 303:853-6

Winterer G, Weinberger DR (2004) Genes, dopamine and cortical signal- to-noise ratio in schizophrenia. Trends Neurosci 27:683– 690.

CHAPTER 5

Concluding Remarks and Remaining Questions

The work presented here elucidates important differences between L5 pyramidal subtypes within the PFC. We explore how distinct projection subtypes differentially express, and respond, to D1 and D2Rs, how these subtypes respond to long-range inputs, and how they receive different forms of feedforward inhibition. Many of the immediate caveats with the experiments are presented here in the Discussion sections of Chapters 2, 3, and 4. In this chapter, I will discuss remaining questions regarding these findings.

In chapter 2 we discussed a novel mechanism by which D2Rs can increase the output of a subpopulation of pyramidal neurons in L5 of PFC via an L-type Ca^{2+} channel and NMDAR-dependent afterdepolarization. We find that D1R activation can oppose this mechanism. It will be important to identify the specific molecular pathway that underlies this effect, i.e. does the quinpirole-mediated afterdepolarization occur by G-protein dependent signaling or via non-canonical, G-protein independent pathways such as β-Arrestin-ergic signaling. Elucidating these mechanisms has potential implications for psychiatric disease since many antipsychotics potently antagonize β-Arrestin 2 recruitment by quinpirole (Masri et al., 2008). Furthermore, if D1R activation opposes the quinpirole-mediated afterdepolarization, does this occur by its effects on PKA and what are the downstream targets? Finally, does D1R activation alone have a measureable effect on Type A neurons?

In the thesis, we discuss the separate computational properties of of PT and IT neurons. PT neurons show facilitating responses to stimulation of long-range contralateral inputs, and are potentially more sensitive to focal inputs in the

spatially and temporal domains. IT neurons, on the other hand, show depressing responses to stimulation of the same inputs and are possibly more sensitive distributed patterns of inputs. These findings provide a framework for a model whereby IT neurons might sustain persistent activity important for working memory or integrate evidence during decision making. This is consistent with findings that IT neurons tend to be D2R-lacking and D1R-expressing and other behavioral studies implicating D1Rs in the PFC with working memory performance (Seong and Carter, 2012; Williams et al., 1995). In contrast, PT neuron activity might then signal to subcortical structures during corollary discharge (Wang, 2004). To validate this hypothesis, it will be important to elucidate the *in vivo* temporal dynamics of activity in these neurons during prefrontal-dependent tasks such as set-shifting (e.g. does type B neuron activity increase during delay periods?). Likewise, future experiments inhibiting these neuronal subtypes during a behavior could illuminate our understanding of how activity in separate neuronal populations contributes to prefrontal-related behaviors.

REFERENCES

Masri B, Salahpour A, Didriksen M, Ghisi V, Beaulieu JM, Gainetdinov RR, Caron MG. Antagonism of dopamine D2 receptor/beta-arrestin 2 I nteraction is a common property of clinically effective antipsychotics. Proc Natl Acad Sci 2008 36:13656-61

Seong HJ, Carter AG. (2012) D1 Receptor Modulation of Action Potential Firing in a Subpopulation of Layer 5 Pyramidal Neurons in the Prefrontal Cortex. J Neurosci 32: 10516–10521.

Wang M., Vijayraghavan S., Goldman-Rakic P. S. (2004). Selective D2 receptor actions on the functional circuitry of working memory. Science 303, 853–856

Williams G. V., Goldman-Rakic P. S. (1995). Modulation of memory fields by dopamine D1 receptors in prefrontal cortex. Nature 376, 572–575

Publishing Agreement

It is the policy of the University to encourage the distribution of all theses, dissertations, and manuscripts. Copies of all UCSF theses, dissertations, and manuscripts will be routed to the library via the Graduate Division. The library will make all theses, dissertations, and manuscripts accessible to the public and will preserve these to the best of their abilities, in perpetuity.

Please sign the following statement:

I hereby grant permission to the Graduate Division of the University of California, San Francisco to release copies of my thesis, dissertation, or manuscript to the Campus Library to provide access and preservation, in whole or in part, in perpetuity.

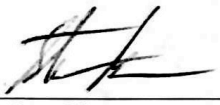

Author Signature

5/27/14

Date